GROWTH KINETICS OF NICKEL SULFATE α-HEXAHYDRATE CRYSTALS IN A FLUIDIZED BED

by

VICTOR ROGER PHILLIPS

B.A. (Hons.), University of Cambridge, 1966

Chem. Eng. Tripos, University of Cambridge, 1967

A THESIS SUBMITTED IN PARTIAL FULFILMENT OF

THE REQUIREMENTS FOR THE DEGREE OF

DOCTOR OF PHILOSOPHY

in the Department

of

Chemical Engineering

We accept this thesis as conforming to the

required standard

THE UNIVERSITY OF BRITISH COLUMBIA

August, 1973

In presenting this thesis in partial fulfilment of the requirements for an advanced degree at the University of British Columbia, I agree that the Library shall make it freely available for reference and study. I further agree that permission for extensive copying of this thesis for scholarly purposes may be granted by the Head of my Department or by his representatives. It is understood that copying or publication of this thesis for financial gain shall not be allowed without my written permission.

Department of Chemical Engineering

The University of British Columbia
Vancouver 8, Canada

Date September 19, 1973

ABSTRACT

Crystal growth rates determined under controlled conditions can be used to test theories of the mechanism of crystallization, while dissolution rates determined under comparable conditions allow an attempt to assess the role of mass transfer in the overall growth process. Laboratory-scale studies of fluidized-bed crystallization are also of interest as aids to the design of full-scale crystallizers of the advantageous suspended-bed ("Krystal") type. Measurements on crystal growth rates under conditions simulating those in industrial crystallizers, especially "Krystal" crystallizers, are still relatively scarce.

In this study, growth and dissolution rates of nickel sulfate α-hexahydrate were measured as functions of the concentration driving force in a laboratory-scale fluidized-bed crystallizer, for the temperature range 35-50°C and the crystal size range 0.5-4.0 mm. The growth of 1 mm crystals at 40°C was measured by two different methods.

Dissolution rates at a given temperature and crystal size were first order in the undersaturation ($c^* - c$). Growth rates were about one-quarter of dissolution rates and depended on a higher power (around 1.3) of the supersaturation ($c - c^*$). This power had no significant dependence on crystal size, but decreased significantly as temperature increased. The apparent variation of growth rate itself with crystal size at constant temperature was slight.

The nature of the dependence of the growth rate on temperature and on crystal size supports the diffusion theory concept

of crystal growth as a two-step process, i.e. mass transfer of solute to the crystal surface, followed by integration into the solid lattice. In the present case, the growth rate appears to be mainly but not wholly controlled by the surface integration step. Making the assumption that the (unknown) rate constant for the mass transfer step of growth can be represented by the (known) rate constant for dissolution, the apparent kinetics of the surface integration step of growth have been extracted from the overall kinetics of growth.

For the growth of 1 mm crystals at 40°C, growth rates found by the "Batch Method," in which the void fraction was 0.998, were in agreement with those found by the "Continuous Method" in which the void fraction was 0.80, close to industrial levels. Since other workers have found agreement for other systems between growth rates from the Batch Method and from single crystal tests, the implication is that only single crystal tests need be made to predict fairly closely the growth rate which would prevail in an industrial type fluidized bed. This should considerably simplify the problem of crystallizer design.

TABLE OF CONTENTS

Section Page

Section Page

Section Page

Page

LIST OF TABLES

LIST OF FIGURES

Figure Page

Figure Page

Figure Page

Figure Page

ACKNOWLEDGMENTS

The author thanks the following:

Dr. Norman Epstein, for consistently wise and considerate supervision.

The Canadian Commonwealth Scholarship and Fellowship Committee and the University of British Columbia, for the award of scholarships.

The National Research Council of Canada, for equipment support through Operating Fund A-2091.

The gentlemen of the Chemical Engineering Department workshop and stores, all of whom gave indispensable help.

The members of the Chemical Engineering Department, both graduate students and faculty, for all those useful discussions.

Mr. Norman Streat, for his kind help with the photography.

"But the way he talks in riddles all the time - it's as if he's frightened of revealing himself. I'd say he knew something about this crystallizing process."

from J.G. Ballard's novel, "The Crystal World" (Jonathan Cape, London, 1966)

1. INTRODUCTION

There were two main purposes behind this work. One was to obtain precise data on crystal growth and dissolution rates, in order to examine current theories of the mechanism of crystallization and investigate the interaction between the mass transfer and the surface phenomena which are believed to contribute to the growth process. Here the use of nickel sulfate α-hexahydrate as the crystallizing substance gave certain experimental advantages (Section 3.2). However, nickel sulfate α-hexahydrate has some commercial significance in its own right, being a by-product of copper refining and being used mainly in electroplating, in the preparation of catalysts and as a fungicide. Hence a second purpose of the work was to provide growth rate data determined under conditions simulating those in industrial "Krystal" crystallizers for a commercially significant compound, one for which no prior growth rate data could be traced. The growth rate data determined might then be useful in the design of full-scale crystallizers for nickel sulfate α-hexahydrate, while some of the conclusions reached for nickel sulfate α-hexahydrate in this work may be generally applicable to the design of "Krystal" crystallizers, regardless of the compounds for which they are intended.

2. LITERATURE REVIEW

2.1 Introduction

The literature on many aspects of crystal growth is voluminous. However, good data which are in a form useful for the design of industrial crystallizers are still relatively scarce.

Only a brief outline of the literature will be attempted here. Mullin [1a,1b] has given a very good account of the chemical engineering aspects of crystallization, with many references to the original literature. Other very useful reference texts with a chemical engineering approach are those by Nyvlt [2], Strickland-Constable [3], Buckley [4] and Bamforth [5].

Until its discontinuation in 1970, the journal "Industrial and Engineering Chemistry" gave very comprehensive annual reviews of the crystallization literature [6]. Since 1970, the annual reviews alone have been continued in book form [7].

2.2 General Kinetics of Crystal Growth from Flowing Solutions

2.2.1 Early work

The existing theories of crystal growth may be put into three main categories, namely, "surface energy," "adsorption layer" and "diffusion" theories. The surface energy theories [1b] have largely been abandoned, but adsorption layer and diffusion theories are both still in use. For a brief description of the adsorption layer theories, see Section 2.2.3.

Unlike the adsorption layer theories, the diffusion theories consider the processes occurring in the solution surrounding the growing crystal as well as the processes occurring at the crystal surface itself. Thus in one of the earliest diffusion-type approaches, Noyes and Whitney [8] considered crystallization to be a simple process of diffusion of solute molecules from the bulk supersaturated solution to the crystal surface, where they believed the saturation concentration to exist. The growth rate was then expressed by

$$r = k_m (c - c^*) \tag{1}$$

where r is the growth rate, c is the bulk (supersaturated) concentration, c* is the saturation concentration and k_m is a constant. Crystal dissolution was also considered to be a diffusion process and crystallization and dissolution were thought to be simply the reverse of one another.

Nernst [9] then concluded from the film theory that

$$k_m = \frac{D}{\delta} \tag{2}$$

where D is the diffusion coefficient and δ is the laminar film thickness. The term δ varied in some inverse manner with the velocity of the solution past the crystal and so the growth rate was expected to increase with solution velocity. Several observations by Marc [10], however, indicated that the above Equation (1) was inadequate. Marc found experimentally that k_m did not increase indefinitely with

increasing solution velocity, but reached some limiting value. He also found that, under similar conditions of temperature and concentration driving force, crystallization was generally slower than dissolution, indicating that the mechanisms of the two processes were different, while Miers [11], by refractive index studies, showed that the solution at the crystal surface was not in fact saturated, but was supersaturated.

Berthoud [12] then considered crystallization as a two-step process: diffusion of solute to the crystal surface, followed by some surface integration process, in which material was incorporated into the solid lattice. The rates of the two processes were written

$$r_m = k_m (c - c_i) \tag{3}$$

$$r_r = k_r (c_i - c^*) \tag{4}$$

where k_m, c and c* are as above, c_i is the (supersaturated) concentration at the crystal surface, r_m is the rate of arrival of solute at the surface by diffusion from the bulk solution and r_r is the rate of integration into the solid lattice.

At the steady state

$$r_m = r_r = r \tag{5}$$

Then, eliminating c_i, which is difficult to find experimentally,

$$r = K(c - c^*) \tag{6}$$

where

$$\frac{1}{K} = \frac{1}{k_m} + \frac{1}{k_r} \tag{7}$$

This rate Equation (6) resembles Noyes and Whitney's original one, except that k_m is replaced by K. The dependence of K on k_r as well as on k_m allows K to remain finite even when k_m becomes very large (i.e. at high solution velocities) and so explains Marc's observations. Dissolution was still thought to be purely diffusive and the absence of a surface integration step in dissolution explained why dissolution was faster then crystallization.

However, Marc had also noticed that, for some solutes, the dependence of crystal growth rate on supersaturation $(c - c^*)$ was greater than first order. This may be expressed empirically by writing

$$r = K(c - c^*)^N \tag{8}$$

where N is now a positive number, greater than unity, not necessarily an integer. Values of N greater than unity have since been found experimentally for many systems. The implication is that the surface integration process may be of higher order than one (the diffusion step is not expected to be of an order other than one) and, instead

of Equation (4), we should really write

$$r_r = k_r(c_i - c^*)^n \tag{9}$$

where n is a positive number greater than unity, not necessarily an integer, and in general

$$1 < N < n \tag{10}$$

Equations (3) and (9) together then express the most general situation, when the surface integration rate is not first-order in the concentration driving force $(c_i - c^*)$ and when the diffusion and surface integration steps occur at comparable rates, that is, neither step is rate-determining.

2.2.2 Attempts to separate the kinetics of the mass transfer and surface integration steps in crystal growth

As is implied in Section 2.2.1, the usual experimental approach to growth kinetics has been to measure the growth rate as a function of supersaturation, holding constant or almost constant other factors such as crystal size, solution velocity and temperature. Once this basic dependence on supersaturation is known, the effect of these other variables can be investigated. Experimental methods by which the growth rate can actually be measured are discussed in Section 3.1.

The kinetics of crystallization would be completely characterized in terms of the diffusion theory if the two rate constants

k_m and k_r (section 2.2.1) could be separately determined, together with the apparent order, n, of the surface integration process. However, because of the complex interdependence of the quantities involved, a general assumption-free separation of the constants has not yet been achieved. Often, one can only express the growth rate in the empirical form of Equation (8).

A novel attempt at a general separation was made (unsuccessfully) in the present work as outlined below. Consider again Equations (3) and (9):

$$r_m = k_m(c - c_i) \tag{3}$$

$$r_r = k_r(c_i - c^*)^n \tag{9}$$

Equating r_m and r_r and eliminating c_i, as before, we have

$$\frac{r}{k_m} + \left(\frac{r}{k_r}\right)^{1/n} = (c - c^*) \tag{11}$$

as an expression relating the separate rate constants for the two steps to the experimentally determinable quantities r and $(c - c^*)$. In general, it is impossible to make r the subject of this expression. Nevertheless, it is expected that estimates may be made of the quantities k_m, k_r and n by a suitable curve-fit of experimentally determined values of r and $(c - c^*)$. This approach has advantages of directness and freedom from assumptions. More details of an attempt to determine k_m, k_r and n by this method are in Section 7.3.2.

The remainder of this section reviews prior work on the separation of the diffusion and surface integration steps. In subsequent discussion, we shall replace the term "diffusion step" by the term "mass transfer step" to emphasize that molecular diffusion is not in fact the only mechanism whereby solute can reach the crystal surface from the bulk solution: eddy diffusion may also be important.

One of the more general separation techniques is as follows. Experimentally, as the solution velocity is increased at constant temperature, a limit on growth rate is reached. There is then assumed to be purely surface integration control of the growth rate and the first term on the left hand side of Equation (11) is assumed to be negligible. Then

$$r = k_r(c - c^*)^n \tag{12}$$

and k_r and n can be obtained directly from a logarithmic plot of r against $(c - c^*)$. Mullin and Garside [13a, 13c] used this technique on potassium alum, finding a value for n of 1.62 for (111) faces, which predominated the crystals: in general both k_r and n are different for different crystallographic faces, even on the same crystal [14, 15, 16]. Substituting their values of n and k_r into Equation (11), they calculated k_m for different solution velocities in the range where growth rate still depended on solution velocity. They found k_m to be much greater than their experimental values of k_d, the rate constant for dissolution, defined by Equation (13), below:

$$r_d = k_d(c^* - c) \tag{13}$$

As they themselves pointed out, the assumption that the mass transfer resistance is completely absent at high solution velocities is suspect. Garside [17] has shown that even at quite high solution velocities, the growth rate, although it may appear experimentally to be independent of the velocity, may actually still be increasing somewhat with velocity. Nevertheless, they found agreement between the form of their measured limiting growth rates[13a] and that of the surface integration rates predicted by Chernov [18], and likewise Cartier et al. [19] found agreement between the form of their data and the form predicted by Amelinckx [20] for surface integration rates. Clontz et al. [21] used this limiting growth rate technique on magnesium sulfate heptahydrate, but found a value of n of unity. Their experimental values of k_m were much higher than values of k_d calculated from the Frossling equation for mass transfer.

Another separation technique can be used when, experimentally, although the growth rate is of higher order than unity at low temperatures, the order tends to unity at higher temperatures. This happens because the surface integration rate increases much more rapidly with temperature than does the mass transfer rate. Thus at the higher temperatures, crystal growth becomes purely mass transfer controlled. In this case, from Equation (11),

$$r = k_m(c - c^*) \qquad (14)$$

and k_m at the different high temperatures can be found directly. Rumford and Bain [22] used this technique on the growth of sodium chloride, in a fluidized bed. They found that there was mass transfer control above 50°C. Their experimental values of k_m were in good agreement with values of k_d calculated from the mass transfer correlation of Chu et al. [23].

As described below, several sets of workers have used a separation technique whereby it was assumed that k_m, the growth mass transfer coefficient, and k_d, the dissolution mass transfer coefficient, were equal. When k_d values, obtained by calculation or directly from dissolution experiments, were substituted for k_m in Equation (11), values for k_r and n could be found.

In a few cases of simple flow, a theoretical expression for the laminar film thickness, δ, has been derived, and so an independent estimate of k_d could be made, using Equation (2). Brice [24], for example, has used such estimates to solve Equation (11) for k_r and n, obtaining n = 2 for two separate cases.

Hixson and Knox [25] calculated k_d values for single crystals by means of a correlation due to Williams [26]. Using these values to solve for k_r and n and permitting only integer values of n, they found the best fit of their data was with n = 2 for copper sulfate pentahydrate and with n = 1 for magnesium sulfate heptahydrate, this latter value agreeing with the findings of Clontz et al., mentioned above.

In cases as below, where it can be established experimentally that n = 1, usually by showing that N = 1 in Equation (8) by a direct plot of r against (c - c*), the separation of k_m and k_r becomes easier, as Equation (7) is then valid. With this technique, Fasoli and Napoli [27] calculated k_d values for a stirred tank, by means of a correlation due to Treybal, and used them as k_m values when plotting 1/K and $1/k_m$ against crystal Reynolds number on the same axes. The distance between the two curves was independent of Reynolds number and represented $1/k_r$. Shirotsuka et al. [28] argued that, by analogy with mass transfer correlations, the dependence of k_m on crystal size and crystal Reynolds number should be of the form

$$k_m \propto \frac{Re^{1/2}}{L} \tag{15}$$

where L is the crystal size. Using Equation (7), they plotted 1/K versus $L/Re^{1/2}$ and obtained a straight line with intercept $1/k_r$. Watts [29] and Bransom et al. [30] studied the growth of magnesium sulfate heptahydrate in a stirred tank, concluding that N and hence n were both unity. They showed that for a stirred tank

$$k_m \propto (\text{stirring rate})^x \tag{16}$$

and substituted this relationship into Equation (7). They then estimated k_r by assuming various values of k_r and, for each one, making a logarithmic plot of $(1/K)-(1/k_r)$ against stirring rate. The value of k_r chosen was that value which gave the best straight line

for this plot. Equation (7) was then used to find k_m. The logarithmic plot also gave the power x. An expression summarizing this investigation of k_m was then used to effect a separation of k_m and k_r in another study using similar equipment [31].

Tanimoto et al. [32] were the first workers to back up their growth experiments (using stirred tanks) with dissolution experiments deliberately made under very similar hydrodynamic conditions so that the values of k_d from their dissolution experiments could be used with more confidence as values of k_m. For copper sulfate pentahydrate they found n = 1. However, in their calculation they had assumed without experimental verification that N = 1 in Equation (8), thus begging the question. Ishii [33] continued this work, measuring growth and dissolution rates of potassium sulfate in both stirred tanks and fluidized beds, again finding n = 1. The constant, k_r, might be expected to be independent of the hydrodynamics and thus values of k_r from stirred tanks and from fluidized beds might be expected to agree. Ishii claimed such agreement, but his data show serious scatter and the agreement is not convincing. Randolph and Rajagopal [34] compared their results from stirred tanks with Ishii's,finding poor agreement. They discuss possible reasons for the difference. Mullin and Garside [13b, 13c] measured growth and dissolution rates of potassium alum in lean fluidized beds (void fraction about 0.95), and performed the separation of k_m and k_r without assumptions about N. They found n was close to two, while k_r still retained some dependence on crystal size.

Although this technique of separation using the assumption of equivalence between dissolution and growth mass transfer has been popular, and indeed is used later in the present work (Section 7.3.1), it must be borne in mind that the assumption has not yet been justified. Mullin and Garside [13c] discuss physical considerations which undermine the assumption (Section 7.3.1) and the difference observed by them and by Clontz et al. [21] between k_d and k_m found using the limiting growth rate method of separation (described above) also undermines the assumption. Again, there is evidence that, in some cases, dissolution is not wholly a mass transfer process itself (see Section 2.2.3). However, the agreement found by Rumford and Bain [22] between k_m from mass transfer controlled growth and k_d calculated from the correlation of Chu et al. [23] is evidence in favour of the assumption.

Nyvlt [35] has reported a separation of k_m and k_r by calculation, for the case of $n = 2$. He derived an equation relating N to k_m, k_r and $(c - c^*)'$, where $(c - c^*)'$ was a constant for given values of N, k_m and k_r, and was the supersaturation obtained by solving together the curve-fitted empirical growth rate expression, i.e. Equation (8), and the curve-fitted theoretical growth rate expression, i.e. Equation (11), with $n = 2$. The experimental value of N was substituted in the derived equation and hence values of k_m and k_r were obtained.

Finally it should be recalled that in general both k_r and n are expected to be different for different crystallographic

faces, even on the same crystal. Thus if the crystal (or crystals) under test shows more than one crystallographic type of face and if the growth rate is found via an overall weight increase rather than by direct measurement of the displacement of separate faces (Section 3.1), then only an average k_r and an average n across the different faces can be found, as has been done in the present work (Section 7.3).

2.2.3 Theories of the surface integration process

So far little has been said to describe the integration process at the crystal surface whereby molecules or ions are accepted into the solid lattice. At the time of their introduction, neither Berthoud's original Equation (4) nor the more general Equation (9) describing the surface integration process had much theoretical justification. However, since then, considerations of the physical situation at the crystal surface have led to the proposal of several mechanisms for the integration process.

It is here that we shall introduce the "adsorption layer" theories of crystal growth referred to at the beginning of Section 2.2.1, as most theories of the surface integration process are in this category. In the original theory, Volmer [36] supposed that crystals grew layer by layer. Molecules or ions arriving at the surface were not immediately integrated, but were initially just loosely adsorbed so that they could still migrate across the surface. For a layer to grow, a critical number of these adsorbed species first had to come together to form a two-dimensional nucleus. The layer was then completed by migration of other adsorbed species, after which the

next layer was nucleated and so on. In a modification of this theory, Kossel [37] considered that kinks could exist along the step at the edge of a partially completed layer and that the kinks would be energetically the most favourable places for newly-migrating species to join the growing layer. However the rates of growth predicted by these theories were many orders of magnitude smaller than those observed experimentally. The difference was explained by Frank [38], who showed that the screw dislocations usually present in crystals allowed growth to continue indefinitely without a need for the slow surface nucleation step. Burton, Cabrera and Frank [39] then reported a theory which allowed for the presence of screw dislocations and which predicted rates much closer to the experimental rates than did the earlier theories. The cases of control by surface diffusion and by volume diffusion were both considered. These theories and a volume diffusion theory due to Chernov [18] all predicted $n = 2$ for very low supersaturations and $n = 1$ for high supersaturations. Brice [40] and Bennema [41] presented data verifying this in a few cases. Brice [40] has also tabulated the values of n predicted for several different types of surface. In a somewhat different approach, Amelinckx [20] had earlier used an analogy to the kinetic theory of gases to calculate the rate of attachment of particles at the crystal surface. The net rate of integration was given by the difference between attachment and detachment rates.

The various modern theories which consider the fundamental processes at the crystal surface in attempts to predict crystal growth rates are discussed in detail in a recent book by Ohara and Reid [42].

Although dissolution is still generally thought to be purely a mass transfer process, in some cases [43, 44, 45] dissolution rates have been found which are greater than first order in undersaturation ($c^* - c$), indicating that sometimes dissolution, like crystallization, may involve a surface process. The phenomenon of etch pits in dissolution is evidence that crystal surfaces do not dissolve homogeneously. Homogeneous dissolution would be expected if the properties of the surface had no influence on the dissolution process.

2.2.4 Dependence of the growth rate on solution velocity and crystal size

Consider again Equation (11)

$$\left(\frac{r}{k_m}\right) + \left(\frac{r}{k_r}\right)^{1/n} = (c - c^*) \qquad (11)$$

The rate constant k_r for the surface integration process is expected to be independent of the mass transfer situation in the solution surrounding the crystal, and thus at constant temperature to be independent of the crystal size and of the velocity of the solution past the crystal. However, k_m is expected to behave as a normal mass transfer coefficient and should thus show a dependence on crystal size L and solution velocity V of the usual form

$$Sh \left(= \frac{k_m \cdot L}{D} \right) \propto (Re)^{\beta} \cdot (Sc)^{\alpha} \qquad (17)$$

when Sh is one or two orders of magnitude greater than unity. Extracting the predicted dependences on V and L only, we have

$$k_m \propto V^{\beta} \cdot L^{\beta-1} \qquad (18)$$

Thus, while in the case of fully surface-controlled growth ($k_m \gg k_r$), we expect no dependence of the growth rate on solution velocity or on crystal size, in the case of fully mass transfer-controlled growth ($k_r \gg k_m$) we expect dependences as given by Expression (18).

Two problems arise when attempting to compare this predicted behaviour with experimental findings. Firstly, much of the experimental data are in the regime where neither surface integration nor mass transfer is fully controlling, and in this regime, justifiable separation of k_m and k_r has been possible only in certain cases (Section 2.2.2). Under these circumstances, often the best that can be done is to look at the size and solution velocity dependence of K, the overall growth rate constant in the empirical Equation (8). Using this approach, Mullin and Garside [13a], for example, found

$$K \propto V^{0.65} \text{ (L constant)} \qquad (19)$$

for $0.003 < V < 0.15$ m/s for a single crystal of potassium alum. Secondly, V and L can only be independently varied if the crystal is anchored. Most work has been done on freely-suspended crystals and in this case V and L are related in some manner, the actual form of

which depends on the hydrodynamics. Also it is often difficult to estimate the effective velocity of the solution over the crystal surface, as usually one can only measure some bulk velocity in the cross-section near the crystal or crystals. Nevertheless such a measured velocity should at least be proportional to the true velocity ("slip velocity") seen by the crystal or crystals.

In an early study, McCabe and Stevens [46] held copper sulfate pentahydrate crystals between parallel screens and passed solution through the screens. Crystals of different sizes grew at the same rate when subjected to the same solution velocity, leading them to make the general statement that growth rate was independent of crystal size at constant solution velocity. However, at most of the solution velocities they used, growth was almost completely surface controlled (that is, the growth rate was almost independent of solution velocity) so the general statement was not justified. They expressed the variation of growth rate with solution velocity V at constant crystal size and supersaturation empirically by

$$\frac{1}{r} = \frac{1}{r_{m0} + B \cdot V} + \frac{1}{r_r} \tag{20}$$

where r is the overall growth rate, r_{m0} is the mass transfer rate at zero solution velocity, r_r is the inherent surface integration rate and B is a constant. Hixson and Knox [25] verified the general form of Expressions (17) and (18) for anchored single crystals of copper sulfate pentahydrate and magnesium sulfate heptahydrate. However, they pre-supposed a value of $\beta = 0.6$ in their initial calculation

of k_d (which they used for k_m).

We now turn to the case of freely-suspended crystals, where V and L are not independently variable. Expression (18) still holds but if we know the relationship between V and L, a simplified form can be obtained. In particular, for fluidized beds, if the range of crystal size considered is not too large and if the void fraction is constant, then approximately

$$V \propto L^a \tag{21}$$

as is found from measurements of crystal fluidization velocities [Figure D.1 and references 5(Figure 77), 47, 48]. (Theoretically, for single spheres, a = 2 in the Stokes flow regime and a = 0.5 in the Newton flow regime.) Hence in fluidized beds

$$k_m \propto L^b \tag{22}$$

where

$$b = \beta(a + 1) - 1 \tag{23}$$

Thus in fluidized beds the growth mass transfer coefficient apparently depends on crystal size only, although in fact part of this dependence on size is really dependence on solution velocity, as seen from the general Expression (18).

As we now recall, k_m itself is generally not available. Some workers have neglected the fact that K of Equation (8) is not a true mass transfer coefficient and have expressed the apparent dependence

of K itself on crystal size in the same form as Expression (22), to give

$$K \propto L^{b'} \tag{24}$$

In their study on the growth of potassium alum crystals at constant void fraction in lean fluidized beds, Mullin and Garside [13b] found $b' = 0.63$, and in a similar study on potassium sulfate Mullin and Gaska [49] found $b' = 0.6$. Bransom [50] arrived at Expression (24) by a more empirical argument and later [51] applied the expression to the growth of potassium nitrate in a fluidized bed, finding $b' \simeq 1$ at 20°C. Some authors have used Expression (24) on growth rates found in equipment other than fluidized beds. Bransom himself [50] applied Expression (24) to the single crystal data of Hixson and Knox [25], finding $b' = 0.65$ for copper sulfate pentahydrate and $b' = 0.3$ for magnesium sulfate heptahydrate. McCabe and Stevens [46] found $b' = 1.1$ for copper sulfate pentahydrate in a stirred tank. The case $b' = 0$ leads to the ΔL law [52].

The simplified Expression (24) is useful in crystallizer design but a more general expression, in which the solution velocity and crystal size dependences of K are not combined, is obtained by replacing k_m directly by K in Expression (17), to give

$$Sh'\left(= \frac{K \cdot L}{D} \right) \propto (Re)^{\beta'} \cdot (Sc)^{\alpha'} \tag{25}$$

Mullin and Gaska [49] found $\beta' = 0.87$ for potassium sulfate at 20°C. By analogy with Equation (23) for pure mass transfer, we can write

$$b' = \beta'(a + 1) - 1 \qquad (26)$$

Rosen and Hulburt [53] expressed the solution velocity dependence of the growth rate of potassium sulfate in a fluidized bed by a semi-empirical equation with an exponential term. Unlike expressions such as (25), this equation could describe the approach of the growth rate to its limit at high solution velocities.

Bujac [47] compared the growth of ammonium alum as single crystals, in fluidized beds and in stirred tanks. For single crystals, he found

$$K \propto V^{0.47} \quad \text{(L constant)} \qquad (27)$$

For fluidized beds, he found $b' = 0.36$ in Expression (24) and for stirred tanks he found the dependences on crystal size and stirring rate to be

$$K \propto L^{0.35} \quad \text{(stirring rate constant)} \qquad (28)$$

$$K \propto N_s^{0.25} \quad \text{(crystal size constant)} \qquad (29)$$

In their stirred tank study of magnesium sulfate heptahydrate growth, Bransom et al. [30] separated k_m and k_r (see Section 2.2.2), showed that there was no effect of crystal size on the growth rate and correlated k_m with stirring rate at constant crystal size by

$$k_m \propto N_s^{0.75} \tag{30}$$

They claimed agreement between this result and an equivalent expression for k_d, found by experiment.

It is important to know the variation of growth rate with crystal size when attempting to predict the product crystal size distribution for an industrial crystallizer. In an early study, McCabe [52] assumed growth rate to be independent of crystal size in deriving the so-called ΔL law. As discussed above, growth rate is expected to be strictly independent of crystal size only when there is full surface control. Bransom [50] used his proposed size dependence, discussed above, in predicting crystal size distribution and other variables for several modes of crystallizer operation. Other empirical size-dependent overall growth rate expressions have been proposed and tested against experimental data by, among others, Canning and Randolph [54], Abegg et al. [55] and Sherwin et al. [56].

2.2.5 Dependence of the growth rate on temperature

Most authors who have measured growth rates at different temperatures have tested them against the Arrhenius relationship:

$$\text{rate constant} \propto \exp[-E/RT] \tag{31}$$

where E is an activation energy for the process in question, R is the gas constant, and T is the absolute temperature. Although almost any

data will yield close to a straight line when plotted in this way, the magnitudes of the resulting values of E have some usefulness in indicating the nature (chemical or physical) of the process being considered. As with the dependence of growth rate on solution velocity and crystal size (Section 2.2.4), the rate constants k_r and k_m should strictly be tested separately against Expression (31), but the separate rate constants cannot always be found and in some cases authors have tested the empirical rate constant K directly.

Rumford and Bain [22], in their fluidized bed study of sodium chloride growth, found that although N in Equation (8) was greater than unity at temperatures below 50°C, N was unity above 50°C, implying that growth was fully diffusion controlled above 50°C. The activation energy over the range 50-73°C was 22.6 kJ/mol (5.4 kcal/mol), while an activation energy calculated from diffusion coefficient data was 20.1 kJ/mol (4.8 kcal/mol). This agreement was more evidence that growth was diffusion controlled at temperatures above 50°C.

Mullin and Gaska [49], in their fluidized bed study of potassium sulfate growth and dissolution, found an overall activation energy for growth, based on K of Equation (8), of 18.0 kJ/mol (4.3 kcal/mol), and an activation energy for diffusion, calculated from diffusion coefficient data, of 20.1 kJ/mol (4.8 kcal/mol), concluding that growth was diffusion controlled, although they found a value for N of 2, whereas N = 1 would be expected in the case of diffusion control. The activation energy for dissolution, found from their own dissolution experiments, was 14.2 kJ/mol (3.4 kcal/mol).

In their study of potassium alum growth and dissolution

at different temperatures in lean fluidized beds, Mullin and Garside [13c] separated k_r and k_m by the method of assuming equivalence between dissolution and the mass transfer step of growth (Section 2.2.2), and found an activation energy for surface integration of 43 kJ/mol (10.3 kcal/mol), while for dissolution the activation energy was 12 kJ/mol (2.9 kcal/mol) from their own dissolution rate data. From diffusion coefficient data, the activation energy for diffusion was 17 kJ/mol (4.1 kcal/mol).

In general, processes with physical mechanisms are expected to have activation energies less than about 30 kJ/mol (7 kcal/mol) and processes with chemical mechanisms are expected to have higher activation energies [2]. For many compounds, dissolution rate data (and diffusion rate data) give activation energies around 20 kJ/mol (5 kcal/mol) and surface integration rate data give activation energies in the range 40-80 kJ/mol (10-20 kcal/mol). Thus for the surface integration step on magnesium sulfate heptahydrate, Hixson and Knox [25], Watts [29], Bransom et al. [31] and Clontz et al. [21], respectively found 102, 64, 50, and 69 kJ/mol (24.3, 15.3, 12.0 and 16.4 kcal/mol) and, for copper sulfate pentahydrate, Hixson and Knox found 57 kJ/mol (13.6 kcal/mol) while Tanimoto et al. [32] found 51 kJ/mol (12.3 kcal/mol). For potassium sulfate, Ishii [33] found 72 kJ/mol (17.2 kcal/mol). These values lend support to the idea that surface integration occurs by a quasi-chemical mechanism (see Section 2.2.3).

2.3 Crystallization in Fluidized Beds

Crystallization work has been conducted using a wide variety of experimental set-ups, including anchored single crystals, both stationary and rotated on rods, stirred tanks, fluidized beds, stationary and reciprocating cages, screw agitated crystallizers and so on. However, in this section, a review is made of kinetics work specifically in fluidized beds.

Particular aspects of several of these papers have already been discussed in Sections 2.2.2, 2.2.4 and 2.2.5. On a laboratory scale, measurements made so far in fluidized-bed crystallizers have mainly been of crystal growth rates, although Bransom and Palmer [51] presented a few data on size classification while Bransom and Trollope [57] measured supersaturation as a function of height in the bed: the supersaturation distribution depends on the growth kinetics and on the degree of mixing in the solution. Bransom and Trollope assumed a certain growth rate law and hence estimated an eddy diffusivity for axial liquid mixing. Mullin et al. [58] and Rumford and Bain [22] have made rough measurements of nucleation rates and hence of the metastable limit during growth on seed crystals. Gaska [59, 49] reported more detailed nucleation measurements.

Rumford and Bain's study [22] was made to investigate the possibility of using a fluidized bed for growing large sodium chloride crystals industrially. Besides their investigations on the effect of temperature on growth rate and on the mechanism controlling growth (Section 2.2.5), they grew sodium chloride crystals in a laboratory-scale (and later a pilot-scale)"Krystal" crystallizer, finding that

large crystals could indeed be successfully grown in such equipment.

Ishii [33, 60] studied growth and dissolution of potassium sulfate in both conical fluidized beds and in stirred tanks. For both types of equipment, he separated k_r and k_m, using the assumption that dissolution and the mass transfer step of growth were equivalent (Section 2.2.2), and he compared k_r values from the two types of equipment. Shirotsuka et al. [61] developed a design method for a fluidized-bed crystallizer and tested it against experimental data on sodium chlorate, with fair success.

Mullin and Garside [13] grew potassium alum both as single crystals and in lean fluidized beds at a constant void fraction of around 0.95. Their method for growth rates in fluidized beds forms the basis of the "Batch Method" in the present work (Sections 3.1 and 5.4). Their separations of k_m and k_r and their investigation of the effects of temperature and of crystal size on the growth rate have been outlined in Sections 2.2.2, 2.2.4 and 2.2.5. When adjusted to equivalent solution slip velocities, the absolute values of the growth rates for single crystals and for crystals in lean fluidized beds were in good agreement, implying that only single crystal tests are needed to predict growth rates in fluidized beds, at least those with high void fraction.

Using similar methods, Gaska [59] grew potassium sulfate as single crystals [16] and in lean fluidized beds [49], but also in much denser fluidized beds with void fraction about 0.85 [62]. He too found agreement between growth rates for single crystals and for crystals in

lean fluidized beds. When working with dense fluidized beds, he used the fore-runner of the "Continuous Method" of the present work (Sections 3.1 and 5.5), following the fall-off of supersaturation by taking a series of solution samples and analyzing them gravimetrically. Provided the crystal size was the same in each, the growth rates in the dense beds and in the lean beds were in agreement [59]. This finding extended the comparison made by Mullin and Garside: it indicated that even growth rates in dense fluidized beds (with void fractions close to industrial levels) could be predicted fairly closely from single crystal tests. The implications for industrial crystallizer design are far-reaching.

Again using similar methods, Bujac [47] grew ammonium alum as single crystals and in both lean and dense fluidized beds, but also in stirred tanks. He again found good agreement between growth rates for single crystals and for crystals in lean fluidized beds. With the dense beds he automated the method [63] with a continuous recording specific gravity meter: this automated method forms the basis of the "Continuous Method" of the present work (Sections 3.1 and 5.5). Verifying Gaska's observations, he found agreement between growth rates in lean beds and in dense beds having void fractions around 0.90. He found that the growth rates in stirred tanks were somewhat higher than the growth rates in the other equipment at comparable solution slip velocities, and he suggested that the difference was due to differences in turbulence levels.

The versatile laboratory-scale fluidized-bed crystallizer [13b] used by Garside, by Gaska and by Bujac (and, in slightly modified

form, in the present work) has been used by several other workers besides: Glasby and Ridgway [64] investigated the growth of aspirin from ethanol, concluding that it was surface integration controlled. Rosen and Hulburt [53] studied the growth of potassium sulfate at constant temperature. They found a value of N in Equation (8) of two, which agreed with Gaska's value [49]. Graeser [65] investigated the effect of temperature and of surfactants on the growth of potassium sulfate. Paxton [66] studied the growth of calcium sulfate dihydrate (gypsum), again finding surface integration control.

2.4 Mass Transfer in Fluidized Beds

As has been seen (Sections 2.2.1, 2.2.2 and 2.2.4), mass transfer is an important part of the crystal growth of many compounds and, since dissolution usually appears to be a pure mass transfer process, some authors have backed up their crystal growth rate measurements with crystal dissolution rate measurements, hoping by a comparison of the two to assess the role of mass transfer in crystal growth. Such dissolution rate measurements have been made on nickel sulfate α-hexahydrate as part of the present work (Section 7.2). We shall now review prior crystal dissolution rate measurements from fluidized beds and outline how they compare with some well-known correlations for mass transfer in fluidized beds.

We shall present the correlations first. That due to Rowe and Claxton [67] for spheres fluidized by water at Reynolds numbers 10^{-3} - 10^{7} is

$$Sh = A + B(Re_s)^m Sc^{1/3} \quad (32)$$

where $$A = 2/[1-(1 - \varepsilon)^{1/3}] \quad (33)$$

$$B = 2/3\varepsilon \quad (34)$$

and $$(2-3m)/(3m-1) = 4.65\ Re_s^{-0.28} \quad (35)$$

The Reynolds number, Re_s, is based on the superficial water velocity, V_s. The form of this correlation makes it suitable for use as void fraction tends to unity. This is an advantage in the present work. The correlation due to Chu et al. [23] is

$$j_D = 5.7[Re_s/(1-\varepsilon)]^{-0.78} \text{ for } 1 < Re_s/(1-\varepsilon) < 30 \quad (36)$$

and $$j_D = 1.77[Re_s/(1-\varepsilon)]^{-0.44} \text{ for } 30 < Re_s/(1-\varepsilon) < 5000 \quad (37)$$

where $$j_D = \left(\frac{k_d}{\rho \cdot V_s}\right) Sc^{2/3} \quad (38)$$

Again, the Reynolds number is based on the superficial fluid velocity, V_s, as is the j-factor. The correlation was originally formulated for the authors' experiments on cylinders and spheres fluidized by air but was found to be effective for many other sets of data, including some from liquid-fluidized beds, although most were from fixed beds.

The form of the correlation makes it unsuitable for use as void fraction tends to unity. This is a disadvantage in the present work.

In the case of crystal dissolution, the particles of course have shapes other than spherical, but the great majority of general heat or mass transfer work has been done on spherical particles. However, in one of the few studies which considered other regular shapes, Glaser and Thodos [68] found no great effect of particle shape on heat transfer in fixed beds of spheres, cubes and cylinders.

Ishii [33, 60] correlated the results of his experiments on the dissolution of potassium sulfate fluidized in vertical cones by

$$(Sh) \cdot \varepsilon^{1/2} = 2 + 0.75(Re)^{1/2} \cdot (Sc)^{1/3} \qquad (39)$$

Here the Reynolds number is based on the interstitial solution velocity. Mullin and Garside [13c] correlated the results of their experiments on the dissolution of potassium alum in lean fluidized beds, at a constant void fraction of 0.95, by

$$Sh = 0.37(Re)^{0.62} (Sc)^{0.33} \qquad (40)$$

again using a Reynolds number based on the interstitial solution velocity. Using the length of an edge as the linear dimension of their (octahedral) crystals, they found a maximum difference of 16% between their values and those predicted by Rowe and Claxton. They found a maximum difference of 18% between their values and those

predicted by Chu et al. Bujac [47] found good agreement between his experimental results from the dissolution of ammonium alum in lean fluidized beds and the values predicted by Rowe and Claxton.

Although they did not themselves conduct dissolution rate measurements, Rumford and Bain [22] compared their values of the growth mass transfer coefficient k_m, found under conditions of full mass transfer control, with values of k_d calculated from the correlation of Chu et al. They found good agreement.

The equating of k_m with k_d permits an extraction of the apparent surface integration kinetics from the overall growth kinetics (Sections 2.2.2 and 7.3.1). There is doubt, however, that the two coefficients are really equal (Section 7.3.1), but even if they are not, we should still be able to express the dependence of either k_m or k_d on the hydrodynamics in the usual way, via Expression (17). Any differences between mass transfer in growth and in dissolution are expected to affect primarily the diffusion coefficient and the mass transfer coefficient.

3. EXPLORATORY WORK

3.1 Possible Methods for Measuring Crystal Growth Rates

The two common ways of expressing a crystal growth rate are as a rate of advance of the crystal surface (m/s) in the direction perpendicular to the surface and as a mass flux, or rate at which unit area of surface gains crystal material ($kg/m^2 \cdot s$). The latter is perhaps more frequently seen, being used in many different mass transfer situations, but the two expressions can easily be related via the density of the crystal material.

Each of the two expressions indicates different possible approaches to the experimental determination of crystal growth rates. Firstly one can measure directly the rate of advance of the crystal surface. When a crystal can be held stationary during growth, the advance of a surface can be followed using a travelling microscope [19, 13a, 16, 47, 21]. When the crystal cannot be held stationary during growth, some reference point within the crystal is necessary, relative to which periodic measurements of the position of the surface can be made. A distinctive flaw such as a veil within the crystal might be used or if the crystal is of a substance for which isomorphous substances exist, then an overgrowth of the substance under test can be made on an initial crystal of an isomorphous substance of a different colour [69, 70]. An advantage of this direct type of method is that the different growth rates on different faces of a crystal may be found independently. A disadvantage is that this method can be used only on single crystals and not on a collection of many crystals. The

second type of method involves finding the overall rate at which one or more crystals gains weight, usually by finding the weight increase occurring in a known time [25, 22, 13b, 49, 47]. The mass flux is then obtained by division of this rate of weight increase by the crystal surface area across which the weight increase has occurred. Alternatively, in the special case of crystal shape being independent of crystal size, the growth rate may be expressed directly as a rate of advance of the crystal surface (in m/s), without having to find the crystal surface area, by equating the ratio of the initial and final sizes to the cube root of the ratio of the initial and final weights [53, 65]. Advantages of this second type of method include basic measurements which are precise and are easy to obtain (weighings and timings) and applicability to collections of many crystals. Disadvantages include the difficulty of finding the crystal surface area and the fact that the method can only give an average growth rate over all the different faces of the crystal. However, if as additional information the ratios of the rates on the separate faces under given conditions are available, then the absolute individual rates on the separate faces under those conditions may be estimated (see Appendix J).

Since the aim of the present work was to measure the growth rates of a collection of crystals in a fluidized bed which was intended to be a model of a full-scale industrial fluidized-bed crystallizer, the second type of method was employed here. Nevertheless there is evidence [13b, 59, 47] that growth rates measured for single crystals (by the first type of method) are directly applicable to collections of crystals growing in a fluidized bed.

Two approaches, both of this second type, have been used in the present work. In the first, called the "Batch Method" (Section 5.4), a series of separate growth experiments was made for each temperature and crystal size considered, the supersaturation level being almost constant within each experiment but different between experiments. Growth rates were found from the weight increase occurring in a known time. In the second, called the "Continuous Method" (Section 5.5) the supersaturation was allowed to fall by a large amount while being continuously monitored. The instantaneous rates of fall of the supersaturation then allowed the determination from a single experiment of growth rates at many different supersaturation levels. Any convenient property of the solution could be monitored in this method, but in the present work, the specific gravity was used (Section 3.3).

3.2 Selection of a Suitable System

After considering various substances for use in the crystal growth rate experiments, nickel sulfate α-hexahydrate was chosen for the reasons outlined below. The α-hexahydrate is the normal commercial form of nickel sulfate. It is that solid form which is in equilibrium with the solution in the temperature range 31.2 - 53.3°C. Some other substances which were considered and the reasons for their rejection are briefly discussed in Appendix A.

Initial considerations indicated that in general inorganic substances would be more suitable than organic substances because of higher mechanical strength of the crystals and better chemical

stability of both crystals and solutions. The two major factors considered next were crystal shape and maximum metastable supersaturation. The crystal shape should be as simple as possible, to facilitate determination of the crystal surface area. The shape of nickel sulfate α-hexahydrate crystals is relatively simple, being a combination of two tetragonal bipyramids (Figure 1 and Appendix J). The maximum metastable supersaturation is the maximum supersaturation which a solution can withstand before nucleating, and should be as large as possible to allow determination of growth rates over a good range of supersaturations. The maximum metastable supersaturation is considerably smaller for a solution in which seed crystals are present than it is for an unseeded solution. Preliminary measurements on nickel sulfate α-hexahydrate in an apparatus as reported by Nyvlt [71] indicated a maximum metastable supersaturation in the presence of seed crystals of 1.5 wt% hexahydrate (or 4.5 °C of supercooling). Later, the maximum metastable supersaturation for seeded solutions in the laboratory-scale fluidized-bed crystallizer was estimated from tests to be 1.3 wt% hexahydrate (or about 4°C of supercooling). This is a relatively high level for a solution of an inorganic salt.

In the laboratory-scale fluidized-bed crystallizer used in the present work, the supersaturations were induced by cooling. Therefore for convenience the substance to be used should have a suitably large temperature coefficient of solubility. Nickel sulfate α-hexahydrate's temperature coefficient of solubility of approximately 0.33 wt% hexahydrate/°C was satisfactory. Other factors in favour of nickel sulfate α-hexahydrate included easy availability in pure

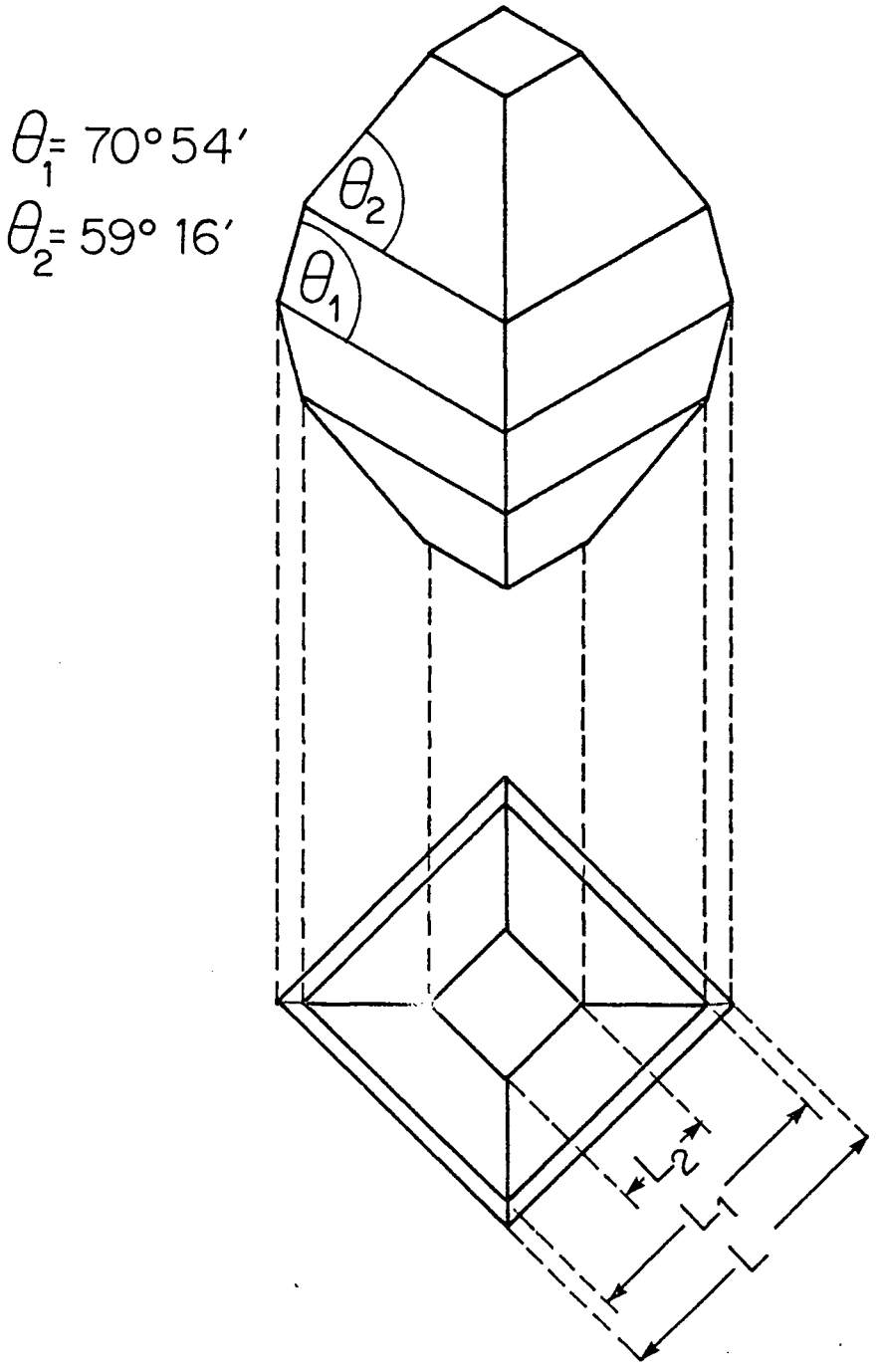

Figure 1 Simplified shape of nickel sulfate α-hexahydrate crystals

form, stability of the solid hexahydrate in ordinary atmospheres, some importance as an industrial product (Section 1) and of course the fact that, despite this latter, crystal growth of this compound had hardly been studied by previous workers. Finally, preliminary growth tests had shown that, even at supersaturations of up to 2.4 wt% hexahydrate, the growth of nickel sulfate α-hexahydrate was well-behaved, proceeding without the development of dendrites, whiskers or other irregular forms.

3.3 Possible Methods for Measuring Solution Concentration

A large variety of methods for measuring concentration have been used in crystallization work. Many could not be considered for the present work as they were not sufficiently sensitive and in fact only two methods were seriously considered. These were specific gravity measurements and direct gravimetric measurements (evaporation of samples of the solution to dryness, followed by heating of the solid residue to a constant weight). Of the two, the former was finally selected.

Specific gravity measurements on any of the solutions were always made in duplicate, using 25 cm^3 bottles, with the temperature controlled to give random fluctuations of not more than 0.05°C and with a systematic (thermometer calibration) error of not more than 0.1°C. The pooled estimated standard error from many pairs of measurements was 0.00004 S.G. A calibration of specific gravity versus concentration was prepared (Appendix D.1). When this was used to convert from the specific gravity of a given solution to the concentration of that solution, the resulting concentration value had an estimated standard

error of 0.006 wt% hexahydrate.

A serious attempt was made to use the direct gravimetric method because this method was expected to give concentrations with a higher precision than did the specific gravity method. It would also have been a more basic method, avoiding the specific gravity method's conversion step with its possibility of introducing further errors. In the direct gravimetric method, weighed samples of the solution were evaporated to dryness and then the solid residues were heated to constant weight. Because of the water of hydration present in nickel sulfate α-hexahydrate, the temperature of this heating was critical. A thermogravimetric analysis was made (on a Du Pont 950 instrument) of nickel sulfate α-hexahydrate to determine its thermal decomposition characteristics, in particular whether any plateaux existed where residue weight was independent of temperature. The analysis (Figure 2) was performed at the minimum heating rate (1°C/min) and the minimum purge air flow (40 cm^3/min), to simulate most nearly the conditions in the drying oven. The analysis indicated that there was no plateau until about 450°C. At that temperature, dehydration had gone to completion and the residue was anhydrous nickel sulfate. This present analysis agreed reasonably with an analysis from the literature [72].

The main disadvantage of the direct gravimetric method was that very long times at 450°C (tens of hours) were needed before the weight of the residue became constant. Also, when the method was tested on known weights of hexahydrate, the actual weight of the residue was usually slightly but significantly lower than calculated,

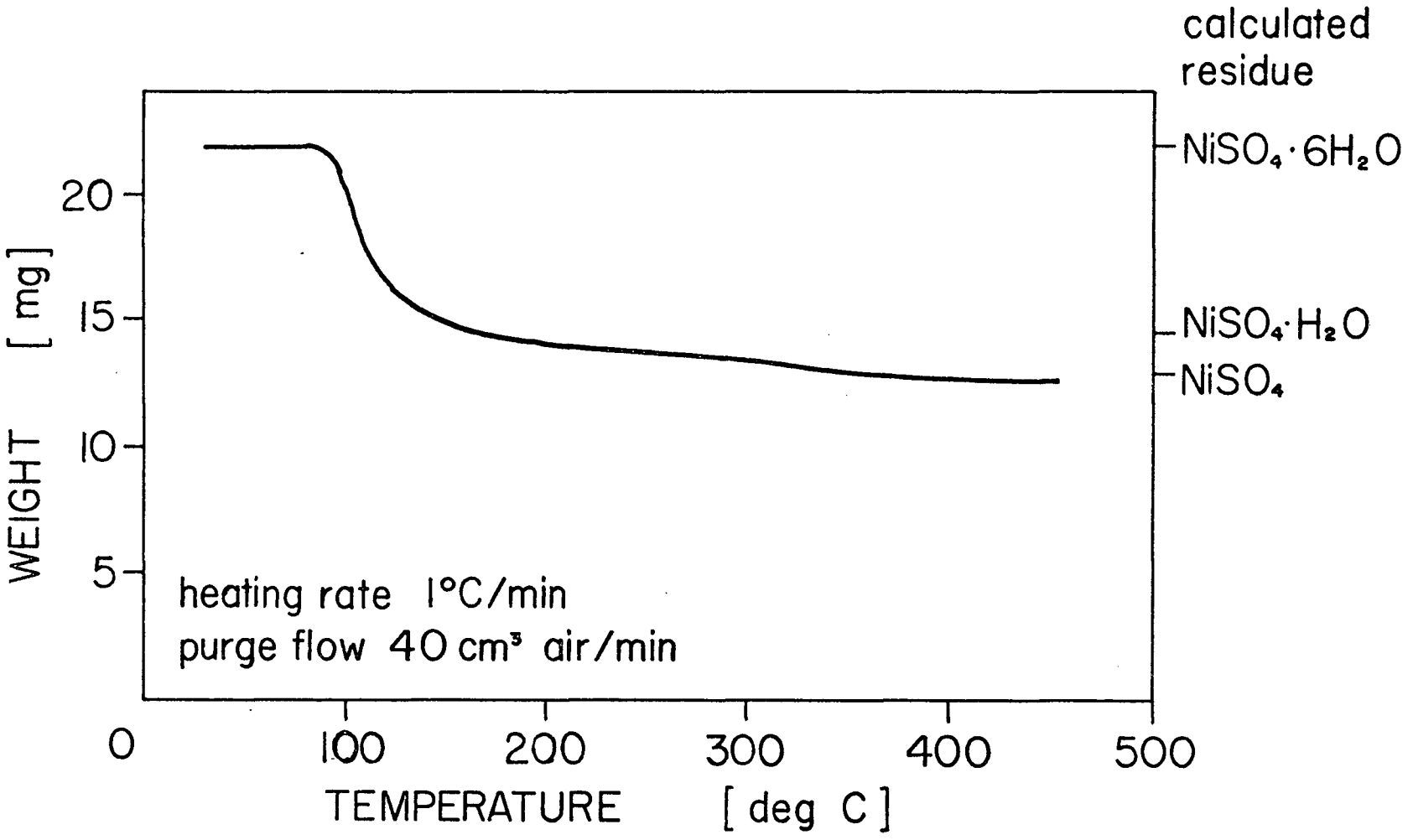

Figure 2 Thermogravimetric analysis of nickel sulfate α-hexahydrate

indicating that perhaps decomposition of the anhydrous nickel sulfate itself (to sulfur trioxide and nickel oxide) had begun. Because of these problems the direct gravimetric method was abandoned in favour of the simpler, more rapid (but less precise) specific gravity method.

Indirect gravimetric methods such as precipitation with dimethylglyoxime would also have been very precise but again would have been very slow and tedious and so were not considered.

The laboratory-scale fluidized-bed crystallizer was equipped with a continuous recording specific gravity meter (Section 4.2) which facilitated the determination of solution concentration via specific gravity, especially during crystal growth by the Continuous Method (Section 5.5), although the meter still had to be calibrated over a suitable range, using specific gravity bottles.

Recently, solution concentrations have been determined in situ via refractive index [73, 74, 75]. A big advantage of this method is that it can be used for the concentration of the interstitial solution in even a thick slurry, while the methods discussed above are really only suitable for use with clear or almost clear solutions.

3.4 Expression of the Concentration Driving Force

Dissolution of a crystal into an undersaturated solution is usually believed to be a purely mass transfer process and crystal growth is believed in general to involve a mass transfer step. For small mass fluxes, mass transfer rates are governed by

$$r_m \propto (\Delta c)_m \qquad (41)$$

where r_m is the mass flux and $(\Delta c)_m$ is the concentration driving force for mass transfer. For dissolution of a crystal,

$$(\Delta c)_m = c^* - c \tag{42}$$

where c* is the saturation concentration (which is the interfacial concentration, in the case of dissolution) and c is the bulk(undersaturated) concentration. For crystal growth:

$$(\Delta c)_m = c - c_i \tag{43}$$

where c is the bulk (supersaturated) concentration and c_i is the interfacial (supersaturated) concentration. Throughout the present work, for both dissolution and crystal growth, the concentration driving forces have been small (not more than 2.4 wt% hexahydrate) and mass fluxes have been small (not more than 130×10^{-5} kg/m^2 • s) so Expression (41) has been considered satisfactory. When large mass fluxes occur, a modified mass transfer expression should be used [76]. Strictly mass transfer involving crystals should be corrected for the rate of advance or retreat of the crystal surface [25, 77] but usually this rate is negligible relative to the mass transfer rate itself.

Many different units of concentration have been used when considering mass transfer rates, particularly in crystallization work. In the present work, two questions arise. In terms of what species should the concentration unit be expressed and what concentration

unit in terms of that species should then be used? It was decided to express concentrations in terms of hexahydrate, as the solid form was itself the hexahydrate. It is doubtful that the real diffusing species is the hexahydrate, but neither would it be the anhydrous sulfate, which is the other obvious candidate for the expression of concentration: the true solvated ion diffusing species is probably nearer to the hexahydrate than to the anhydrous form. In any case, a concentration expressed in terms of hexahydrate should at least be proportional to a concentration expressed in terms of the true diffusing species and any constant of proportionality can be taken up by the mass transfer coefficient. The concentration unit then decided upon was weight percent hexahydrate. Concentrations as weight of solute per unit volume of solution have more theoretical justification but, because of thermal expansion, the concentration of a given solution is somewhat temperature-dependent when expressed in these units. This is a serious disadvantage. A weight ratio (weight of solute per unit weight of solvent) could have been used instead of a weight percentage, but this was rejected as being even further from the basic theoretically justifiable unit. Nevertheless when calculating the results of experiments by the Continuous Method (Section 6.2) it was convenient to convert concentrations temporarily into these units.

4. THE LABORATORY-SCALE FLUIDIZED-BED CRYSTALLIZER

4.1 Basic Construction

The crystallizer (Figure 3) was a slightly modified version of that reported originally by Mullin et al. [58] and in later form by Mullin and Garside [13b]. It consisted basically of a vertical rectangular circuit of total capacity about 0.012 m^3 (12 ℓ) built from industrial glass piping (Q.V.F. Ltd., Scarborough, Ontario). Supersaturated solution was continuously pumped round the circuit by a small stainless steel centrifugal pump. Technical specifications for the pump and for other mechanical and electronic components of the apparatus are given in Appendix B.

Most of the glass piping was 25 mm internal diameter, but the 900 mm long crystallization section was 50 mm internal diameter, while directly above the crystallization section was a calming section of 150 mm internal diameter. Unlike a conventional fluidized bed, the crystallization section had no bottom grid. Instead, the position of the bottom of the bed of crystals was defined by the tapering reducer between the 50 mm I.D. crystallization section and the 25 mm I.D. feed pipe below it, since the upward velocity of the solution decreased sharply at the reducer. Similarly the top of the bed of crystals was defined by the tapering reducer between the 50 mm I.D. crystallization section and the 150 mm I.D. calming section. Above the calming section, the crystallizer was closed at the top by a lid of 2 mm Teflon sheet, secured by a metal flange. In the lid was a central 25 mm hole, for

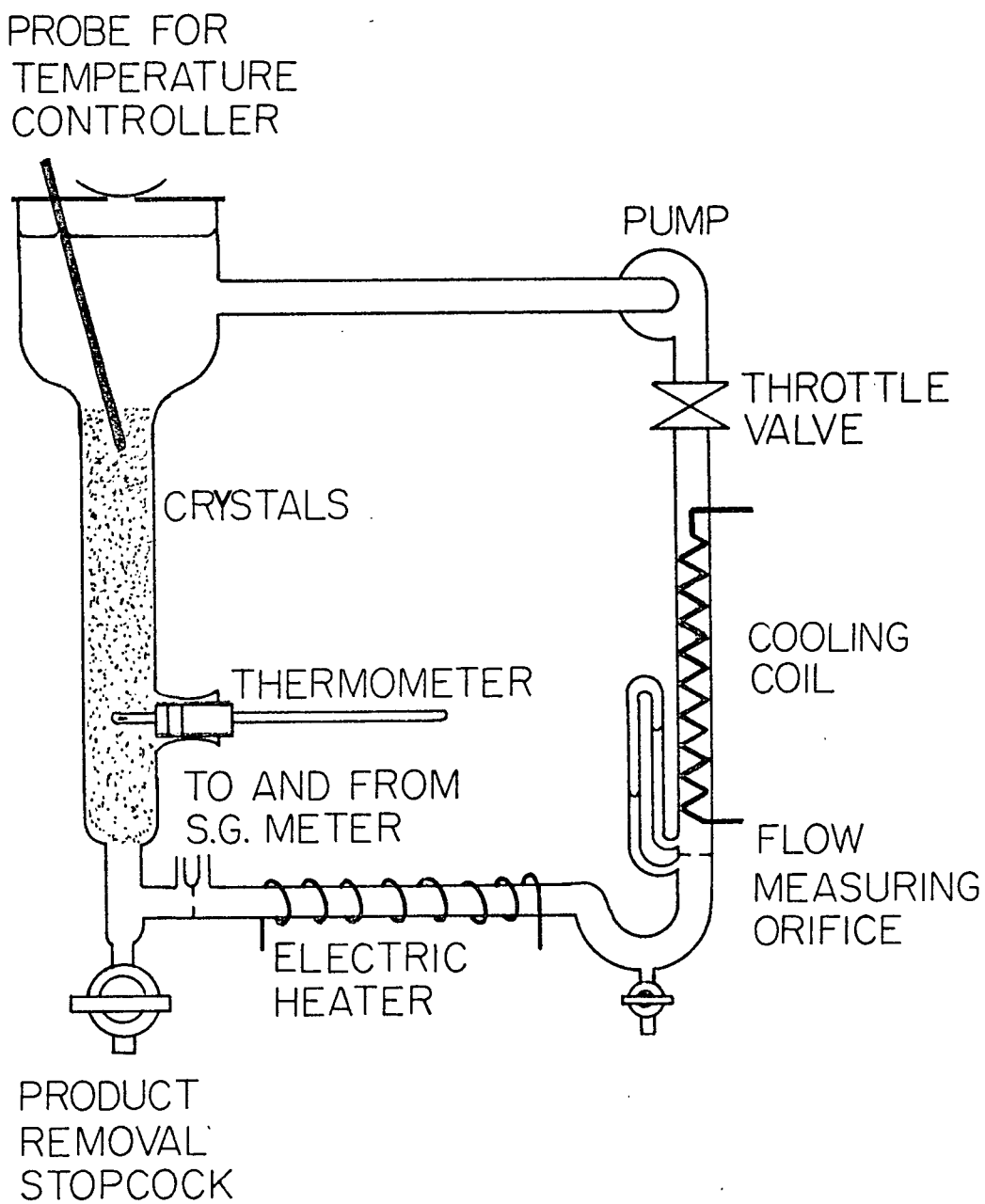

Figure 3 The laboratory-scale fluidized-bed crystallizer

charging make-up solution or seed crystals, and also a 6 mm hole at the side, through which passed the platinum resistance probe of the temperature controller. When not in use, the charging hole was covered by a clock glass to keep out dust and to prevent evaporation. The product crystal removal valve was a conventional Standard Taper glass stopcock (Pyrex brand) of 12 mm bore, fused to a standard Q.V.F. 25 mm I.D. flared end-piece. An auxiliary drain valve was provided by a conventional Teflon-barrel stopcock of 8 mm bore, fused to the Q.V.F. U-section at the low point. Connections between the glass piping and the pump were via Teflon bellows, to prevent the transmission to the glass of vibration from the pump motor.

When working with smaller crystals (size less than 1 mm) it was found that a few of these crystals tended to be carried through the calming section and were then drawn into the pump inlet pipe. To prevent this occurrence by deflecting these crystals from their upward path, a conical Teflon baffle of bottom face diameter 25 mm was fitted to the platinum resistance probe just above its bottom end, at the top of the crystallization section.

Most of the gaskets between the glass pipe sections were equipped with standard Q.V.F. U-section Teflon sheaths. However, because the end-pieces of the pipe sections had I.D.'s up to 2 mm oversize while the I.D.'s of the standard gaskets were always exactly on size, the joints between pipe sections in the vertical crystallization section presented ledges on which crystals smaller than 1 mm could be trapped. Therefore, in the crystallization section only, the standard gaskets were replaced by gaskets machined from solid

sheet Teflon, individually sized so as to give a smooth inside wall across each joint.

The maximum capacity of the crystallizer was about 0.012 m^3 (12 ℓ), while the minimum volume of solution necessary for operation (that is, sufficient to flood the pump inlet) was about 0.011 m^3 (11 ℓ).

Because of the deep colour of concentrated nickel sulfate solutions, crystals growing in the crystallizer could not be viewed properly by daylight alone. Additional lighting was installed behind the crystallization section, the product crystal removal valve and the calming section, so that the growing crystals could be observed more easily, by transmitted light. The crystallization section and product crystal removal valve were illuminated by fluorescent gas tubes while the calming section, being thicker, required the more intense light provided by a bank of three 150 W tungsten filament reflector floodlamps.

For the Continuous Method (Section 5.5) it was necessary to reduce the effective bed volume. This was achieved by fitting inside the crystallization section a 25 mm I.D. constriction (Figure 4) machined from Teflon. The lower section of the constriction simply tapered gradually from 50 mm I.D. to 25 mm I.D., but the upper section of the constriction reproduced the shape of the lower glass reducer which had previously defined the bottom of the crystal bed. Thus the constriction defined the new higher position of the bottom of the bed. The constriction was sized externally such that it was a tight sliding fit inside the crystallization section, so by pushing or pulling it to different positions within the section, large changes of the effective bed volume could conveniently be made.

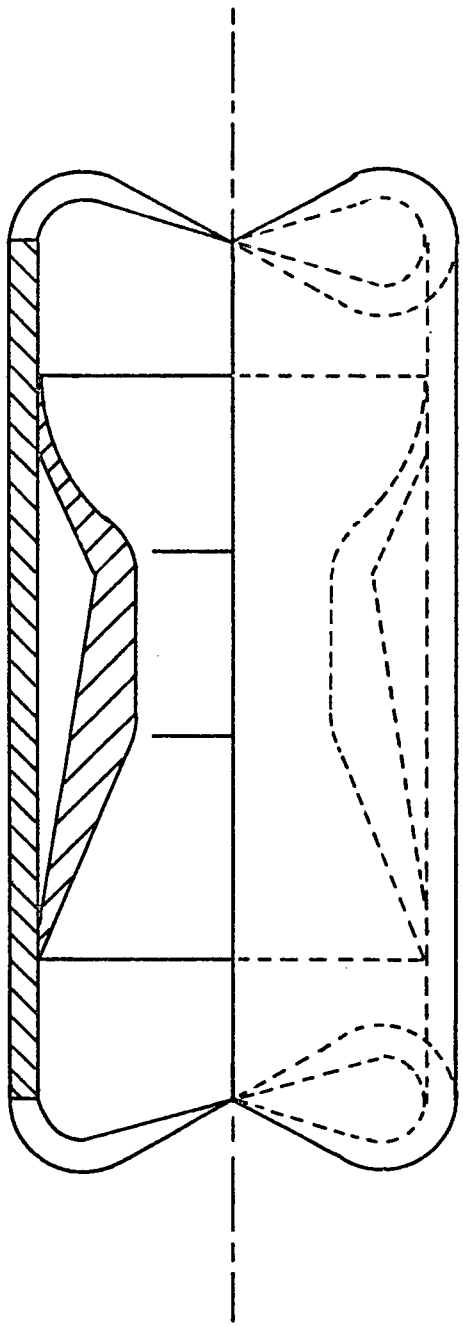

Figure 4 Teflon constriction for reducing bed volume

4.2 Solution Concentration Measurement

The solution concentration, c, and hence the supersaturation level, (c - c*) was found from measurements of the solution specific gravity at a known temperature, the relationship between solution specific gravity and concentration having previously been precisely determined (Appendix D.1). The crystallizer was equipped with a sensitive continuous recording specific gravity meter (Appendix B) which had a flow-through sampling chamber. The chamber was mounted in a short by-pass loop in which connections to and from the main crystallizer circuit were made by 250 mm lengths of 6 mm I.D. Teflon-lined tubing. A pressure drop to cause sufficient flow through the loop was induced by an orifice plate placed in the main circuit between the inlet and outlet ports of the loop. The orifice diameter was 5 mm for crystal sizes below 3 mm and 9 mm for crystal sizes above 3 mm. As the output of the specific gravity meter was sensitive to variations in the sampling chamber flow-rate (0.0001 S.G. per cm^3/s) this flow-rate was held constant at 10 cm^3/s by adjusting a conventional Teflon-barrel stop-cock mounted in the inlet tube to the sampling chamber. The sampling chamber flow-rate was measured by a small calibrated rotameter tube mounted in the outlet tube from the chamber.

The output of the specific gravity meter was a d.c. signal which was in the range 0-100 mV and which was almost linear with the solution specific gravity. For the small specific gravity ranges (0.02 S.G.) used in this work, the non-linearity was negligible. The sensitivity of the meter under the conditions of this work was approximately 0.00025 S.G./mV. The signal was recorded with a

conventional strip chart Recorder (Model 7101 B, Hewlett-Packard Co., Palo Alto, California) with an input impedance of 1 MΩ and fitted with a damping capacitor of1000 μF. This combination gave very rapid responses (full response to a step change of density within a few seconds) and had a final sensitivity of 0.0025 S.G./chart inch. Thus when readjusting the concentration after a change, any given concentration could be reproduced during the same day to within 0.0001 S.G. or, in terms of concentration, to within 0.01 wt% hexahydrate. However, day-to-day variations in the response of the meter to a solution of given concentration were typically 0.0001 S.G., so to achieve the highest precision and accuracy the main specific gravity measurements at the beginning and end of each main experiment (Section 5) were made with 25 cm^3 specific gravity bottles. Two bottles were used each time and the estimated pooled standard error from many pairs of measurements was 0.00004 S.G. The solution samples were drawn from a conventional Teflon-barrel stopcock in a T connection at the outlet of the meter sampling chamber. After the first 30 cm^3 had been discarded, the samples were allowed to flow directly into the bottles, which were held in a thermostatic water jacket surrounding the sampling chamber. The temperature of the jacket was held within 0.1°C of the temperature of the growth experiment. When sampling at the end of a growth experiment, the sampling jet was fitted with a piece of 38 μm stainless steel wire cloth to filter out any nuclei and a visual check of the bottles for absence of nuclei was always made immediately after they had been filled. This precaution was to ensure that the final specific gravity

measurements of the experiment were made on the clear solution rather than on a slurry containing nuclei as well as solution.

Despite the fact that the main specific gravity measurements were in the end made with specific gravity bottles, the meter was invaluable throughout the work as it permitted very rapid adjustment of concentration to within a small margin of any desired value: only then for the highest accuracy measurements were the bottles needed in the Batch Method (Section 5.4). Meanwhile in the Continuous Method (Section 5.5), although the meter was calibrated by bottle measurements of the initial and final specific gravities, the specific gravities prevailing during the run could be conveniently obtained only from the meter trace.

4.3 Flow-Rate Measurement and Control

The solution flow-rate was measured with an orifice meter, the pressure drop across which was registered in millimetres of the solution itself in an inverted glass manometer tube with air entrapped at the top. (A safety switch sensed the pressure of this air. If this pressure fell during unattended running, for such reasons as solution leakage or pump seizure, the switch cut off all power to the equipment.) The orifice was mounted between pipe sections of 25 mm I.D. and two orifice sizes were used, a 10 mm orifice when crystal sizes were below 3 mm and a 16 mm orifice when crystal sizes were above 3 mm.

Particularly because of the orifice's non-standard location, with an obstruction (the heat exchanger coil) upstream and a pipe bend

downstream, it was decided to perform a calibration. Since large volumes of liquid were needed, the nickel sulfate solution itself could not be used. Instead, after the experiments had been completed, the orifices were calibrated over the appropriate range of orifice Reynolds numbers (700-7000), using mains water. It was found that the coefficient of discharge was within the range 0.64 ± 0.01 throughout the range of flow-rates used. Literature values of the coefficient of discharge [78] are somewhat higher at the lower Reynolds numbers but these values are for orifices installed far from obstructions in the pipe.

The solution flow-rate was controlled by a straight-through glass valve (Q.V.F. Ltd.) of the globe type, in which a Teflon-sheathed plunger could be tightened down on to a seat. The valve was mounted in the circuit immediately on the outlet side of the pump. The valve offered perfectly satisfactory flow control except when large numbers of crystal nuclei (estimated total weight of nuclei greater than 100 g) were circulating with the solution (see Section 5.6), when there was a tendency for the flow to fall off as nuclei partially plugged the annular space between the valve's plunger and seat. Frequent re-adjustments of the flow-rate were then necessary.

4.4 Temperature Measurement and Control

The temperature of the solution in the crystallization section was measured by a sensitive mercury-in-glass thermometer. The thermometer was graduated from -1 to 101°C in divisions of 0.1°C. Each division had an actual length of 0.5 mm and as the readings were taken with a

four-power magnifier, the temperature could be read to 0.01°C. The thermometer was calibrated against a standard quartz thermometer (Model 2801 A, Hewlett Packard Co., Palo Alto, Calif.) to give a calibration error of not more than 0.03°C.

For heating the solution, the crystallizer was equipped with three separate 600 W mineral-insulated, copper-sheathed heating cables (Pyrotenax Ltd., Trenton, Ontario) wound directly on to the horizontal glass pipes, one on the upper pipe and two on the lower pipe. The cable on the upper pipe was simply used for rapid heating between runs while the two cables on the lower pipe, both equipped with variable transformers, were used respectively as the"maintenance" heater and "trimmer" heater of the temperature control system. The "maintenance" heater was adjusted to a steady wattage just insufficient to hold the required temperature and then the "trimmer" heater, switched by a temperature controller and usually adjusted to 50 W output, supplied the final control heating. The temperature controller itself (Appendix B) was a sensitive electronic controller of the "on-off" type, employing as a sensor a platinum resistance of base resistance one hundred ohms, and having a switching differential of 0.025°C.

The errors on the steady state temperature in the crystallization section, as measured by the main thermometer, were as follows. The difference between the mean temperature given by the thermometer and the reported set temperature was never more than 0.05°C. The half-wave amplitude of the sinusoidal variations in the instantaneous temperature, caused by the temperature control system, was never more than 0.07°C.

For cooling the solution, the crystallizer had a glass heat-exchanger section in which the solution flowed past a coil of glass tubing which carried water at 9°C from the mains supply.

4.5 The Thermostatic Water Jackets

Previous forms of the crystallizer had been operated with solutions having viscosities not greatly different from that of water. These were reported [13b] to give temperature differences between the ends of the crystallization section of only 0.05°C even at an operating temperature of 50°C. However the solutions used in the present work had viscosities several times that of water (Appendix D.2) and consequently the solution circulation rates necessary to fluidize the crystal bed were correspondingly smaller. Hence at 50°C, the temperature difference between the ends of the crystallization section was greater than 0.05°C, particularly along the wall. Therefore the crystallization section was fitted with a clear acrylic jacket (Plexiglas brand). Between the jacket and the glass pipe inside it was pumped water at a temperature within 0.2°C of the temperature of the crystallization experiment. With the jacket fitted, the temperature difference along the crystallization section fell to not more than 0.05°C. Because of the deep colour of nickel sulfate solutions, this temperature difference could not be measured directly by observing thermometers suspended inside the crystallization section. Instead, the following indirect method was used. With the temperature controller set at a value near 50°C, and the solution circulation rate at the maximum which the manometer could accommodate (about 180 cm^3/s), the mean temperature shown by the main

thermometer was noted. The circulation rate was then reduced to the lowest value that would be encountered (about 25 cm^3/s), all temperatures were allowed to re-equilibrate without the controller set temperature having been changed, and the main thermometer was then reread. At high circulation rates, the temperature difference along the crystallization section was negligible, as shown by the fact that for all high circulation rates, the main thermometer registered the same mean temperature. Therefore the difference between the mean temperature registered by the main thermometer at high circulation rates and the (higher) mean temperature registered by the thermometer at the minimum circulation rate gave the maximum temperature difference along the crystallization section.

The sampling chamber of the specific gravity meter was immersed in a well-stirred plastic tank containing water at a temperature within 0.1°C of the temperature of the growth experiment. This was intended to prevent nucleation and possible errors in the specific gravity measurements. Both could have been caused if the solution cooled as it passed through the sampling chamber.

Except briefly, when in use, the product crystal removal stopcock was also immersed in a similar well-stirred tank of water. This prevented the stopcock from seizing up by preventing crystallization in the film of solution between the ground surfaces of the stopcock and thus allowed the stopcock to be used without grease.

Finally, the flow-rate measuring manometer and its leads were also equipped with a jacket through which water was pumped.

Without a jacket, the solution in the manometer and leads, being essentially stagnant, would have been particularly susceptible to crystallization through excessive cooling.

Although not an integral part of the crystallizer itself, the sintered glass Buchner funnel which was used to collect the crystals on draining them from the crystallizer at the end of an experiment was also equipped with a thermostatic jacket. This prevented the cooling which would have caused unwanted further weight increases in the product crystals during their filtration prior to the final washing and rinsing operations (see Section 5.4.1).

4.6 Materials of Construction

Even parts per million of certain impurities can radically alter crystal growth [1b], so efforts were made to ensure that the crystallizer was highly inert to its contents. (The author visited an ammonium sulfate plant (Cominco Ltd., Trail, B.C.) having two large "Krystal" crystallizers in parallel. One crystallizer was of rubber-lined steel, the other of stainless steel. Thus both were supposedly relatively inert to their contents. Nevertheless from similar feed solutions, the stainless steel crystallizer produced crystals with flat faces and sharp edges while the rubber-lined crystallizer produced fully rounded "rice grain" crystals with no definite faces or edges.)

In the present crystallizer, all Q.V.F. parts were of the standard borosilicate glass and all other glass tubes, connections and so on were of Pyrex. Most wetted parts of the centrifugal pump were of Type 316 stainless steel, although the mechanical seal contained

minor parts of Teflon, ceramic and graphite. Both orifice plate assemblies were of Type 316 stainless steel. The sheath of the platinum resistance probe and the holder for the main thermometer were of Type 303 stainless steel. All gaskets were either Teflon-sheathed or of solid Teflon. The flexible tubing leading to the manometer and to the specific gravity meter sampling chamber was of Teflon. In the specific gravity meter itself, the plummet was gold-plated but its housing and the sampling chamber were both of epoxy resin, the composition of which is in Appendix B. All through its use the resin retained the smooth surface and high gloss it had shown when new so there was no indication that it was losing components into the solution.

All of the stopcocks in the crytallizer had Teflon barrels except the large product crystal removal stopcock, which had a glass barrel but which was kept immersed in a hot water jacket as described above (Section 4.5). Therefore all need for grease, a possible contaminant, was eliminated.

After the crystallizer had been assembled in its final form, but before the proper crystal growth experiments were begun, all parts of the crystallizer except the specific gravity meter sampling loop were cleaned by circulating sulfuric acid/dichromate mixture at 50°C for three hours.

5. THE EXPERIMENTAL METHODS FOR OVERALL CRYSTAL GROWTH AND DISSOLUTION RATES

5.1 Filling the Crystallizer

About 0.012 m^3 (12 ℓ) of solution were needed. Reagent specifications are given in Appendix C. The solutions were initially made up in a 0.020 m^3 (20 ℓ) Pyrex glass bottle and were preheated to about 20°C above their saturation temperature in a large pot containing water heated by electrical immersion heaters. Meanwhile the crystallizer was filled with distilled water which was circulated and heated to 60°C to preheat the crystallizer parts. Then this water was quickly drained out, the preheated solution was quickly poured in at the top and circulation was started again.

5.2 Running Conditions Between Experiments

Between experiments and overnight the solution was circulated at the maximum rate at a base temperature of 60°C, which for all the solutions used was well above the saturation temperature. All the thermostatic water jackets were also heated to 60°C. Thus any crystal nuclei and any stray crystals remaining from the previous experiment were completely redissolved (as indicated by a steady output signal from the specific gravity meter) before the next experiment was begun. With this technique the crystallizer could be run continuously for many weeks, even on solutions having saturation temperatures over 50°C. The crystallizer was shut down and the solution drained out only when maintenance was necessary. Inspection revealed no visible corrosion of the wetted stainless steel parts of the crystallizer at any time.

An estimated 50 cm^3 of solution was lost from the crystallizer per experiment, mainly through normal product crystal washing operations and inevitable leakage. This loss was made up with fresh solution poured in at the top. Thus although the crystallizer was run for long unbroken periods, this loss and make-up provided a useful purge of any impurities which might have been building up in the solution.

5.3 Preliminary Adjustments of the Concentration

When possible, necessary adjustments of the concentration of the solution in the crystallizer were made when the solution was still at 60°C, before it had been cooled to the actual temperature of the ensuing experiment, because mixing-in of added solution was more rapid at the higher temperature. A 10 mm diameter Teflon stirring rod was used to assist mixing in the calming section. Here again, the specific gravity meter was invaluable as it rapidly showed when mixing had been completed.

Stocks of solutions of concentrations up to saturation, for use in the adjustment of concentration, were held in a water bath at 60°C. All additions of solution were filtered through 38 μm stainless steel wire cloth on their way into the crystallizer. When gross increases or decreases in concentration were necessary, pure solid nickel sulfate or pure water were used respectively.

After adjustment of the concentration, the high-accuracy specific gravity measurements for the initial solution concentration of an experiment were usually taken (with 25 cm^3 specific gravity bottles) at 60°C, again for reasons of convenience, since, before

cooling, the solution was in an undersaturated state. However, in a few cases, to check the previously determined effect of temperature on solution specific gravity (Appendix D.1), another pair of measurements was made after the solution had been cooled to the temperature of the experiment, the solution then being in a supersaturated state. No significant difference was ever found between the concentrations derived from the specific gravity measurements at the two different temperatures.

5.4 The Batch Method

5.4.1 Crystal handling losses

In order to check that the weight change in the crystals observed during an experiment could be attributed solely to crystal growth or dissolution and not to other factors such as hold-up of crystals within the crystallizer, dummy runs were made as follows. A solution with its concentration accurately adjusted to a saturation temperature of 32°C was circulated within the crystallizer at 32°C. This temperature was used in order to minimize possible errors due to cooling: it was the lowest temperature at which the α-hexahydrate was the equilibrium solid form of nickel sulfate. Ten grams of crystals of size 425-500 μm (this was the smallest crystal size used and so was the most susceptible to hold-up within the crystallizer) were preheated for fifteen minutes in a bath at 32°C. The flow control valve was then completely closed and the crystals were quickly charged into the crystallizer, where they settled through the crystallization section and on to the product crystal removal stopcock. For 425-500 μm crystals this settling

took several minutes. During this time, although the solution circulation rate was zero, the thermostatic water jackets prevented cooling of the solution in the crystallization section and above the product crystal removal stopcock.

After 210 s, when no crystals could be seen still settling, the flow control valve was opened for a few seconds to give a burst of flow at the maximum rate and then closed once more. This burst of flow brought down a few more crystals (estimated maximum weight 50 mg) which had been held up in such places as piping joints, on the bulb of the main thermometer and on the sloping surface of the lower glass reducer. Then, sixty seconds after the burst of flow, when these crystals had joined the others on the product crystal removal stopcock, all the crystals were drained out through the cock, filtered of accompanying solution, washed quantitatively, rinsed and dried. Details of the washing and rinsing operations are given in Appendix E.

The weight of crystals charged and the weight of crystals recovered differed by not more than 25 mg. Corresponding tests on the larger crystal sizes produced still smaller weight differences. Thus there was no serious hold-up of crystals inside the crystallizer. The use of the burst of flow was retained during the tests on the larger crystal sizes, but in practice bursts never brought down a significant weight of crystals for sizes greater than 1.0 mm.

The sieving of the product crystals to determine their size distribution subsequently caused a weight loss not exceeding 20 mg. Thus the overall handling loss of crystals through all stages of the experiment did not exceed 45 mg.

5.4.2 End correction tests

Although the weight of crystals suffered no significant change due to hold-up (Section 5.4.1), the weight of crystals suffered considerable increases when the crystals were settled through a supersaturated solution, as at the beginning or end of a growth experiment by the Batch Method, because of crystal growth. Weight increases were also expected to occur during the time the majority of the crystals were delayed on the product crystal removal stopcock while the stragglers finished settling and again weight increases occurred during filtration of the supersaturated solution from the product crystals after drainage into the Buchner funnel assembly. The growth rates at which these weight increases were produced were expected to be very different from the growth rates prevailing during the main period of the experiment. Therefore these weight increases were treated as end effects. Corrections were made for them to the raw overall weight increase to give the weight increase occurring only during the steady period of the experiment, that is, after charging was complete and before final settling was begun. The corresponding growth time for the steady period alone was then taken as the time between (a) opening the flow control valve when the seed crystals had settled into position in the crystallization section after charging and (b) closing the flow control valve to allow the product crystals to begin settling on to the product crystal removal stopcock at the end of the experiment.

The magnitudes of the end corrections were found by performing dummy runs similar to those of Section 5.4.1 except that they were now performed with supersaturated solutions rather than with saturated solutions. Thus known weights of sized crystals were preheated and were

then settled through stagnant solutions which were at the appropriate temperatures. The crystals were removed for filtration, washing, rinsing, drying and re-weighing as soon as settling was complete. The crystals used in an end correction test had the same starting size as had the seed crystals used in the corresponding main experiment, so as to reproduce as nearly as possible in the end correction test the size changes occurring during that main experiment (see Section 5.4.3). Standard time delays (Table I) were used between the various stages of the tests such as the burst of flow and the draining of crystals into the Buchner funnel. These same delays were then used in the charging and withdrawing stages of the main Batch Method experiments themselves, in order to ensure the validity of the end corrections. Different delays were used with different crystal sizes. The overall duration of the end correction tests varied greatly with crystal size as most of the time for a test was needed for the crystal settling itself (see Table I).

Preliminary tests confirmed that for a given crystal size the magnitude of the end correction, as expected, was proportional to the weight of crystals settled. Therefore all end correction tests were performed with weights of crystals close to that mean weight of crystals which would occur during the batch growth experiments (that is, close to seven grams) and the end corrections were then expressed as weight increases per unit of the average weight occurring during the end correction test or growth experiment. For each temperature and crystal size considered, two replicate end correction tests were made at each of three different supersaturation levels. Fresh crystals were used for each end correction test. In all cases the curve of end correction

Table I Standard times in seconds between the various stages of the end correction tests and of the main experiments, in the Batch Method

For the end correction tests, t = 0 and the crystals settle straight through. For the main experiments, t is the duration in seconds of the steady period of the experiment

	Crystal size	0.5 mm	1 mm	2 mm	4 mm
	start clock				
	crystals enter solution	10	10	10	10
main experiments only	start flow	40	20	10	5
main experiments only	stop flow	t	t	t	t
	burst of flow	160	45	20	10
	remove water jacket from product valve and fit drip guard	60	30	15	10
	drain and begin washing	25	25	25	25
	total time between starting clock and draining	t + 295	t + 130	t + 80	t + 60

(per unit of average weight) against supersaturation could be fitted without statistically significant lack of fit by a straight line through the origin. These lines are given in Appendix L.1.

Exactly the same procedure was used to obtain end corrections for batch dissolution experiments except of course that in this case the solutions through which the crystals were settled were undersaturated. In the case of 0.5 mm crystals at 40°C only, the straight line fit through the origin gave some significant lack of fit. Therefore, in this case only, a quadratic fit through the origin was used instead. This curve then gave no significant lack of fit. The dissolution end correction curves are given in Appendix L.4.

5.4.3 The main procedure for growth experiments by the Batch Method

This procedure was based on that reported by Mullin and Garside [13b] for experiments on the growth of potassium alum. As discussed in Section 5.3, before cooling from 60°C to the temperature of the experiment, the solution concentration was first adjusted to the desired value and specific gravity measurements were made with 25 cm^3 bottles to determine this the initial concentration for the experiment. The solution and the water in the thermostatic jackets were then rapidly cooled to the temperature of the experiment and temperatures were allowed to stabilize at this new value with the solution circulation rate set at the value expected for the experiment: this depended on crystal size. The specific gravity meter was very useful here for indicating when the temperatures had fully re-stabilized. Meanwhile an accurately known weight (about five grams) of highly regular

seed crystals all within one size interval in the full U.S.A. Standard Sieve Series [79] was preheated for fifteen minutes at the temperature of the experiment. Preliminary tests had demonstrated that even the smallest crystals used (425-500 μm), with the largest specific surface, showed no dehydration when heated to the highest experimental temperature (50°C) for fifteen minutes. Details of the preparation of seed crystals are in Appendix G. The flow control valve was then fully closed and the preheated seed crystals were quickly charged into the top of the crystallizer. When they had settled into position in the crystallization section, the flow control valve was re-opened and the flow-rate adjusted to fluidize the crystals so that they were uniformly distributed throughout the crystallization section. The moment of re-opening of the valve was taken as the start of the crystal growth period for the corrected weight increase. Some instability of the temperature was inevitable after the valve was re-opened but this always decayed within about two minutes. Even during the instability, the mean temperature was close to the steady state mean value, as the instability was basically a damped oscillation.

Growth was continued until the total weight of crystals was about nine grams. The times needed for this amount of growth varied from about five minutes to several hours, depending on the growth conditions.

As the crystals grew, the solution circulation rate had to be increased slightly (by about 15%) to maintain uniform distribution of the crystals within the crystallization section. Slight readjustments of the specific gravity meter sampling loop stopcock were then also

necessary, to maintain the sampling loop flow-rate constant at 10 cm^3/s.

Because the bottom of the crystal bed was defined by the change in cross-section at the lower pipe reducer and because there was no grid at the bottom of the bed, the velocity profile across the bed was unlike that occurring in a conventional fluidized bed (which is approximately plug flow). Rather, there was a central core of fast-moving solution with a surrounding annulus of much slower-moving solution. This caused a circulation pattern of the crystals similar to that of a spouted bed. The central core contained only a few, fast-rising crystals. Most of the crystals remained in the annulus, falling slowly until they were caught in the core once more and thrown upwards. That this pattern differs from that in a conventional fluidized bed is not necessarily a disadvantage, as the crystal bed in an industrial "Krystal" crystallizer, which the present apparatus is intended to model, has the same lean and dense regions. The lean region occurs below the central downcomer through which feed solution enters the crystallizer and the dense region occurs where the solution rises in the annulus surrounding the downcomer.

In all experiments by the Batch Method, the supersaturation level was almost constant throughout an experiment. The calculated fall-off of supersaturation due only to loss of solute to the growing crystals (ignoring the effects of nucleation) was only about 0.02 wt% hexahydrate or 0.0002 in terms of specific gravity. For supersaturations below about 1.3 wt% hexahydrate, the observed fall-off agreed with the calculated and thus the percent fall-off in supersaturation ranged from 1.5% when the supersaturation was 1.3 wt% hexahydrate to a maximum of 15% when the supersaturation was 0.13 wt% hexahydrate, the

smallest value used. At supersaturations above 1.3 wt% hexahydrate, significant amounts of nucleation occurred, causing increases in the observed fall-off over the calculated fall-off. This was actually the main factor limiting the maximum supersaturation which could be used. As at the low end of the supersaturation range a limit of 15% was set on the allowable percent fall-off. This in turn proved to limit the maximum useable supersaturation to around 2.4 wt% hexahydrate (see Section 5.6). The supersaturation then reported for a given batch experiment was the arithmetic mean of the supersaturations found from the initial and final specific gravity measurements of that experiment.

Another consequence of the requirement that supersaturation not fall off substantially during a Batch Method experiment was the relatively low limit of five grams on the weight of seed crystals which could be used. This in turn meant that the void fraction of the fluidized bed of crystals was very high. When calculated directly from the overall bed volume and the volume occupied by the crystals themselves, the mean void fraction was 0.998, the same value of course applying to all batch experiments. However, lower void fractions, closer to the industrial levels, could be and in fact had to be used in the Continuous Method (Section 5.5).

After sufficient growth had occurred, the flow control valve was completely closed and the product crystals began to settle towards the product crystal removal stopcock. The moment of closing of the valve was taken as the end of the crystal growth period for the corrected weight increase. After allowing the standard settling

times both before and after the burst of flow (see Sections 5.4.1 and 5.4.2), the crystals were drained directly into a Buchner funnel assembly which was already under suction.

The Buchner funnel was of 600 cm^3 volume and had sintered glass of "coarse" grade (pore size range 40-60 μm). The funnel was equipped with a jacket through which circulated water at the temperature of the experiment. Suction was provided by a rotary vacuum pump. The funnel was mounted on a 2000 cm^3 collecting flask and was fitted with a glass extension tube 200 mm long and 90 mm O.D. which was connected to the funnel by a Teflon adapter piece. The extension tube prevented loss of crystals or solution by splashing during draining. Roughly 300 cm^3 of solution were drained into the funnel: this volume was sufficient to ensure that all product crystals were flushed through the product crystal removal stopcock. The suction took ten seconds to draw off all the solution in the funnel except that left coating the crystals. The funnel and extension tube were then quickly transferred to another collecting flask and the crystal washing and rinsing operations were performed immediately. Full details of these operations are in Appendix E.

Right after this, specific gravity measurements were taken for the final solution concentration of the experiment, the samples of solution being filtered of possible nuclei as discussed in Section 4.2. Solution circulation was then re-started and the water jackets and the solution in the crystallizer were re-heated to 60°C.

After a final drying, the product crystals were sieved by hand according to A.S.T.M. recommendations [80], to separate them from any nuclei which may have accompanied them from the crystallizer, and

to obtain their size distribution, which was in general a little wider than that of the seed crystals. The product crystal specific surface average size was then calculated (see Appendix H). Hand sieving was used because the crystals were relatively fragile and machine sieving was found to cause severe abrasion of their edges. All the sieving done in this work was done with the same set of previously unused sieves.

For any given temperature or crystal size, once one or two growth experiments had been made at different supersaturations, a close estimate could be made, by the extrapolation of growth rates, of the growth time necessary to reach the target product weight in subsequent experiments. The target product weight was such that nearly all the product crystals would fall within one size interval in the full U.S.A. Standard Sieve Series. If this condition was fulfilled, errors in the calculation of the mean product crystal size were minimized (see Appendix H). As indicated above, for nickel sulfate α-hexahydrate crystals the condition implied that a product weight close to nine grams should be grown from a seed weight close to five grams. The main product crystal size interval was then the next larger to the seed crystal size interval in the full U.S.A. Standard Sieve Series. Thus, for example, seed crystals of 850 μm - 1.00 mm would be grown until they were almost all 1.00 - 1.18 mm, a size increase of about 20%.

The smallest size of crystals which could be considered was 0.5 mm (that is: seed size range 425-500 μm, product size range approximately 500-600 μm) because for crystals smaller than this, the fluidization velocity and hence the solution circulation rate was too

small to allow satisfactory temperature control. Because these crystals, being small, had a high specific surface, only short growth times (a few minutes) were needed to achieve the weight increase from five grams to nine grams, while because of their small settling velocity, they gave long end correction test times and hence large end correction weight increases. Thus for high supersaturations the end correction weight increase became a considerable fraction of the main uncorrected weight increase. Therefore, because the end correction weight increases showed greater standard errors than did the weight increases from the main experiments, an arbitrary limit was set that the overall end correction weight increase should not exceed 20% of the overall uncorrected weight increase due to growth. Applying this limit to the growth of 0.5 mm crystals meant that no supersaturation above 1.0 wt% hexahydrate could be used.

In order to estimate the standard error of the weight increase from the main experiments, at least one pair of replicate growths at the same supersaturation was made for each temperature and crystal size considered.

5.4.4 The main procedure for dissolution experiments by the Batch Method

As far as possible, the procedure for dissolution experiments by the Batch Method was made the same as for growth experiments by the Batch Method. Thus approximately nine grams of seed crystals were dissolved down to approximately five grams of product crystals, so that both the average weight of crystals and the average crystal size during an experiment were close to those of the corresponding growth experiment.

The dissolution rate at a given dissolution driving force (c* - c) was several times the growth rate at a growth driving force (c - c*) of the same magnitude. Thus dissolution experiments lasted shorter times than the corresponding growth experiments, end correction weights were larger and the arbitrary limit mentioned in Section 5.4.3 that the overall end correction weight change should not exceed 20% of the uncorrected main weight change was used to define the maximum undersaturation which could be investigated. In the case of dissolution, where nucleation was of course absent, no reheating and recooling of the solution in the crystallizer was necessary between experiments. Inevitably some rounding of the edges of the crystals occurred during dissolution but the crystal shape was still well-defined at the end of a batch dissolution experiment.

A phenomenon observed during dissolution experiments which had not been observed during growth experiments was that of crystal cleavage. The tendency to cleave was more marked for larger crystals. Not more than an estimated 12% of the crystals were observed to cleave, usually symmetrically, along the (001) plane (see Figure J.1) during the main stage of an experiment. This was not expected to affect the overall crystal surface area greatly: besides, any small increase in the surface area due to cleavage would be offset by the slight decrease in the surface area due to rounding of edges.

A good deal more cleavage occurred during the product crystal draining and washing stages and again during the final sieving of the product crystals to determine their size distribution. Thus

the final total proportion of crystals which had cleaved was up to about 50% for the largest product crystals (size range approximately 3.35 - 4.00 mm) although it was much lower for all smaller crystals. Of course only the cleavage occurring during the actual dissolution stage could affect the overall crystal surface area available for dissolution. Microscopic inspection of the cleaved surfaces after an experiment was used to estimate the amount of cleavage occurring during the dissolution stage alone. When cleavage had occurred during the dissolution stage, the cleaved surfaces had lost their fine structure by dissolution and appeared "polished," while the edges bounding the cleaved surfaces had become rounded. When cleavage had occurred only after the dissolution stage, the cleaved surfaces retained their fine structure and therefore appeared somewhat rough, while the edges bounding the cleaved surfaces were still sharp.

When sieving to find the size distribution of a set of product crystals containing some cleaved crystals, the effects of cleavage were treated as follows. If a particular sieve size interval was found to contain only or almost only cleaved fragments then the weight of these fragments was considered to belong with the next larger size interval (which in all cases contained nearly all the uncleaved crystals), on the grounds that during the actual dissolution experiment most of these cleaved crystals were still in the form of whole crystals from this larger size interval. Unless a size interval contained only or almost only cleaved fragments, the weight in the interval was reported without any such adjustment.

5.5 The Continuous Method

5.5.1 Design of the experiments

This method was based on that reported by Bujac and Mullin [63] for experiments on the growth of ammonium alum. As with the Batch Method, the Continuous Method can be used for both growth and dissolution experiments. In applying the Batch Method for a given temperature and crystal size, a series of separate experiments was performed, each experiment at a different supersaturation, this supersaturation being held almost constant within each experiment. In the Continuous Method, in contrast, the supersaturation, initially at a high level, was permitted to fall by a large amount as the solution gave up solute to a large weight (several hundred grams) of growing crystals. This gross fall of supersaturation with time was continuously monitored with the specific gravity meter. Then, by equating instantaneous rates of reduction of the supersaturation (obtained from the meter trace) with instantaneous rates of growth on the seed crystals, growth rates for a whole range of supersaturations could be found from a single experiment. More details of the method of calculating growth rates from the meter trace are in Section 6.2.

While void fractions were necessarily high (around 0.998) in the Batch Method, they were necessarily much lower (around 0.80) in the Continuous Method. An advantage of this was then that in the Continuous Method, the fluidized bed of crystals more nearly represented the bed in a full-scale industrial fluidized-bed crystallizer, where operating void fractions are usually around 0.80 [81, 82].

The lower void fraction in the Continuous Method was a consequence of the very large weight of seed crystals (several hundred grams) which had to be used: only a very large weight of seed crystals could undergo the large weight increase necessary to absorb the gross reduction in solution supersaturation, without meanwhile suffering an excessive increase in size. In the present experiments the weight of seed crystals was so chosen that their size increase would be the same as that in the Batch Method experiments, that is from one size interval in the full U.S.A. Standard Sieve Series to the next larger one. This was intended to make comparison of results from the two methods more valid, for the average crystal size during an experiment by the Continuous Method was then close to that during any one experiment by the Batch Method. However, the equivalence of results from the two methods was not exact, as can most easily be seen by considering the following example. In all of the Batch Method growth experiments at average crystal size 1 mm, whatever the supersaturation, the seed crystals were of size 850 μm - 1.00 mm and the product crystals were of size approximately 1.00 - 1.18 mm. However in the corresponding experiment by the Continuous Method, the crystals were of size 850 μm - 1.00 mm at the initial (high) supersaturation, and gradually increased to size approximately 1.00 - 1.18 mm at the final (low) supersaturation. Therefore each of the growth rates calculated for different supersaturations in the Continuous Method strictly applied to a slightly different crystal size. As it happened, the growth rate was found to depend only weakly on crystal size (Section 7.1.2), so this was not a serious source of error.

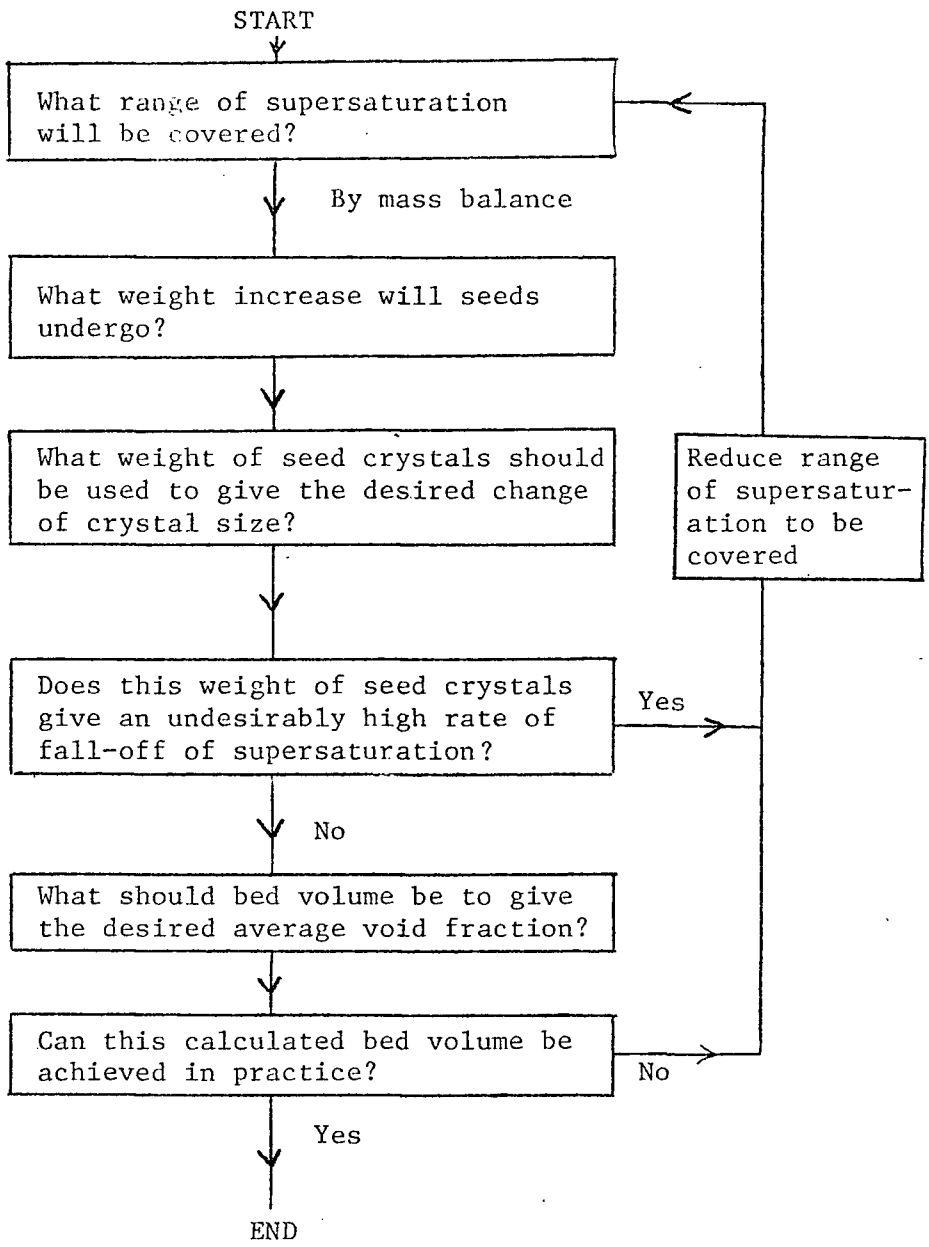

Figure 5 Chart for design of experiments by the Continuous Method

Once the weight of seed crystals had been chosen, the bed volume was adjusted by the use of the moveable Teflon constriction (Section 4.1) so as to give an average calculated void fraction during the experiment of 0.80. (The initial calculated void fraction was 0.85 and the final calculated void fraction was 0.75.) The value of 0.80 was used so as to approximate the voidage conditions in an industrial fluidized-bed crystallizer.

The mass balances on which the Continuous Method was based assumed that all solute lost from the supersaturated solution was transferred to the seed crystals as crystal growth. Thus no significant nucleation could be tolerated in growth experiments by the Continuous Method. This meant that the maximum useable supersaturation for growth by the Continuous Method was well below that for the Batch Method (in which considerable nucleation could be tolerated), particularly as the amount of nucleation occurring at a given supersaturation was observed to depend on the weight of seed crystals added (perhaps because nucleation occurred by the "initial breeding" mechanism; see Section 5.6) and the weight of seed crystals used in the Continuous Method was over sixty times the weight used in the Batch Method. All seed crystals used in growth by the Continuous Method were, before use, treated for the removal of crystal dust from their surfaces (see Appendix F) but even so, crystal growth without significant accompanying nucleation could not be achieved in the Continuous Method at supersaturations above about 1.3 wt% hexahydrate.

A supersaturation of 1.30 wt% (representing a supercooling of about 4°C) was therefore chosen as the starting supersaturation for a

growth experiment by the Continuous Method at 40°C with an average crystal size of 1 mm. The amount of growth which would have been produced if this supersaturation had been allowed to fall to zero in one stage would have been unacceptably large: to observe the limit stated above on the increase of crystal size during an experiment, such a large weight of seed crystals would have been needed that the void fraction, even with the bed volume at a maximum, would have been well below 0.80. Also, with such a large weight of seed crystals, the rate of fall-off of supersaturation would have been undesirably high. Therefore the supersaturation range was covered in two separate experiments, both of which were duplicated. In the first experiment, supersaturation was allowed to fall from a starting value of 1.30 wt% hexahydrate to a final value of around 0.67 wt% hexahydrate, while in the second experiment it fell from a starting value of 0.67 wt% hexahydrate to a final value close to zero. Both experiments used 320 g of seed crystals and a bed volume of 1080 cm^3 (adjusted with the Teflon constriction). These appropriate values of seed crystal weight and bed volume were calculated as explained above (see also Figure 5).

5.5.2 The experimental procedure

In most aspects the procedure for experiments by the Continuous Method was the same as that for experiments by the Batch Method. Thus the solution concentration was adjusted and measured at 60°C, the solution was then cooled to the temperature of the experiment and after temperatures had re-stabilized, the preheated seed crystals were added.

Because of the lower void fraction, however, the solution flow-rate to fluidize the crystals uniformly throughout the bed volume was somewhat less (by about 10%) than for the Batch Method. Also, in the Continuous Method, the overall solution volume must be accurately known, for use in the mass balance calculation for the growth rates. In the present experiments the solution volume was found directly from a prior calibration of the crystallizer volume. Alternatively it can be calculated from the overall weight increase on the seed crystals, by mass balance [63].

When the supersaturation had fallen to the desired end value, as estimated from the specific gravity meter trace, the solution circulation was stopped and the bottle specific gravity samples for the final supersaturation were quickly taken. Then the product crystals were drained out, washed, rinsed and dried by the usual method (Appendix E).

Because of the finite volume (350 cm^3 when assembled) of the specific gravity meter sampling chamber, there was a lag in the sampling system. Thus at a given time the solution in the sampling chamber did not have exactly the same concentration as did the solution in the main body of the crystallizer at that same time. Instead it had the concentration which had been present in the main body of the crystallizer a short time beforehand. The sampling chamber was assumed to behave as if well-stirred, an assumption which had been verified by Bujac and Mullin [63]. The concentration in the sampling chamber ($\bar{c}$) and the concentration in the main stream at the same

time (c) could then be related (Section 6.2).

To minimize the lag in the sampling system, the flow-rate through the sampling loop was kept as high as possible. In practice a constant flow-rate of 10 cm^3/s was used, giving a mean residence time in the sampling chamber of 35 s. When higher flow-rates were tried, there was a significant level of electrical noise on the specific gravity meter output trace.

Of course the trace from the specific gravity meter referred to the sampling chamber concentration, $\bar{c}$, and so did the calibrating specific gravity measurements, because the stopcock used for the specific gravity samples was located directly at the outlet of the meter sampling chamber. Thus the variation of c with time had to be calculated from the observed variation of $\bar{c}$ with time before the main calculation of the growth rate could be made. For all experiments by the Batch Method, the lag ($\bar{c}$ - c) was negligible for all times. Even for experiments by the Continuous Method, ($\bar{c}$ - c) was never larger than 0.02 wt% hexahydrate.

Because in the present work the overall solution volume was found directly, the overall weight increase on the seed crystals was available for an independent mass balance check on the experiment. Thus the calculated total weight of solute lost by the supersaturated solution was obtained from the solution volume and the known initial and final supersaturations. This was then compared with the observed weight increase on the seed crystals. In the present work, because of the large weight of product crystals, a few grams of them were inevitably left in the crystallizer when draining out the product

crystals. Also no check was made that the washing operation was exactly quantitative for such a large weight of product crystals. Nevertheless, the calculated and observed values of the weight transferred from solution to seed crystals never differed by more than 3%.

5.6 Nucleation during Crystal Growth Experiments

In the present work, nucleation was considered only as a nuisance, and was studied only to the extent necessary to be able to minimize its effects. Theoretical work on nucleation by most mechanisms [1b, 3] predicts that below some critical range of supersaturation (the "metastable limit") the rate of nucleation is small, but that it increases very rapidly as soon as supersaturations increase above the critical range. Many factors influence the value of this critical supersaturation, but the main one is the presence or absence of seed crystals: the critical supersaturation is much lower when seed crystals are present in the solution then it is when the solution is unseeded.

Observations during the present experiments generally upheld the predicted behaviour, but the value of the critical supersaturation in the presence of seed crystals appeared in addition to depend greatly on the properties of the seed crystals themselves. It was believed that the main factor here was the amount of crystal dust (microscopic crystal fragments) present on the surfaces of the seed crystals. The surfaces of the seed crystals could never be completely free of crystal dust, while any sieving operation on the seed crystals greatly increased the amount of surface crystal dust.

Thus with seed crystals which had not been sieved before use, the critical supersaturation was estimated from tests to be 2.0 wt% hexahydrate, while with seed crystals which had been sieved before use it was about 1.3 wt% hexahydrate. This difference indicates that nucleation by the "initial breeding" mechanism [3] was important.

Where necessary, to reduce the amount of nucleation, the seed crystals were treated before use (but after all sieving) for removal of much of their surface dust by settling them through a saturated solution. More details of this procedure are in Appendix F.

Of course the absolute amount of nucleation occurring during an experiment depended not only on the value of the critical supersaturation, but also on the duration of the experiment and on the weight of seed crystals used. Thus in the Batch Method supersaturations of over 2 wt% hexahydrate could be used with the smaller crystals without treatment for surface dust removal, as, with their larger specific surface, they required shorter growth times, while in order to use supersaturations up to 2 wt% hexahydrate with the larger crystals requiring longer growth times, surface dust removal was necessary. Meanwhile in the Continuous Method with its very large weights of seed crystals, long experiments and, unlike the Batch Method, an inability to tolerate much nucleation at all, surface dust removal was highly necessary for supersaturations above 0.7 wt% hexahydrate. In fact, as a precaution, all seed crystals used in the Continuous Method, regardless of the supersaturation range they were intended for, were treated for the removal of surface crystal dust.

6. DATA HANDLING

6.1 Calculation of Growth or Dissolution Rates from the Batch Method

The following procedure, based on that reported by Garside [83], is discussed in terms of growth rates, but an analogous procedure was used for dissolution rates.

Having found the raw weight increase undergone by the seed crystals during the experiment, the first step towards calculating the growth rate was to apply the end corrections which had been obtained as explained in Section 5.4.2. The end corrections were expressed as the weight increases during charging and withdrawing, per unit of the average weight of crystals occurring during the experiment. This average weight was taken to be the arithmetic average of the weight of seed crystals and the uncorrected weight of product crystals. This uncorrected average weight exactly equalled the true average weight occurring during the steady period of the experiment only if the total end correction weight increase resulted from equal increases during charging and during withdrawing. From physical considerations, the contributions to the total end correction from charging and from withdrawing should have been of the same order. Besides, the end correction was never more than 20% of the uncorrected weight increase, so the errors in the calculation of the average weight could never be large.

The total end correction was thus found and hence the corrected weight increase occurring only during the steady period of the experiment. The duration of the steady period was known, so the

corrected weight increase per unit time was then found. This had to be divided by the average overall crystal surface area, to give the growth rate as a mass flux. The method of calculating the overall surface area of a known weight of particles having a regular shape and known size distribution is given in Appendix H. This method was used to find both the seed crystal and product crystal overall surface areas. As above, the uncorrected final weight was used, in the case of the product crystals. The average overall crystal surface area was then taken as the arithmetic average of the initial and final overall surface areas and the crystal growth rate was thus found. The procedure discussed here is illustrated by a sample calculation in Appendix K.1.

6.2 Calculation of Growth or Dissolution Rates from the Continuous Method

The following procedure, based on that reported by Bujac and Mullin [63], is discussed in terms of growth rates, but an analogous procedure would be used for dissolution rates. In the present work, the Continuous Method was only applied to growth of 1 mm crystals at 40°C.

The basic data from the Continuous Method were recorder traces giving the specific gravity of the solution in the sampling chamber of the specific gravity meter as a function of time. Points were picked from these traces and, using a table of specific gravity against concentration (Appendix D.1), the concentrations $\bar{c}$ of the solution in the sampling chamber at different times after starting were found. For each of the two supersaturation ranges used, duplicate experiments were made. The values of $\bar{c}$ at a given time from the duplicate experiments

never differed by more than 0.01 wt% hexahydrate. By least squares fitting, the average concentrations from the duplicates were represented by a polynomial function of time, of the lowest order which gave no significant lack of fit. These concentrations $\bar{c}$ differed slightly from the main-stream concentrations c at the same times, because of lag due to the finite volume of the sampling chamber. The chamber was assumed to be well-stirred. This assumption was verified experimentally by Bujac [47] for calculated residence times of one or two minutes. In the present work, the residence time found directly from the known constant sampling loop flow-rate was 35 s, so the assumption is even more justified here. By mass balance [63], $\bar{c}$ is then related to c by

$$c = \bar{c} + \tau \left(\frac{d\bar{c}}{dt} \right) \tag{44}$$

We thus obtain the main-stream concentration c as a function of time. In the present work, the lag $(\bar{c} - c)$ in fact never exceeded 0.02 wt% hexahydrate. We now perform an instantaneous mass balance on the contents of the crystallizer [63]. Assuming no nucleation, all solute lost by the solution is gained by the seed crystals:

$$dW = -W_s \cdot d\hat{c} \tag{45}$$

where W is the instantaneous total weight of crystals, W_s is the total weight of water (a constant for each experiment) and $\hat{c}$ is the solution concentration, now expressed as kilograms of hexahydrate per kilogram of water. The instantaneous growth rate r is given by

$$r = \frac{1}{A} \cdot \frac{dW}{dt} \tag{46}$$

where A is the instantaneous overall crystal surface area. Thus

$$r = -\frac{W_s}{A} \cdot \frac{d\hat{c}}{dt} \tag{47}$$

To find A, we use

$$\frac{A}{A_0} = \left(\frac{W}{W_0} \right)^{2/3} \tag{48}$$

where subscript zero denotes the starting value. In this expression it is assumed that crystal shape is independent of size. This is a good assumption with nickel sulfate α-hexahydrate crystals (Table J.I). The initial overall surface area of the crystals is given by

$$A_0 = \left(\frac{F}{\rho_c \cdot L_0} \right) \cdot W_0 \tag{49}$$

(see Appendix H) and, by cumulative mass balance, the instantaneous total crystal weight is given by

$$W = W_0 - W_s (\hat{c} - \hat{c}_0) \tag{50}$$

A computer was used to perform these calculations. Using time t as a dummy variable, growth rates at a series of different supersaturations were found. As discussed in Section 5.5.2, W_s was found directly from a calibration of the crystallizer volume and from the known initial

solution concentration. The procedure discussed above is illustrated by a sample calculation in Appendix K.2.

6.3 Calculation of Other Experimental Variables

In a fluidized bed, the true solution velocity seen by the crystals is the interstitial solution velocity, V. This is related to the superficial velocity (or "empty-tube velocity"), V_s, by

$$V = \frac{V_s}{\varepsilon} \tag{51}$$

In the present work, for both Batch and Continuous Methods, V_s was calculated from the flow-rates found from the orifice meter, assuming plug flow in the crystallization section. The reported value of V_s was the arithmetic average of the initial and final values. The void fraction ε was calculated directly from the average volume of crystals during an experiment and from the calculated bed volume. This gave a value of $\varepsilon = 0.998$ for all experiments by the Batch Method, so for this method the differences between V_s and V were in fact negligible (Table II). In this work, for a given crystal size, V_s and V appeared to be independent of temperature. Because the true velocity distribution across the crystallization section was far from plug flow (Section 5.4.3), the calculated value of V was not expected to equal but only to be proportional to the true average velocity seen by the crystals, but since this true average was difficult to find, use of the calculated value of V was retained. Values of V and of single crystal terminal velocities V_t (Appendix D.4) as functions of crystal size

Table II Solution velocities, void fractions and crystal Reynolds numbers corresponding to different crystal sizes

	average crystal size L [mm]	average superficial solution velocity, V_s, from orifice meter [mm/s]	average void fraction ε [dimension-less]	average interstitial solution velocity V [mm/s]	approximate crystal Reynolds number $\frac{V \cdot L}{\nu}$ [dimension-less]
Batch Method	0.51	12.1	0.998	12.1	1.5
	1.01	29.4	0.998	29.5	7.1
	2.03	68.9	0.998	69.0	33
	4.03	130	0.998	130	125
Continuous Method	1.01	26.5	0.80	33.1	8.0

at 40°C are plotted in Figure D.1.

Other workers have used different methods to find both V and ε. Mullin and Garside [13b] found V_s as in the present study, but then used the Richardson-Zaki [84] equation, with measured single crystal terminal velocities V_t, to calculate ε and hence V. This method gave much lower values of ε (around 0.95), but the Richardson-Zaki equation is not strictly valid when, as in this study, there is particle circulation in the bed. Gaska [59] calculated the void fraction directly, as here, but used measured single crystal terminal velocities V_t as values of V in the Batch Method. At void fractions close to unity, the differences between V, V_s and V_t are all small.

Bujac [47] used the Richardson-Zaki equation to estimate the differences of interstitial velocity in beds of particles of the same size but with different void fractions. He calculated that the interstitial velocity was reduced by 20% when the void fraction was reduced from 0.995 in the Batch Method to 0.90 in the Continuous Method, remarking that differences of technique in the two methods may mask any effect of this velocity difference. In the present work, the observed superficial velocity was reduced by only 10% when the void fraction was reduced from 0.998 in the Batch Method to 0.80 in the Continuous Method. This is a much smaller reduction than that predicted by Richardson and Zaki. Again, the difference may be due to the circulation occurring in these beds. The difference in the calculated interstitial velocities for the two methods used in this work is then only about 12% (see Table II). Also shown in Table II are the approximate crystal Reynolds numbers, based on the interstitial velocities.

The reported crystal size during an experiment was the arithmetic average of the initial and final values of the specific surface average size. The variation of this reported size between experiments within a series in the Batch Method was always small (see Appendix L.2 and L.5). The variation was also small between corresponding series of growth and dissolution experiments.

Supersaturations were expressed as actual concentration minus saturation concentration and undersaturations as saturation concentration minus actual concentration. Saturation concentrations had previously been precisely determined (Appendix D.3). In the Batch Method, the reported supersaturation or undersaturation was the arithmetic average of the initial and final values.

7. THE EXPERIMENTAL RESULTS

7.1 The Crystal Growth Rates

7.1.1 General results from Batch and Continuous Methods

The growth rates found by the Batch Method for different crystal sizes at 40°C and for different temperatures at a crystal size of 1.01 mm are plotted as functions of supersaturation in Figures 6 and 7 respectively. The rates are fully tabulated in Appendix L.2. All the growth rates measured in this work are strictly growth rates averaged over the different types of face present on the crystal: strictly, each type of face grows at a different rate, but these different rates on the different types of face cannot be separately determined solely from overall weight increases of the crystal. With nickel sulfate α-hexahydrate, there is evidence (Appendix J) that in fact the differences in the growth rates on the different types of face are not great.

The estimated absolute standard error (estimated standard deviation of the sample mean) on the supersaturations was constant at 0.007 wt% hexahydrate. The estimated percentage standard error on the growth rates was constant within each series of experiments at a given temperature and crystal size, but was different for different series, ranging from 1.1% to 2.2%. Replicate experiments were made to estimate the standard error of the crystal weight change itself, but in most cases, the major contribution to the standard error of the growth rates was from the standard error of the calculated overall

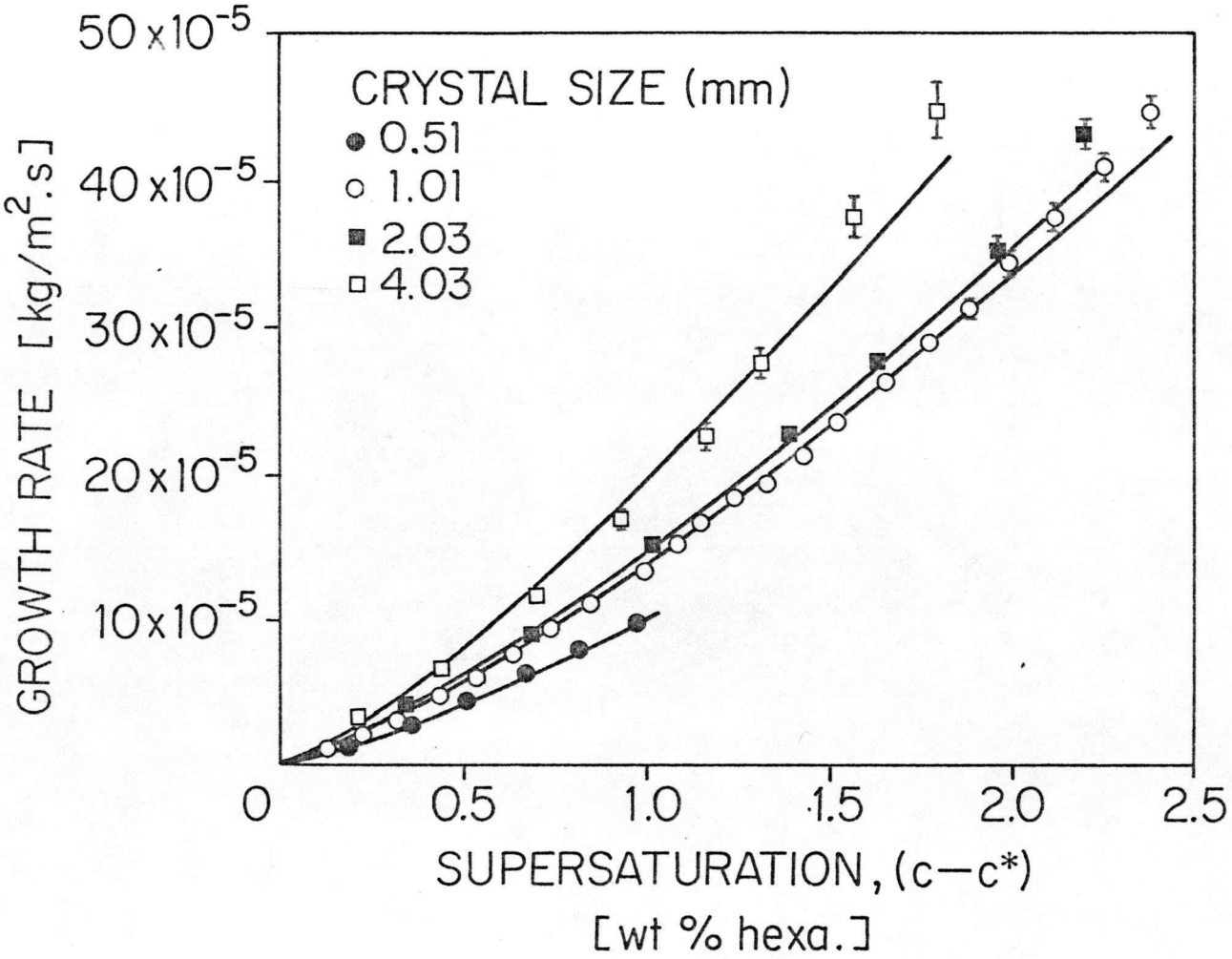

Figure 6 Growth rates by Batch Method of different sized nickel sulfate α-hexahydrate crystals at 40°C. Bars show the 95% confidence limits when these extend beyond the point symbols

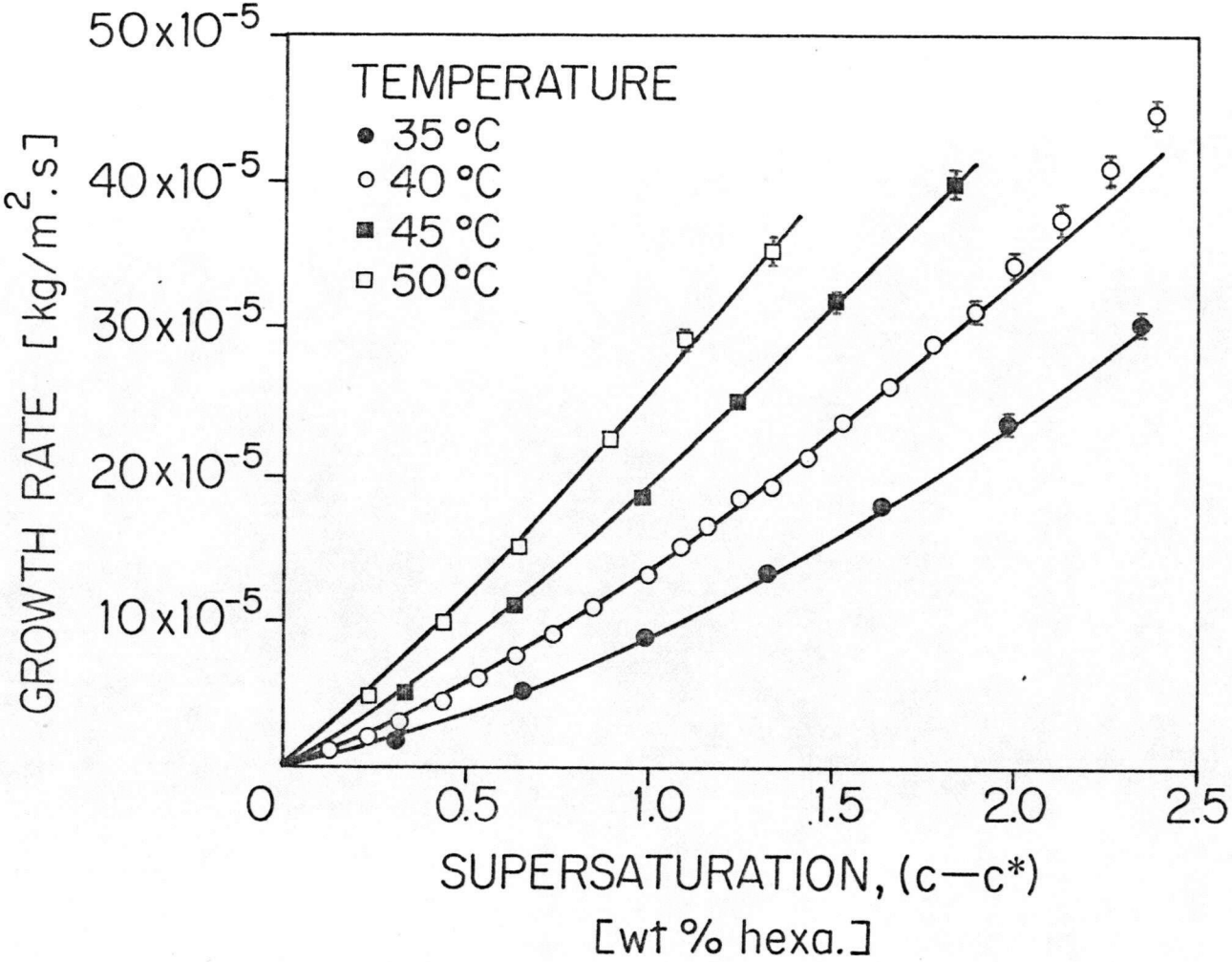

Figure 7 Growth rates by Batch Method of 1.01 mm nickel sulfate α-hexahydrate crystals at different temperatures. Bars show the 95% confidence limits when these extend beyond the point symbols

surface-volume shape factor, due to the variations of L_1/L and L_2/L (Appendix J) between individual crystals.

In the present work, the Continuous Method was only applied to growth and only at a temperature of 40°C and for a crystal size of 1.01 mm. In separate experiments, the supersaturation ranges 0.00 - 0.67 and 0.67 - 1.30 wt% hexahydrate were covered, duplicate experiments being made for each range. The resulting curves of growth rate against supersaturation are shown in Figure 8 and are also tabulated in Appendix L.3. The estimated percentage standard error of the growth rates was 1.1%, the major contribution again being from the calculated overall surface-volume shape factor. For comparison, results from the Batch Method for 1.01 mm crystals at 40°C are also shown in Figure 8. The agreement is good over the range of supersaturation 0.00 - 0.67 wt% hexahydrate, but over the range 0.67 - 1.30 wt% hexahydrate, the results from the Continuous Method are about 15% lower than those from the Batch Method.

The reason for this difference is uncertain. Nucleation can be ruled out as a cause: hardly any nucleation was observed and, besides, nucleation would increase the rates of fall-off of supersaturation and hence apparently increase rather than decrease the growth rates. Another factor is that the true (interstitial) solution velocities past crystals of a given size are somewhat different in the two different methods, because the interstitial solution velocity varies with the void fraction, as discussed in Section 6.3. However if this were the cause of the observed differences in the results from the two methods, it would be expected to affect not one but both of

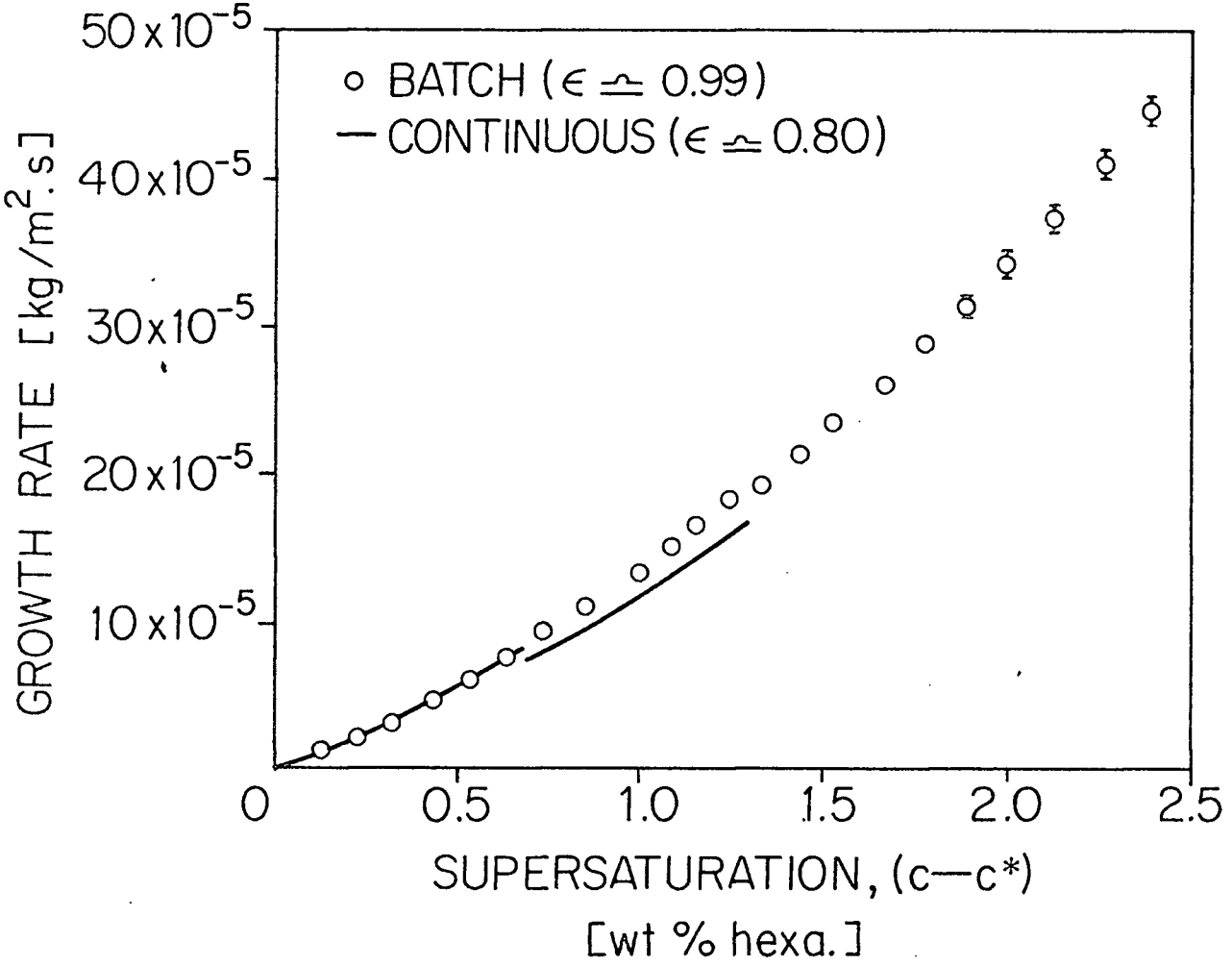

Figure 8 Growth rates of 1.01 mm nickel sulfate α-hexahydrate crystals at 40°C by the Batch and Continuous Methods. Bars show the 95% confidence limits when these extend beyond the point symbols

the ranges of supersaturation used in the Continuous Method. With higher supersaturations, the growth rates are higher and hence the rates of fall-off of supersaturation are higher. The calculation of these rates of fall-off from the recorder trace is expected to be more susceptible to error for the higher rates of fall-off. This would explain why a difference from the Batch Method is observed with the higher supersaturation range but not with the lower one.

All the (1 mm) seed crystals used in the Continuous Method had been previously treated for the removal of surface dust (Appendix F), to reduce the likelihood of nucleation during the experiments, while none of the 1 mm crystals used in the Batch Method were so treated. The agreement between results from the two methods (good, for the low supersaturation range; fair, for the higher supersaturation range) therefore helps to verify that the dust removal treatment did not otherwise affect the seed crystals.

There has been criticism [85, 86] of the methods used in this work to the effect that large undetected changes in the effective overall crystal surface area may be occurring at the beginning of a growth experiment, because of the "healing" of imperfections in the surface or the presence of crystal dust on the surface. These changes would then cause large errors in the calculated growth rates. However, when end corrections are made in the Batch Method, as has been done in this work, any such changes in the surface area should be at least partly absorbed in the end corrections. Also, the agreement between results from the Batch Method and the Continuous Method, in which latter

no such changes of surface area can occur except at the very beginning of an experiment, is evidence that errors from such causes are not great.

Curves of the empirical form

$$r = K \cdot (c - c^*)^N \qquad (8)$$

were fitted to the Batch Method growth rate measurements as follows. Logarithms were taken of both growth rates and supersaturations. In this form, the absolute estimated standard errors on the growth rates were constant within each series, so unweighted linear least squares fits were performed on these logarithmic values. In most cases these fits gave no statistically significant lack of fit. The slope of the linear fit directly gave N, together with its estimated standard error and the intercept of the linear fit gave log K together with the estimated standard error of log K. From these, K and the estimated standard error of K were calculated. These values of K and N are given in Tables III and IV, and the fitted lines are shown in Figures 6 and 7.

7.1.2 The effects of solution velocity and crystal size on the growth rate

As has been discussed in Section 2.2.4, the most general way of expressing the dependence of the overall growth rate constant K on solution velocity V and crystal size L is in the form of a pseudo-mass

Table III Best fit parameters of Equation (8) for growth of crystals of different sizes at 40°C

mean crystal size [mm]	K [$kg/m^2 \cdot s \cdot (wt\%\ hexa.)^N$]	estimated absolute standard error of K	N [dimensionless]	estimated absolute standard error of N
0.51	10.07×10^{-5}	0.11×10^{-5}	1.267	0.013
1.01	13.68×10^{-5}	0.11×10^{-5}	1.282	0.011
2.03	14.93×10^{-5}	0.26×10^{-5}	1.245	0.029
4.03	19.54×10^{-5}	0.61×10^{-5}	1.232	0.047

Table IV Best fit parameters of Equation (8) for growth of crystals of size 1.01 mm at different temperatures

temperature [deg C]	K [$kg/m^2 \cdot s \cdot (wt\%\ hexa.)^N$]	estimated absolute standard error of K	N [dimensionless]	estimated absolute standard error of N
35.00	9.02×10^{-5}	0.05×10^{-5}	1.390	0.009
40.00	13.68×10^{-5}	0.11×10^{-5}	1.282	0.011
45.00	19.10×10^{-5}	0.07×10^{-5}	1.216	0.007
50.00	25.41×10^{-5}	0.17×10^{-5}	1.155	0.011

transfer correlation such as Expression (25), which, for convenience, is restated here:

$$Sh' \left(= \frac{K \cdot L}{D}\right) \propto (Re)^{\beta'} \cdot (Sc)^{\alpha'} \qquad (25)$$

This expression is valid when, as in this work, Sh' is one or two orders of magnitude greater than unity. In fluidized beds at constant temperature and constant void fraction only, when V is related to L by

$$V \propto L^{a} \qquad (21)$$

the simplified expression

$$K \propto L^{b'} \qquad (24)$$

is also valid.

When attempting to apply Expression (24) or Expression (25) in order to find the value of b' or of β', a problem arises if the value of N is different at different values of L. When this is so, the dimensions of K, $kg/m^2 \cdot s \cdot (wt\%\ hexa)^N$, are different for different values of L and it is therefore of doubtful meaning to plot log K directly against log L. In the present work the differences in the values of N at different values of L (Table III) were not statistically significant, so the arithmetic average value of N

was found (1.257) and the growth rate curve-fits for different crystal sizes at 40°C were re-determined all with this fixed value of N. This gave the values of K shown in Table V. These values were numerically close to the previous values of K (Table III) but, unlike them, were all of the same dimensions, $kg/m^2 \cdot s \cdot (wt\%\ hexa)^{1.257}$, and thus their logarithms could be plotted against the logarithms of the values of L. When this was done, and a straight line fit made (Figure 9), the resulting value of b' for nickel sulfate α-hexahydrate at 40°C was 0.31, with an estimated standard error of 0.05. Values of b' found by other workers are given in Section 2.2.4, and the expected range for b' is discussed in Section 7.3.1.

In order to present the direct dependences of K on solution velocity and on crystal size fully in the form of Expression (25), suitable diffusion coefficient data are needed so that the Schmidt number can be calculated. In the present case such data were not available: the only diffusion coefficient measurements for nickel sulfate solutions which could be traced were those by Oholm [87], but these were at 20°C and for low concentrations, and extrapolation to other temperatures and concentrations is dangerous [88]. Nevertheless, the exponent β' can still be found, by plotting log (K • L) against log (V • L) at constant temperature. When this was done, using the dimensionally consistent values of K from Table V, and a straight line fit made (Figure 10), the resulting value of β' for nickel sulfate α-hexahydrate at 40°C was 0.61, with an estimated standard error of 0.03.

Table V Values of K for different crystal sizes at 40°C when growth rate curves were refitted using N = 1.257 for all crystal sizes

mean crystal size [mm]	K [$kg/m^2 \cdot s \cdot (wt\%\ hexa.)^{1.257}$]
0.51	10.04×10^{-5}
1.01	14.14×10^{-5}
2.03	15.10×10^{-5}
4.03	20.22×10^{-5}

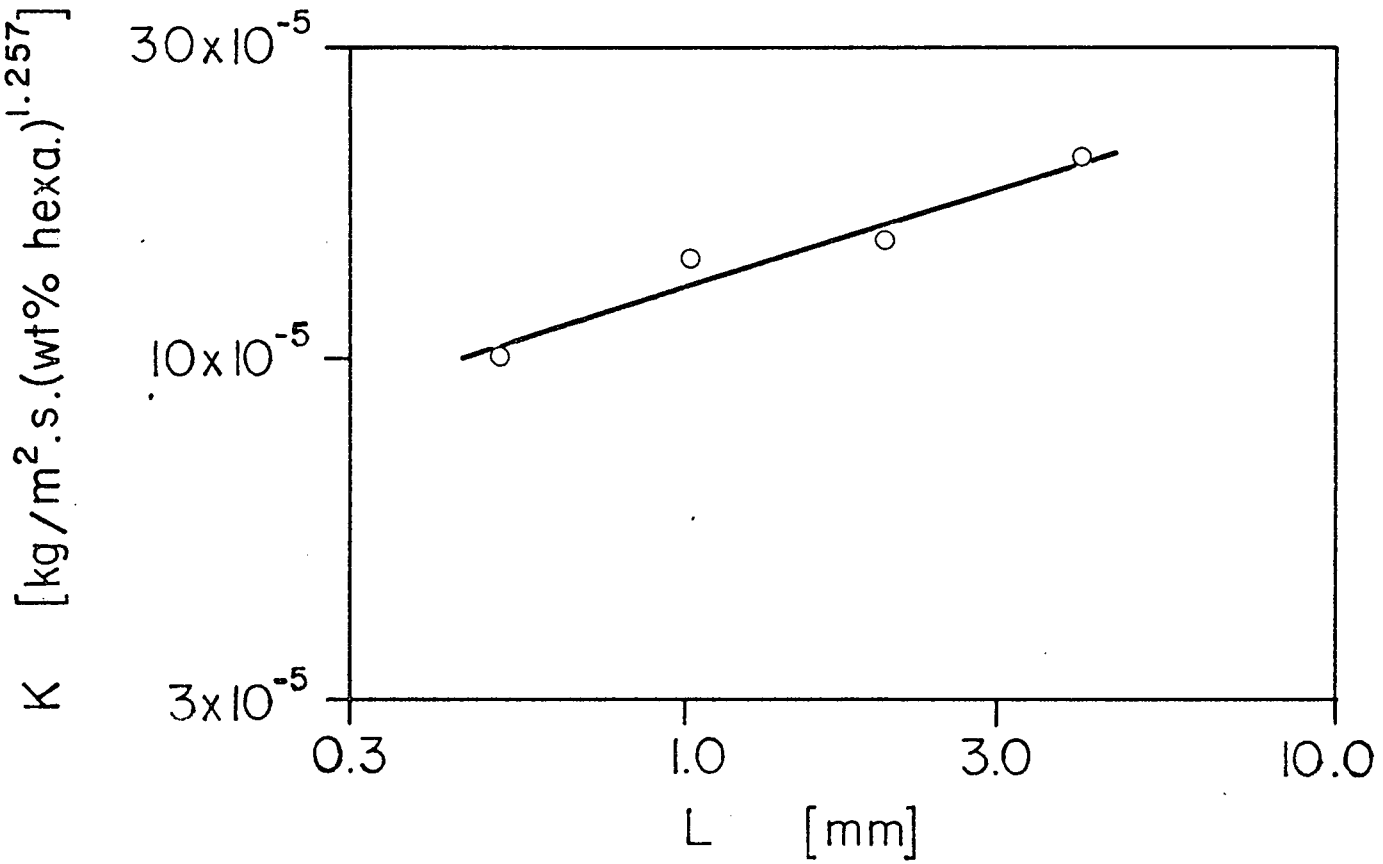

Figure 9 Logarithmic plot of overall growth rate constant (K) against crystal size (L) to find the exponent b'

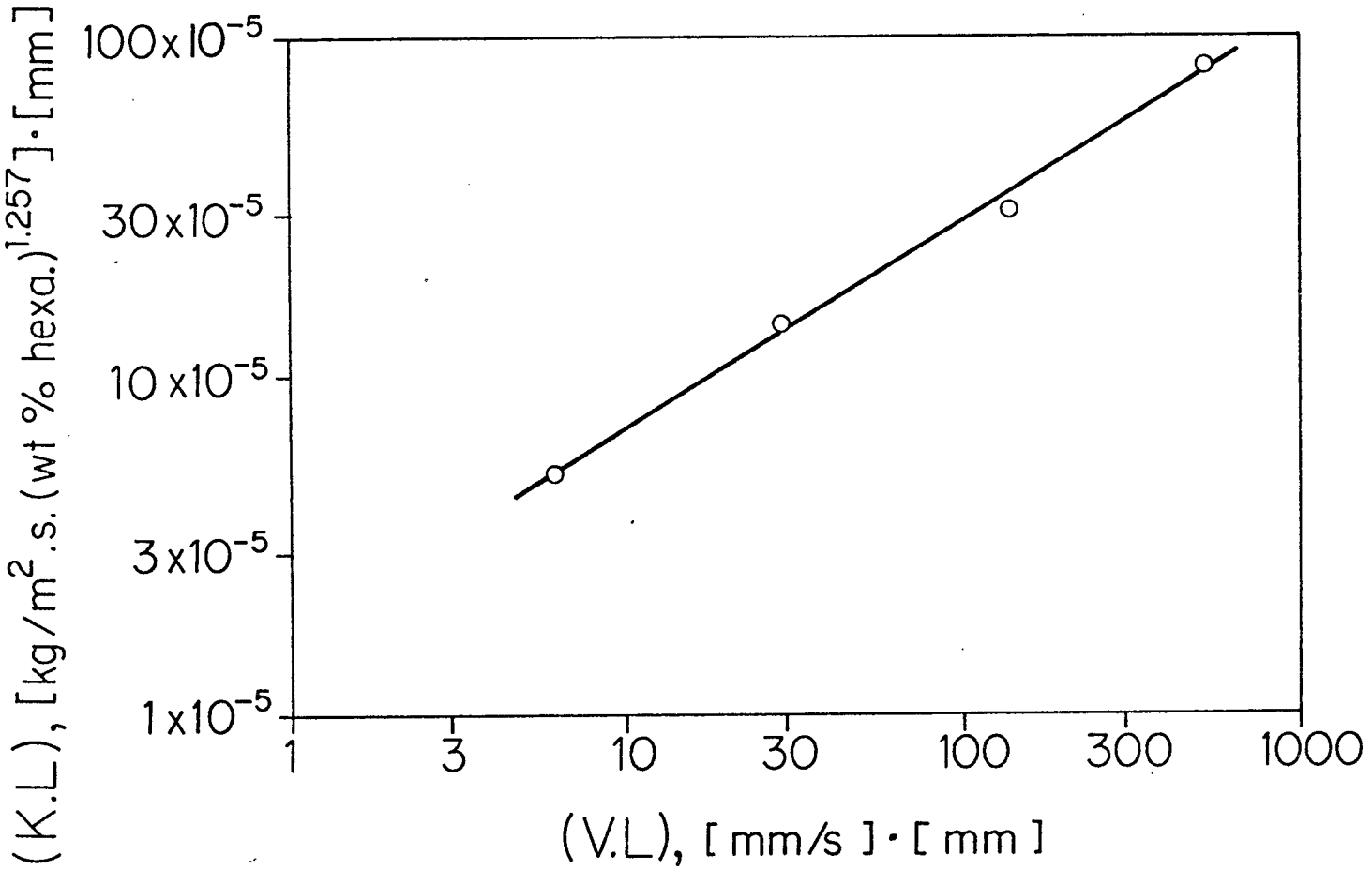

Figure 10 Pseudo-mass transfer correlation of overall growth rate constant (K) with interstitial solution velocity (V) and crystal size (L) at 40°C

When growth is fully mass transfer controlled, that is, when k_r is much greater than k_m, then K tends to k_m and β' tends to β. On the other hand, when growth is fully surface controlled, that is, when k_m is much greater than k_r, then K tends to k_r. Since k_r is expected to be independent of the hydrodynamics and hence of both V and L, it follows that, in the general case of neither step fully controlling, which we have in the present work, β' is expected to be between 0 and β. The experimental value from this work ($\beta' = 0.61$) as well as the experimental value obtained by Mullin and Gaska [49] of $\beta' = 0.87$ fall within the conceivable range of β' of 0 to 1, the possible range for β being 0.33 to 1 [89].

7.1.3 The effect of temperature on the growth rate

The usual way of presenting the temperature dependence of a process rate is via the Arrhenius relationship:

$$\text{rate constant} \propto \exp [- E/R \cdot T] \qquad (31)$$

As discussed in Section 2.2.5, if the rate constants k_m and k_r were available, each could be tested separately against this expression, but unfortunately k_m and k_r are usually unavailable and we have to make do with K. At constant crystal size, the present values of N are different at different temperatures (Table IV). Therefore the dimensions of K, $kg/m^2 \cdot s \cdot (wt\% \text{ hexa})^N$, are different for different temperatures and a direct plot of log K against 1/T is again of

doubtful meaning. The variation of N with temperature was too great to justify using a mean value of N, as was done above for the dependence of K on crystal size. In fact only upper and lower bounds could be set on the apparent activation energy of the overall growth process. This was done as follows. The growth rate curve-fits at different temperatures with a crystal size of 1.01 mm were re-determined, first all with N = 1.155 (the lowest value, from the unconstrained curve-fit at 50°C) and then all with N = 1.390 (the highest value, from the unconstrained curve-fit at 35°C). This gave two sets of dimensionally consistent values of K at the different temperatures (Tables VI and VII). An Arrhenius plot was then made of each set (Figure 11) and the resulting apparent activation energies of 49 and 56 kJ/mol (11.7 and 13.4 kcal/mol) were taken to be lower and upper bounds on the apparent activation energy of the overall growth process for a crystal size of 1.01 mm. The values are of the order of magnitude expected for a process occurring by a chemical mechanism.

7.1.4 Variations in the exponent N

We have considered in some detail the effect of temperature and crystal size on K. What can be said about their effects on N? Quantitatively, little can be said, but qualitatively their effects lend more support to the concept that crystallization involves a mass transfer step and a surface integration step in series. Experimentally, the mass transfer rate (as represented by dissolution rates) increases more slowly with temperature than does the surface integration rate (as represented by the limiting growth rate at high solution

Table VI Values of K for different temperatures at crystal size 1.01 mm when growth rate curves were refitted using N = 1.155 for all temperatures

temperature [deg C]	K [$kg/m^2 \cdot s \cdot (wt\%\ hexa.)^{1.155}$]
35.00	10.43×10^{-5}
40.00	14.97×10^{-5}
45.00	19.55×10^{-5}
50.00	25.45×10^{-5}

Table VII Values of K for different temperatures at crystal size 1.01 mm when growth curves were refitted using N = 1.390 for all temperatures

temperature [deg C]	K [$kg/m^2 \cdot s \cdot (wt\%\ hexa.)^{1.390}$]
35.00	9.09×10^{-5}
40.00	13.07×10^{-5}
45.00	17.91×10^{-5}
50.00	25.22×10^{-5}

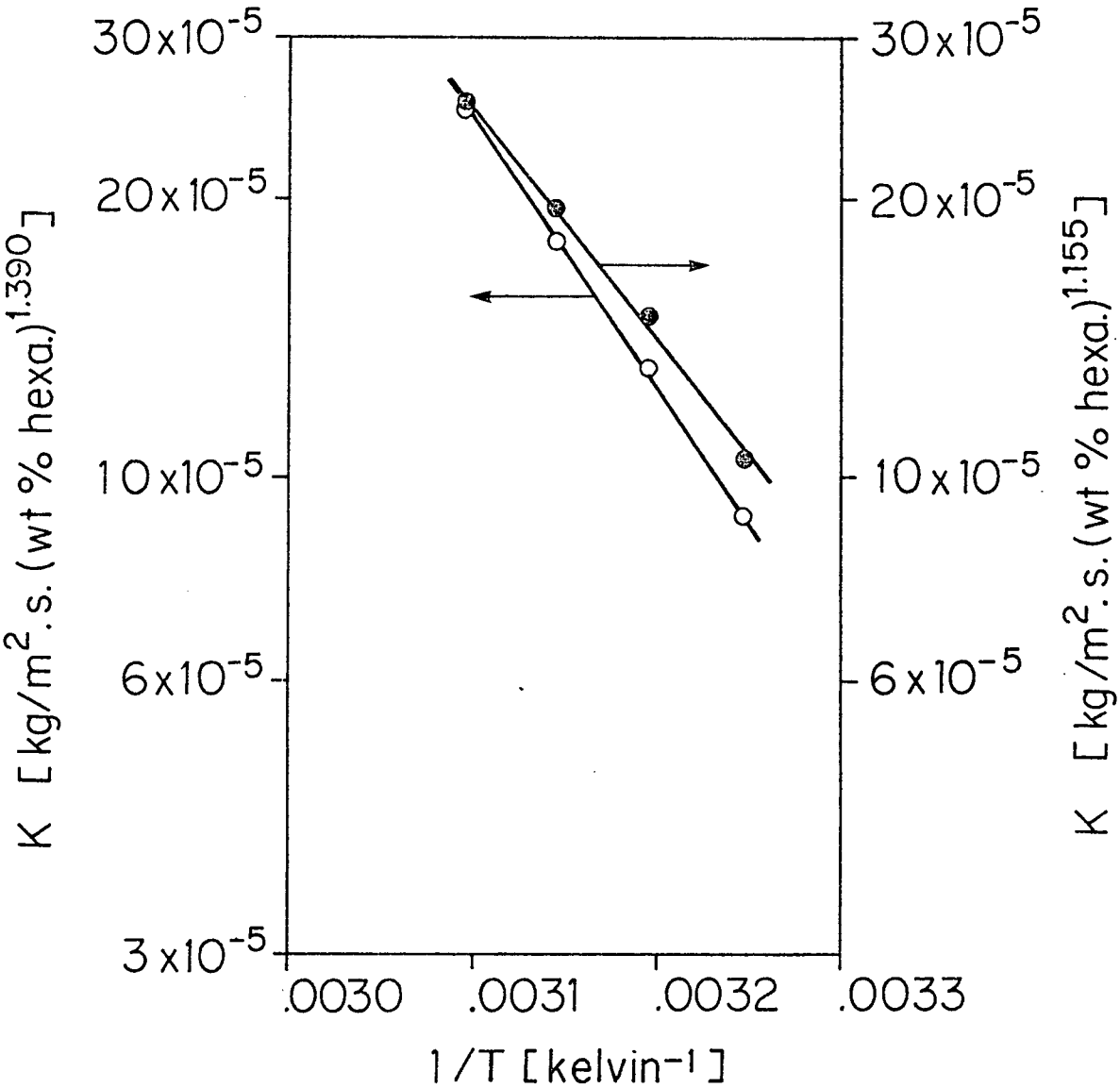

Figure 11 Arrhenius plots to find the apparent activation energy for the overall growth process

velocity). Thus as temperature increases, growth becomes more nearly fully mass transfer controlled and N is therefore expected to decrease. In this work the observed values of N for constant crystal size do indeed decrease as temperature increases (Table IV).

In general, the mass transfer rate increases with solution velocity while the surface integration rate is expected to be independent of solution velocity. Thus as solution velocity (or, in a fluidized bed, crystal size) increases, growth becomes more nearly surface controlled and N is therefore expected to increase. In this work the observed values of N for constant temperature do not appear to increase with crystal size (Table III), although, taking into account their different standard errors, the hypothesis that N increases slowly with crystal size cannot be discounted.

In this respect, a plot of growth rate itself at a given supersaturation against solution velocity is also of interest (Figure 12). At high solution velocities the growth rate begins to level out, indicating an approach to full surface control. However Garside [17] has indicated that even at very high solution velocities some resistance to mass transfer may persist.

7.2 The Crystal Dissolution Rates

7.2.1 General results

The dissolution rates found by the Batch Method for different crystal sizes at 40°C and for different temperatures at a crystal size of 1.00 mm are plotted as functions of undersaturation in Figures 13 and 14 respectively. The rates are fully tabulated in Appendix L.5.

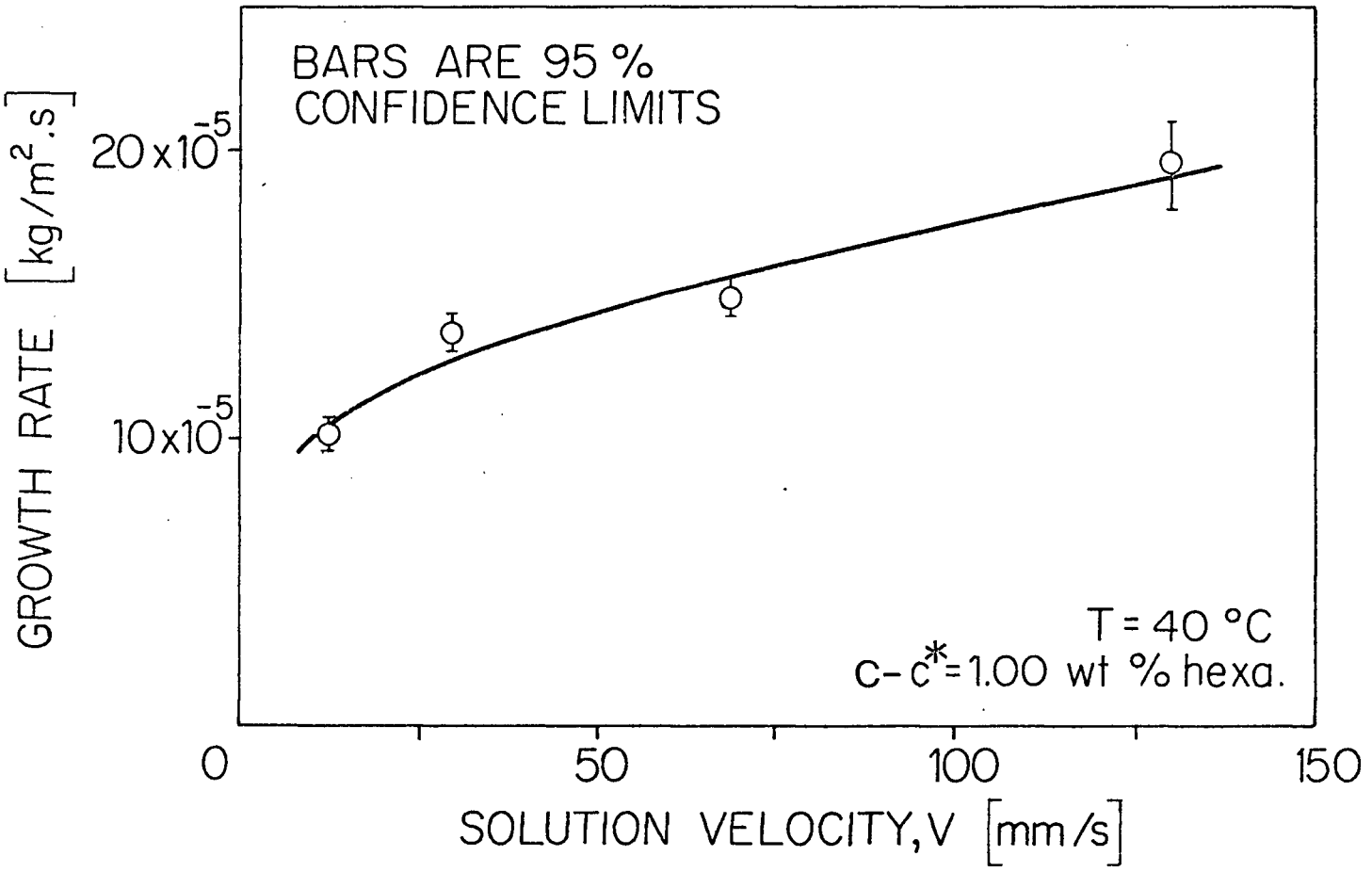

Figure 12 Apparent dependence of growth rate on crystal/solution relative velocity (interstitial solution velocity), V, in a fluidized bed

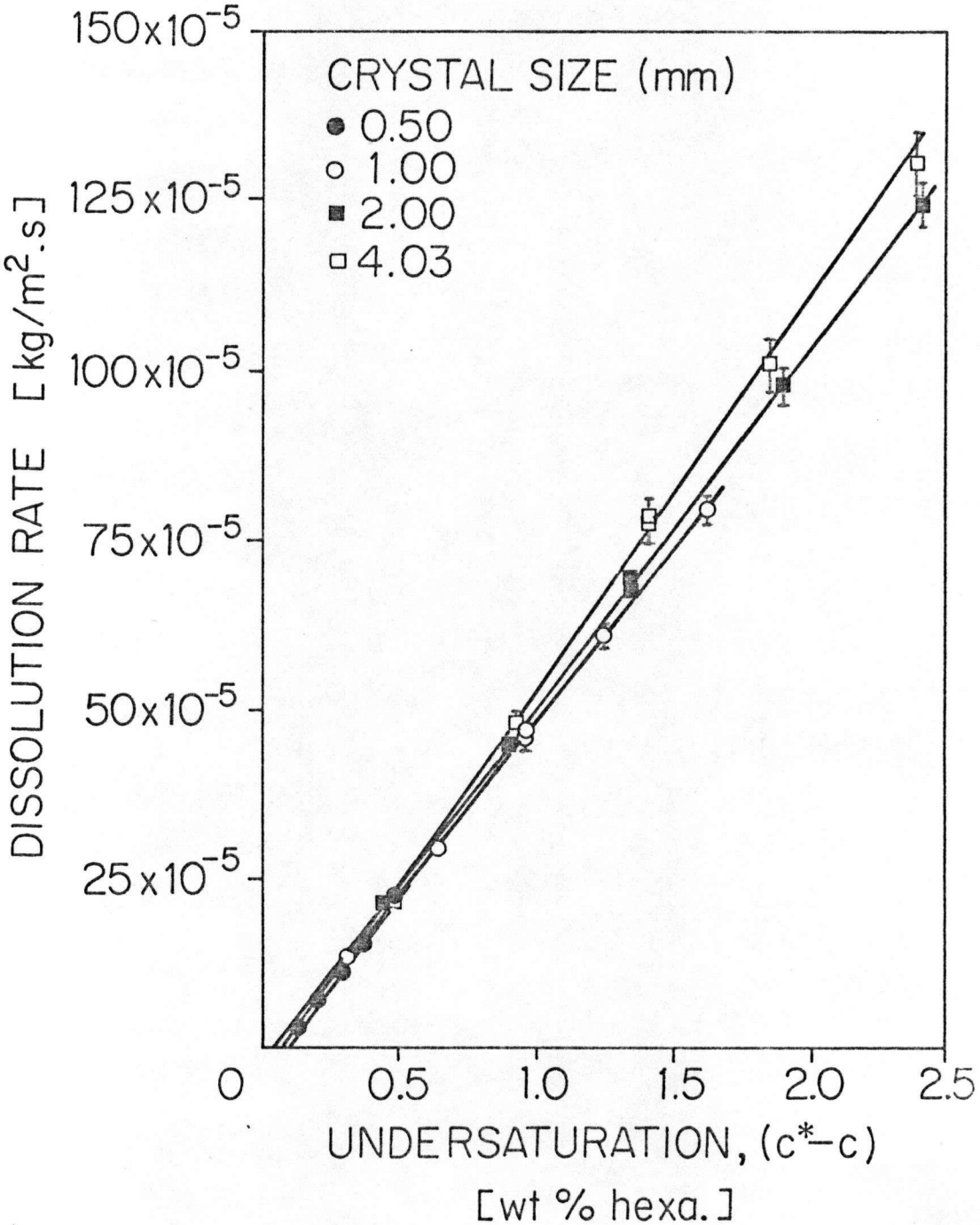

Figure 13 Dissolution rates by Batch Method of different sized nickel sulfate α-hexahydrate crystals at 40°C. Bars show the 95% confidence limits when these extend beyond the point symbols

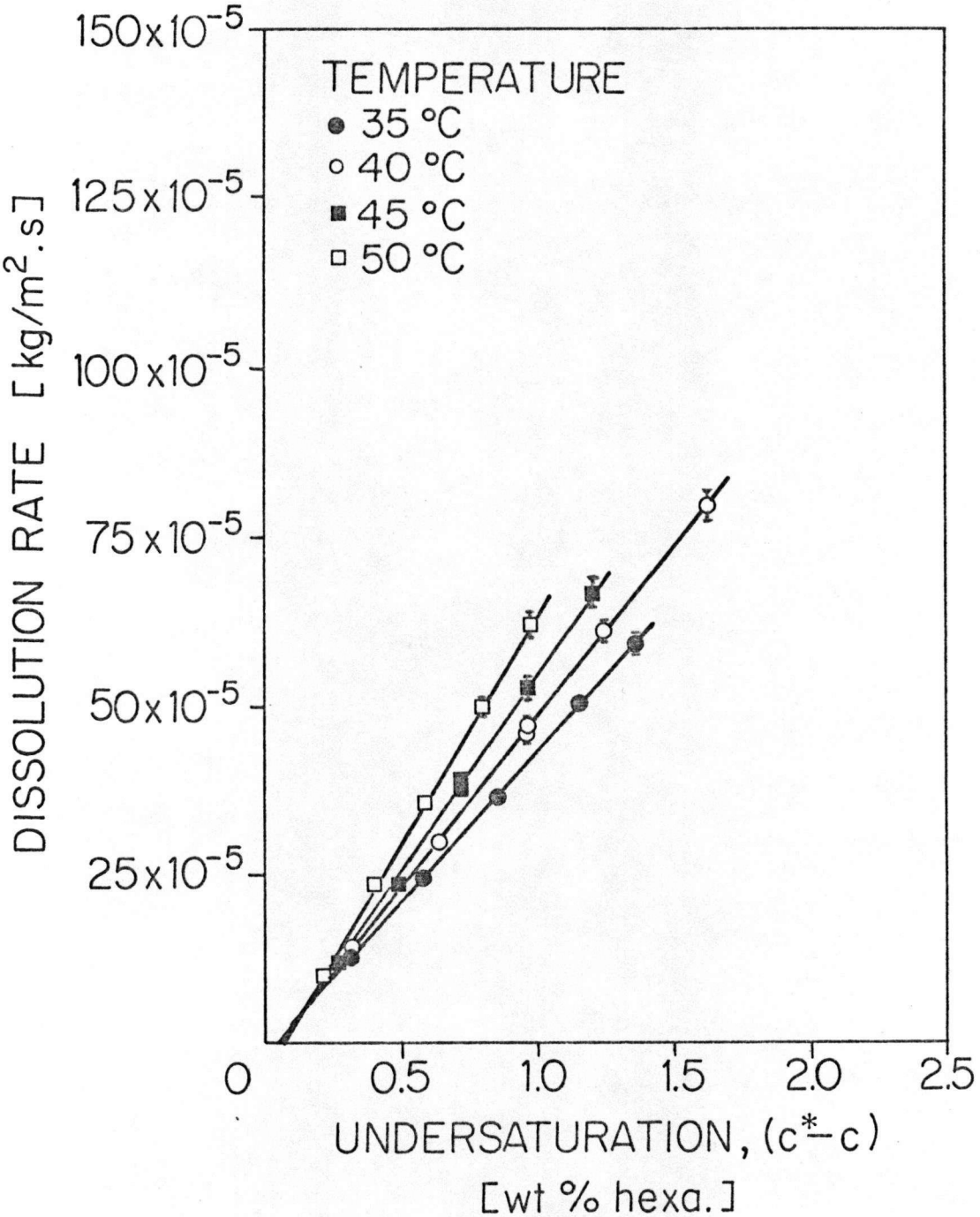

Figure 14 Dissolution rates by Batch Method of 1.00 mm nickel sulfate α-hexahydrate crystals at different temperatures. Bars show the 95% confidence limits when these extend beyond the point symbols

The estimated standard errors on the undersaturations and dissolution rates are the same as for the supersaturations and growth rates respectively.

The dissolution rate measurements were first fitted by least squares straight lines constrained to pass through the origin. As their percent error, rather than their absolute error, was constant, the measurements were weighted accordingly. However, in all cases these constrained lines gave a statistically significant lack of fit, so instead, unconstrained straight lines were used, again with weighting. These latter lines are shown in Figures 13 and 14. In most cases thay gave no statistically significant lack of fit. The meaning of the small, but significant, positive intercepts on the undersaturation axis is not certain. Possibly the actual saturation concentration had fallen below the expected value because of a build-up of impurities. In the case of growth, such intercepts have been observed by other workers [e.g.,22,49] but in the present work they were observed only in the case of dissolution. Cooke [90] has reported that with sodium chloride, intercepts exist for both growth and dissolution. The dissolution rate constants k_d in the equations

$$r_d = k_d \cdot (c^* - c) \qquad (13)$$

were taken as the slopes of the unconstrained lines, ignoring the intercepts. These constants and their estimated standard errors are given in Tables VIII and IX.

Table VIII Best fit values of k_d from Equation (13) for dissolution of crystals of different sizes at 40°C

mean crystal size [mm]	k_d [kg/m^2 · s · (wt% hexa.)]	estimated absolute standard error of k_d
0.50	51.33×10^{-5}	1.47×10^{-5}
1.00	50.62×10^{-5}	0.35×10^{-5}
2.00	52.52×10^{-5}	0.34×10^{-5}
4.03	58.57×10^{-5}	0.83×10^{-5}

Table IX Best fit values of k_d from Equation (13) for dissolution of crystals of size 1.00 mm at different temperatures

temperature [deg C]	k_d [$kg/m^2 \cdot s \cdot$ (wt% hexa.)]	estimated absolute standard error of k_d
35.00	43.96×10^{-5}	0.17×10^{-5}
40.00	50.62×10^{-5}	0.35×10^{-5}
45.00	57.22×10^{-5}	1.37×10^{-5}
50.00	66.97×10^{-5}	0.70×10^{-5}

7.2.2 The effects of solution velocity and crystal size on the dissolution rate

In this work, as is usual, dissolution appeared to be purely a mass transfer process, and since the Sherwood number was one or two orders of magnitude greater than unity, the dependence of k_d on crystal size and solution velocity could be expressed directly in the form of Expression (17). As outlined in Section 7.1.2, an absolute comparison with published fluidized bed mass transfer correlations could not be made here, because of a lack of diffusion coefficient data, but a plot of log ($k_d \cdot L$) against log ($V \cdot L$) at constant temperature (Figure 15) yielded $\beta = 0.49$ (with estimated standard error 0.03), a value close to those given by Rowe and Claxton [67] for spheres at similar Reynolds numbers. For the dissolution of potassium alum, Mullin and Garside [13c] found $\beta = 0.62$.

7.2.3 The effect of temperature on the dissolution rate

For the dependence of k_d on temperature, an Arrhenius plot for 1.00 mm crystals gave a good straight line (Figure 16) leading to an activation energy of 23 kJ/mol (5.5 kcal/mol), which is of the order expected for processes occurring by physical mechanisms. If diffusion coefficient data at different temperatures were available, the activation energy for dissolution could be compared with that for molecular diffusion. The two are expected to be of the same order when molecular diffusion through a laminar sublayer is the main mechanism of dissolution mass transfer.

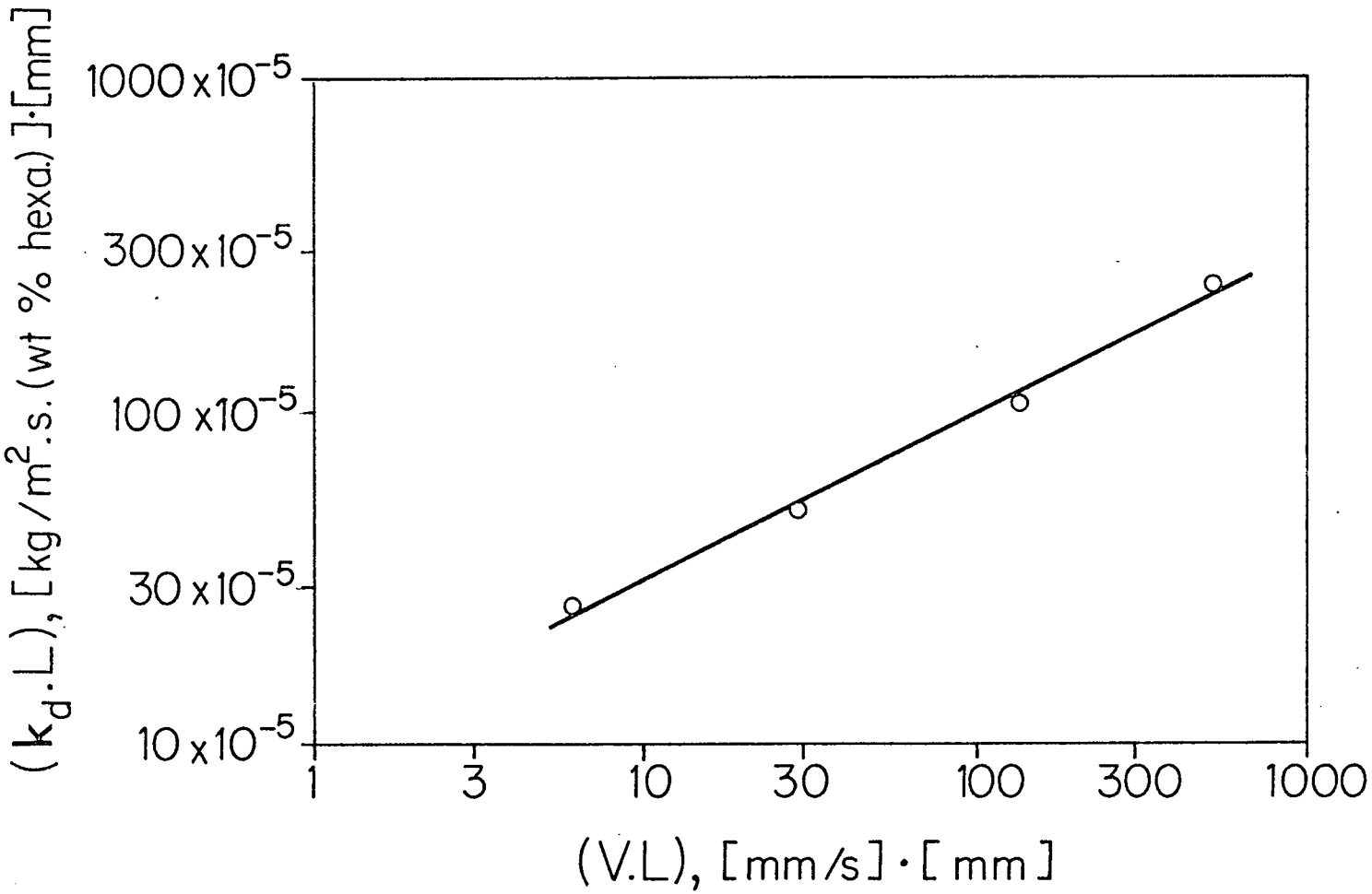

Figure 15 Mass transfer correlation of dissolution rate constant (k_d) with solution velocity (V) and crystal size (L) at 40°C. The 95% confidence limits are all within the point symbols

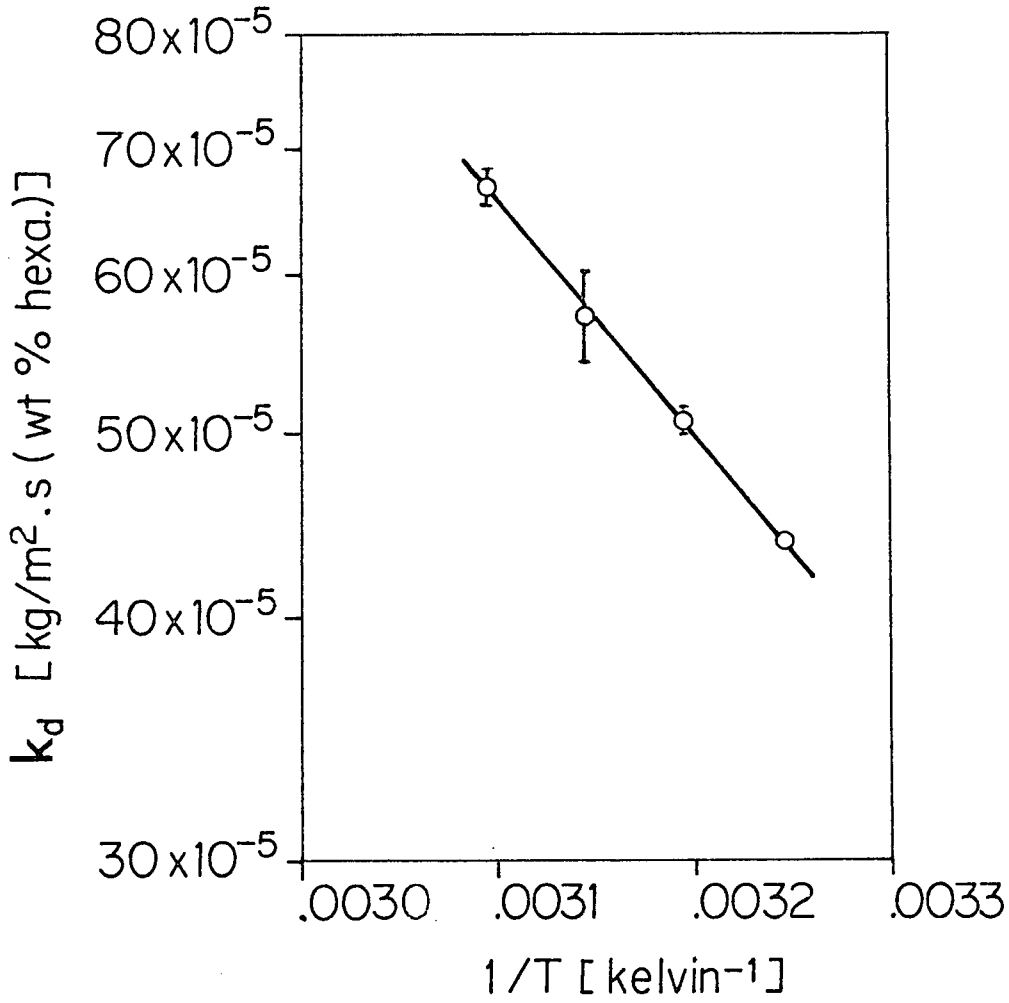

Figure 16 Arrhenius plot of dissolution rate constants for 1.00 mm crystals. Bars show the 95% confidence limits when these extend beyond the point symbols

7.3 The Apparent Kinetics of the Surface Integration Step of Growth

7.3.1 Isolation of the apparent surface integration kinetics, using dissolution rate data

In this work, both growth and dissolution rates have been found under hydrodynamic conditions deliberately made as similar as possible in the two cases. In this section, the apparent kinetics of the surface integration step of growth (Equation 9) are extracted from the overall kinetics of growth (Equation 8), by assuming that the mass transfer step of growth can be represented by dissolution rate expressions, in other words that under given conditions k_m equals k_d. Before proceeding, it is emphasized that although it has been used by several workers (Section 2.2.2), this assumption is open to dispute. Illustrating this point, Mullin and Garside [13c] write: "During growth, solute molecules are diffusing towards the crystal surface, whilst during dissolution they are travelling in the opposite direction. It is possible that electrostatic charges attracting solute molecules to the crystal surface would increase the rate of diffusion in the former case but decrease the rate in the latter." Indeed, the values of k_m which they themselves calculated by estimating k_r from measurements of the limiting growth rate at high solution velocities are considerably greater than the values of k_d for similar conditions, and the same kind of discrepancy was found by Clontz et al. [21]. However, the values of k_m found by Rumford and Bain [22] from mass transfer controlled growth were in good agreement with values of k_d calculated from the mass transfer correlation of Chu et al. [23].

Having made the assumption discussed above, we substitute $k_m = k_d$ in Equation (3) and hence calculate

$$r/k_m = (c - c_i) \tag{52}$$

Then

$$(c - c^*)-(r/k_m) = (c - c^*)-(c - c_i) = (c_i - c^*) \tag{53}$$

Plots of r against $(c_i - c^*)$ thus computed are shown in Figures 17 and 18. Logarithmic curve-fits then yielded the apparent values of k_r and n (Tables X and XI). The exponent n is expected to be independent of crystal size, and the present values of n at different crystal sizes are indeed not significantly different. The rate constant k_r might also be expected to be independent of the hydrodynamics and thus of crystal size. However, as yet there is no convincing experimental verification of this prediction by the present method. Certainly in this work the values of k_r retain a dependence on crystal size (Table X), and despite their smaller range of crystal size and larger standard error of k_r, Mullin and Garside [13c] similarly report some dependence of k_r on crystal size. In the next paragraph, this dependence on crystal size is considered more fully.

Consider the dependences of k_m, K and k_r on solution velocity and on crystal size, as expressed in combined form for fluidized

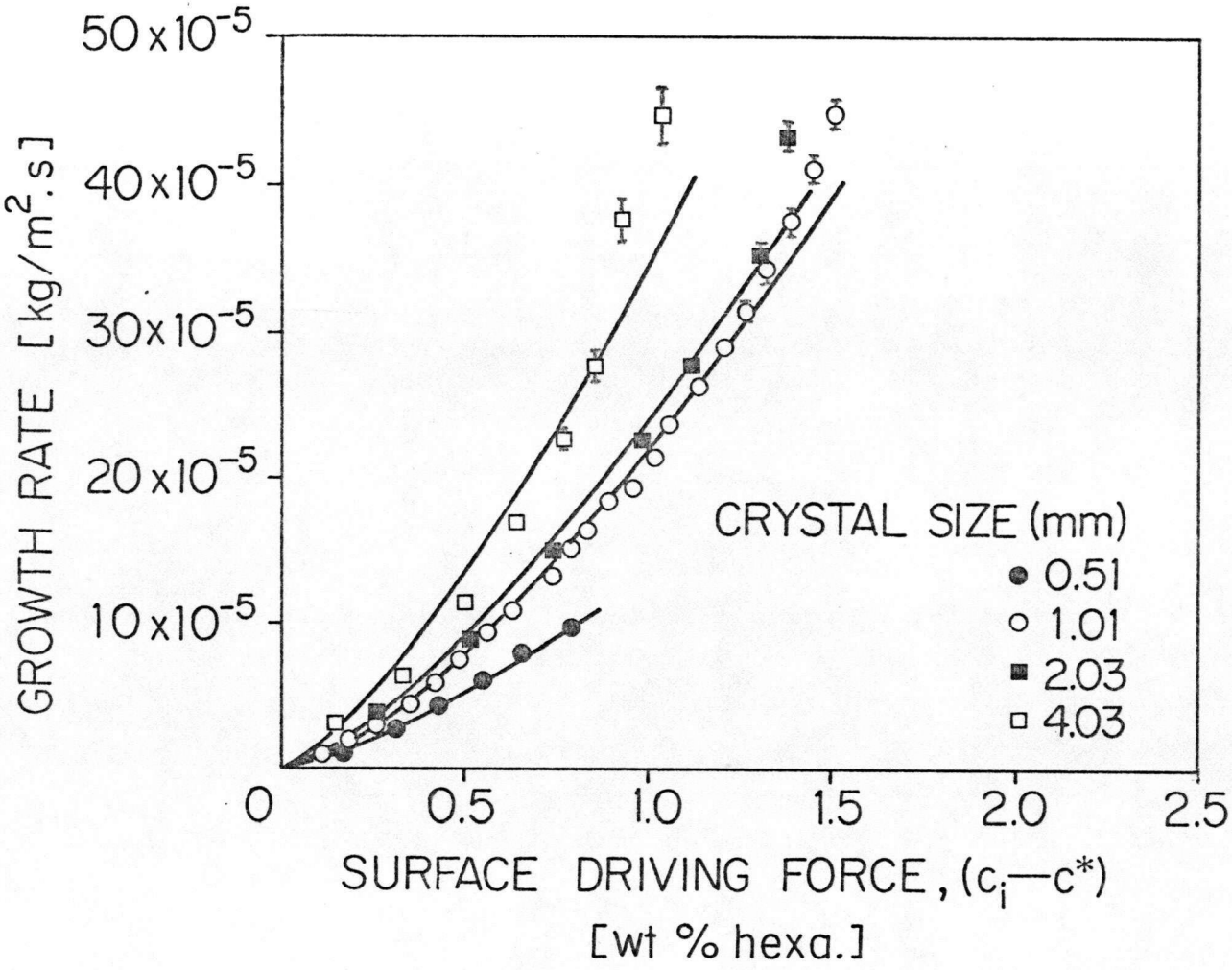

Figure 17 Apparent surface integration rates of different sized nickel sulfate α-hexahydrate crystals at 40°C. Bars show the 95% confidence limits when these extend beyond the point symbols

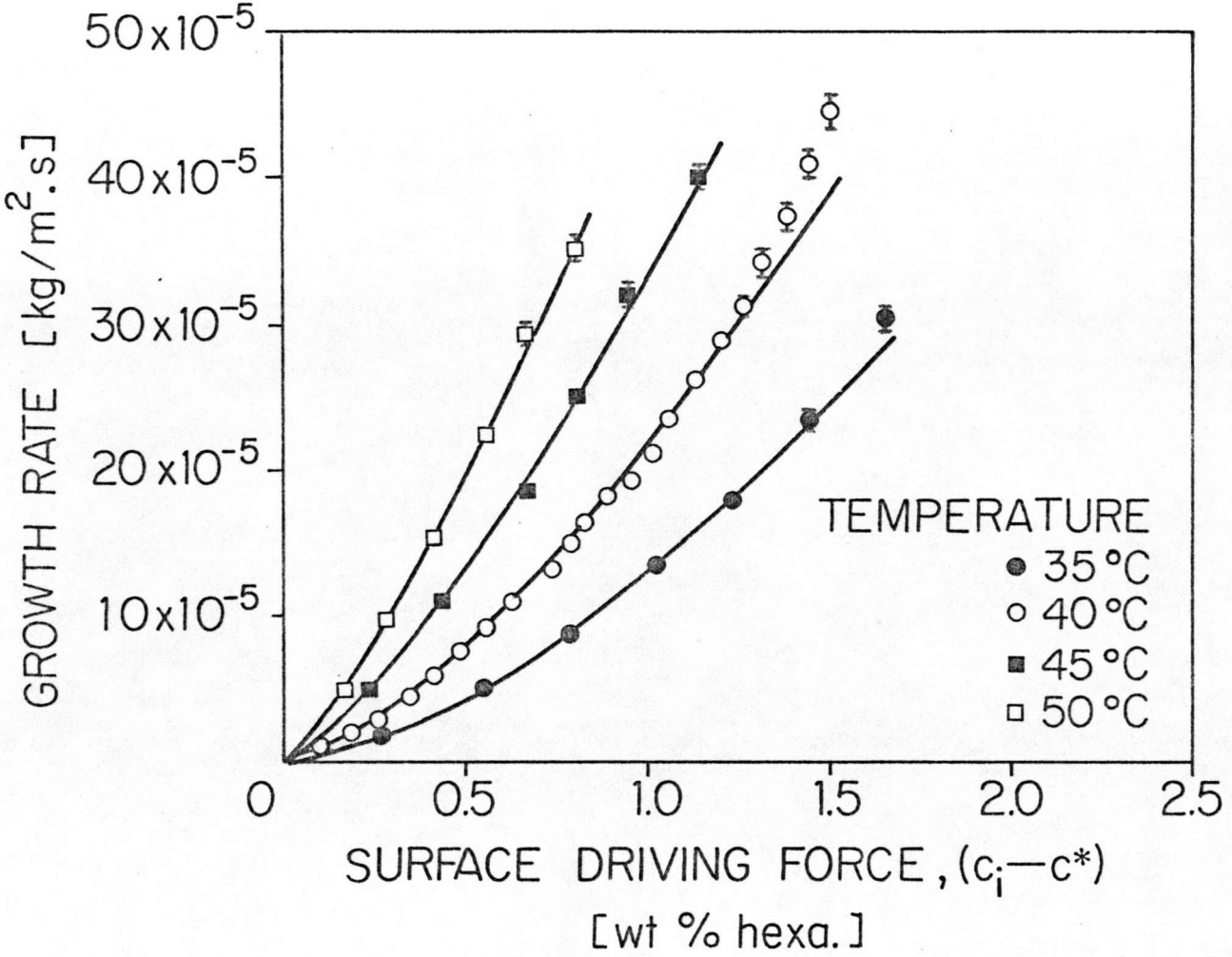

Figure 18 Apparent surface integration rates of 1.01 mm nickel sulfate α-hexahydrate crystals at different temperatures. Bars show the 95% confidence limits when these extend beyond the point symbols

Table X Best fit parameters of Equation (9) for growth of crystals of different sizes at 40°C

mean crystal size [mm]	k_r [$kg/m^2 \cdot s \cdot (wt\%\ hexa.)^n$]	estimated absolute standard error of k_r	n [dimensionless]	estimated absolute standard error of n
0.51	13.43×10^{-5}	0.24×10^{-5}	1.349	0.020
1.01	21.78×10^{-5}	0.35×10^{-5}	1.426	0.021
2.03	23.82×10^{-5}	0.76×10^{-5}	1.371	0.059
4.03	34.36×10^{-5}	2.70×10^{-5}	1.351	0.097

Table XI Best fit parameters of Equation (9) for growth of crystals of size 1.01 mm at different temperatures

temperature [deg C]	k_r [$kg/m^2 \cdot s \cdot (wt\%\ hexa.)^n$]	estimated absolute standard error of k_r	n [dimensionless]	estimated absolute standard error of n
35.00	13.00×10^{-5}	0.18×10^{-5}	1.544	0.025
40.00	21.78×10^{-5}	0.35×10^{-5}	1.426	0.021
45.00	33.11×10^{-5}	0.50×10^{-5}	1.342	0.023
50.00	46.67×10^{-5}	0.56×10^{-5}	1.269	0.015

beds at constant temperature by

$$k_m \propto L^b \tag{22}$$

$$K \propto L^{b'} \tag{23}$$

$$k_r \propto L^{b''} \tag{54}$$

When there is full mass transfer control, K tends to k_m. When there is full surface control, K tends to k_r. Thus in the general case of neither step fully controlling, we expect

$$b < b' < b'' \quad \text{if} \quad b < b'' \tag{55}$$

or

$$b > b' > b'' \quad \text{if} \quad b > b'' \tag{56}$$

These expressions should hold regardless of whether or not k_m and k_d are equal. Now for the present crystals, $a \simeq 1$ in Expression (21) (Figure D.1). Also, for octahedral alum crystals, whose shape is not greatly different from that of the present crystals, Bujac [47] found $a \simeq 1$ and Ishii [33] used $a \simeq 1$ for potassium sulfate. Then, taking the usual $\beta \simeq 0.5$ and using Equation (23), we find $b \simeq 0$, that is, in fluidized beds, at constant temperature, growth mass transfer coefficient k_m is predicted to be apparently approximately independent of crystal size. Ishii [33] reached the same conclusion. In support of this

prediction, for the present values of k_d (Table VIII) b = 0.06, with a standard error of 0.03, while Bujac [47] has also reported that experimentally b is close to zero. Now in theory, k_r is independent of both solution velocity and crystal size, so theoretically b" is zero also. But as we have shown, b' should never fall outside the range b to b" (Expressions 55 and 56). Therefore, in fluidized beds, theoretically, b' is also zero, even without full surface or full mass transfer control. In practice b' is often, as it is in this work (b' = 0.31), greater than zero, but Expression (55) should still hold, so in practice b" should be greater than both b' and zero. Thus if, in fluidized beds, the overall growth kinetics are apparently size-dependent, as they are here, the apparent surface integration kinetics can never by the present method be found to be size-independent, and, more specifically, must be found to be at least as size-dependent as are the overall kinetics. This prediction appears to hold for the present data: when the values of k_r were re-estimated using the mean value of n (as was done above for the variation of K with crystal size) and the logarithms of these values of k_r were plotted against the logarithms of L, the resulting value of b" was 0.45, with an estimated standard error of 0.08, compared with b' = 0.31.

There is some prior experimental evidence both for and against the idea that k_r varies with crystal size. For example, at high solution velocities, when the growth rate was almost independent of solution velocity, McCabe and Stevens [46] and Rosen and Hulburt [53] found the growth rate to be independent of crystal size as well. Mullin and Gaska [47] found that their crystal growth rates varied

with crystal size. This fact, together with the fact that the activation energy for growth was low, led them to conclude that growth of potassium sulfate was diffusion controlled. However, they found $N = 2$ for all crystal sizes, whereas for diffusion control $N = 1$ would be expected. Another interpretation of their data is that, since $N = 2$ for all crystal sizes, surface integration at least partly controls the growth rate and the surface integration rate is size-dependent. Bujac [47] has concluded from his experimental observations that the surface integration rate does depend on the hydrodynamics, and he therefore considers the simple diffusion theory of growth of the type used in the present work to be inadequate. It is conceivable that some property of the surface (such as dislocation density) which may influence the surface integration rate, may change during the growth of batches of seed crystals to their different intended sizes, thereby causing seed crystals of different sizes to have different surface properties and hence causing a variation of the surface integration rate with crystal size.

An inequality similar to Expression (55) holds for n as well. Again by considering the extremes of full mass transfer control and full surface control, we can state that, at constant temperature,

$$1 < N < n \tag{10}$$

and from Tables III and X this condition is seen to hold for the present data. Considering the effect of temperature on the apparent surface integration kinetics, the observed behaviour of k_r and of n

is very similar to that of K and of N respectively. Using the same recalculation technique that was used on K, the lower and upper bounds on the apparent activation energy of the surface integration step were found to be 65 and 76 kJ/mol (15.4 and 18.0 kcal/mol) respectively. These values for the activation energy of the isolated surface integration process show the chemical nature of this process still more clearly than did the lower values of the activation energy of the overall growth process.

7.3.2 An attempt to separate the kinetics of the mass transfer and surface integration steps by a general method

We recall Equations (3) and (9)

$$r_m = k_m (c - c_i) \tag{3}$$

$$r_r = k_r (c_i - c^*)^n \tag{9}$$

and also Equation (11), obtained from them by equating r_m and r_r and eliminating c_i, the surface supersaturation, which is difficult to evaluate.

$$\frac{r}{k_m} + \left(\frac{r}{k_r}\right)^{1/n} = (c - c^*) \tag{11}$$

It is expected that k_m, k_r and n can be estimated directly and without assumption by a suitable curve-fit of values of r and $(c - c^*)$. Such a curve-fit was attempted as follows.

Equation (11) has the form

$$p_1 x + p_2 x^{p_3} = y \qquad (57)$$

where p_1, p_2, and p_3 are to be determined. This form cannot be linearized, by taking logarithms or by any other method. A curve-fit of the growth rates from the Batch Method of 1.01 mm crystals at 40°C was attempted using a conventional non-linear least squares computer program [91] which used an iterative procedure based on Taylor expansions. However no convergence was achieved. A series of curve-fits were therefore made using a linear least squares program, holding p_3 constant within each fit but varying p_3 between fits. The standard errors of estimate of $(c - c^*)$ from each of these fits were compared in the hope of finding a minimum standard error of estimate at a certain value of p_3. However there was no physically meaningful minimum.

Mathematical limitations in the curve-fitting programs may be the immediate factor preventing the success of this approach. However, in this particular case, failure may also be caused by shortcomings of the data themselves. For example, if we re-write the empirical Equation (8) in the form

$$\left(\frac{r}{K}\right)^{1/N} = (c - c^*) \qquad (8)$$

and compare this with Equation (11), we see that curve-fitting Equation (11) requires the determination of three parameters rather

than the two of Equation (8). Since Equation (8) in most cases fitted the present data without statistically significant lack of fit (Section 7.1.1), it is not in the present case statistically justifiable to introduce the third parameter. However, this is not necessarily true of other sets of data. The main contribution to the standard error of the growth rates in this work was from the standard error of the parameter L_1/L of the crystal shape (Appendix J). Measurements on other compounds, where the crystal shape does not have this source of variation, may therefore produce growth rates with smaller standard errors, so that introduction of the third parameter may then be justified. Also, in the present work the term (r/k_m) was expected to be considerably smaller than the term $(r/k_r)^{1/n}$, since k_d was observed to be several times k_r, and k_m is expected to be greater than or equal to k_d. Both these factors help to prevent the success of the approach described here, when it is applied to the data from this work. However, when applied to data which do not give these disadvantages, the approach may be more successful.

In the derivation of the least squares method of curve-fitting, it is assumed that only the y quantities are subject to error. In the present work, the errors in r are greater than the errors in $(c - c^*)$ (Section 7.1.1). It would therefore be theoretically more justifiable to use r as the y quantity when curve-fitting Equation (11) than to use $(c - c^*)$ as the y quantity, as has been done here. However, in general, r cannot be made the subject of Equation (11). Some authors have restricted the value of n to an integer (usually n = 2),

although there is little theoretical justification for doing so. When $n = 2$, r can be made the subject of Equation (11). The result is given by Mullin and Garside [13c], but it is complicated. When the present data for 1 mm crystals at 40°C were curve-fitted using $n = 2$ (but still with $(c - c^*)$ as the y quantity), the value obtained for k_m was 30.7×10^{-5} kg/m^2· s · (wt% hexa) and for k_r was 43.5×10^{-5} kg/m^2· s · (wt% hexa)^2. However this curve gave a highly significant lack of fit, so this approach was not pursued.

8. SUMMARY AND CONCLUSIONS

Growth and dissolution rates of nickel sulfate α-hexahydrate crystals have been measured, the growth rates by two different methods. It has been clearly shown that growth and dissolution are not reciprocal processes. At a given concentration driving force (supersaturation or undersaturation), dissolution was about four or five times as fast as growth. Also, the dissolution rate was first order in undersaturation ($c^* - c$) while the growth rate depended on a somewhat higher order of the supersaturation ($c - c^*$). Dissolution appeared to be a pure mass transfer process and the dissolution rate constant has been expressed in the usual form of mass transfer correlation. The dissolution measurements made in this work are a contribution in their own right to the rather sparse data on mass transfer from non-spherical particles. The growth rate constant depended on solution velocity and crystal size and this dependence has been expressed in the form of a pseudo-mass transfer correlation.

The nature of this dependence and also of the dependence of the growth rate on temperature supports the diffusion theory concept of crystal growth as a two-step process, i.e. mass transfer of solute to the crystal surface, followed by integration into the solid lattice. In the present case, the growth rate appears to be mainly but not wholly controlled by the surface integration step. Making the assumption that the (unknown) rate constant for the mass

transfer step of growth can be represented by the (known) rate constant for dissolution, the apparent kinetics of the surface integration step of growth have been extracted from the overall kinetics of growth. The surface integration rate, thus isolated, still apparently depended on crystal size, and the significance of this observation has been briefly discussed.

The diffusion theory concept of crystal growth used in this work does have shortcomings. The diffusion theory cannot account for the formation of plane faces and sharp edges on crystals. The diffusion theory takes little account of the physical conditions at the crystal surface, and cannot explain variations of c_i with position on the crystal surface nor the occurrence of periodic growth rates, both of which have previously been observed experimentally [92]. Nevertheless, as demonstrated by the present study, the diffusion theory retains some usefulness by virtue of its simplicity and ease of application, particularly in an engineering context, where the evaluation of phenomena at the crystal surface is not essential.

These are believed to be the first growth rate measurements reported for nickel sulfate, a compound of some commercial significance. While it is realized that in the industrial crystallization of nickel sulfate, the feed solutions are not pure, it is suggested that the present measurements represent the asymptotic growth rates as impurity levels tend to zero. The absolute values of the growth and dissolution rates were comparable to those published for other simple inorganic salts.

In the supersaturation range 0.0 - 0.7 wt% hexahydrate, which includes the usual industrial levels [82, 93, 94] results from the Continuous Method agreed well with those from the Batch Method, despite different void fractions in the two methods. This agreement reinforces and extends to lower void fractions similar findings by Bujac and Mullin [63] for ammonium alum and Garside et al. [62] for potassium sulfate. Since Mullin and Garside [13b] and Mullin and Gaska [16] have found agreement for other systems between growth rates from the Batch Method and from single crystal tests, the strong implication is that only single crystal tests need be made to predict fairly closely the growth rate which would prevail in an industrial-type fluidized bed. This should considerably simplify crystallizer design.

9. SUGGESTIONS FOR FURTHER WORK

Single crystal studies of the growth rate of nickel sulfate α-hexahydrate would be a valuable complement to the work presented here. The growth rates on the different types of face present on the crystal could then be separately determined and compared with each other and with the overall growth rates given here. If the crystal were anchored, the effects of solution velocity and of crystal size on the growth rate could be separately studied. Also, the limiting growth rate at high solution velocities gives another estimate of the surface integration rate. The mass transfer coefficient during growth can then be isolated and compared with the mass transfer coefficient during dissolution.

Diffusion coefficients in near-saturated nickel sulfate solutions should be determined over a range of temperatures. The comparison of the dissolution rate data given here with standard mass transfer correlations could then be completed.

More measurements should be made in dense beds so that their behaviour can be more closely compared with that of lean beds and single crystals. If more evidence can be found that growth rates in all three situations are quite similar, then the problem of crystallizer design is considerably simplified. Again, more results on the relationship between solution velocity and void fraction in the fluidized bed would be valuable in crystallizer design. The effect

of impurities on the growth rate should be examined. Growth rates from typical industrial solutions would be particularly useful. Systematic investigations of the effects of impurities on growth rates have been undertaken only in the last very few years.

A challenging but worthwhile project would be the direct determination of the surface supersaturation c_i during crystal growth from flowing solutions. Some work has already been done on finding c_i in stagnant solutions [92, 95, 96], but c_i may be very different with flowing solutions. If c_i were determined directly, an assumption-free separation of the kinetics of the mass transfer and surface integration steps of growth could be made.

N O T A T I O N

a	exponent of L in Expression (21) [dimensionless]
A	overall surface area of a collection of crystals [m^2]
b	exponent of L in Expression (22) [dimensionless]
b'	exponent of L in Expression (24) [dimensionless]
b"	exponent of L in Expression (54) [dimensionless]
B	constant in Equation (20) [$kg/m^2 \cdot s \cdot (mm/s)$]
c	concentration of bulk solution, supersaturated in the case of growth, undersaturated in the case of dissolution [wt% hexahydrate]
$\bar{c}$	concentration of the solution in the sampling chamber of the specific gravity meter [wt% hexahydrate]
$\hat{c}$	in Section 6.2 and Appendix K.2, concentration of the solution, expressed as [kg hexa./kg water]
c*	saturation concentration [wt% hexahydrate]
c_i	in the case of growth, the (supersaturated) solution concentration at the crystal surface [wt% hexahydrate]
$(\Delta C)_m$	concentration driving force for mass transfer; used in Expression (41) [wt% hexahydrate]
D	diffusion coefficient [m^2/s]
E	activation energy; used in Expression (31) [kJ/mol]
f_s	surface area shape factor, defined by Equation (H1) [dimensionless]

f_v volume shape factor, defined by Equation (H2) [dimensionless]

F overall surface-volume shape factor, defined by Equation (H3) [dimensionless]

k_d dissolution mass transfer coefficient; defined by Equation (13) [$kg/m^2 \cdot s \cdot (wt\%\ hexa.)$]

k_m growth mass transfer coefficient; defined by Equation (3) [$kg/m^2 \cdot s \cdot (wt\%\ hexa.)$]

k_r surface integration rate constant; defined by Equation (9) [$kg/m^2 \cdot s \cdot (wt\%\ hexa.)^n$]

K overall growth rate constant; defined by Equation (8) [$kg/m^2 \cdot s \cdot (wt\%\ hexa.)^N$]

L crystal size [mm]

L_1, L_2 parameters of the crystal shape; see Figure J.2 [mm]

L_i size of the i'th size fraction of a polydisperse collection of crystals; used in Equation (H10) [mm]

$\bar{L}_s$ specific surface average size of a polydisperse collection of crystals [mm]

n exponent of $(c_i - c^*)$ in Equation (9) [dimensionless]

N exponent of $(c - c^*)$ in Equation (8) [dimensionless]

N_s stirring rate; used in Expression (29) [radians per second]

p_1, p_2, p_3 parameters in Equation (57)

r growth rate [$kg/m^2 \cdot s$]

r_d dissolution rate [$kg/m^2 \cdot s$]

r_m mass transfer rate [$kg/m^2 \cdot s$]

r_r surface integration rate in growth; used in Equation (4) [$kg/m^2 \cdot s$]

r_{m0} mass transfer rate at zero solution velocity; used in Equation (20) [$kg/m^2 \cdot s$]

R gas constant [= 8.31 J/mol • kelvin]

t time [s], or, in Appendix D, temperature [deg C]

T in Expression (31), absolute temperature [kelvin]

V interstitial solution velocity = true velocity of solution past crystals [mm/s]

V_s superficial solution velocity = "empty-tube velocity" [mm/s]

V_{t50} terminal velocity of single crystals in the 50 mm section [mm/s]

$V_{t\infty}$ terminal velocity of single crystals in an infinite medium [mm/s]

W overall weight of a collection of crystals [kg]

W_s total weight of water present in the solution in the crystallizer: used in Section 6.2 [kg]

w_i weight of the i'th size fraction of a polydisperse collection of crystals; used in Equation (H10) [kg]

x exponent in Expression (16) [dimensionless]

α exponent of Schmidt number in Expression (17) [dimensionless]

α' exponent of Schmidt number in Expression (25) [dimensionless]

β exponent of Reynolds number in Expression (17) [dimensionless]

β' exponent of Reynolds number in Expression (25) [dimensionless]

δ laminar film thickness; used in Equation (2) [mm]

ε void fraction of a fluidized bed [dimensionless]

ν kinematic viscosity of the solution [m^2/s]

ρ density of the solution [kg/m^3]

ρ_c density of the crystals [kg/m^3]

τ residence time [s]

Re particle Reynolds number = $\frac{V \cdot L}{\nu}$. In fluidized beds, this Reynolds number is based on the interstitial fluid velocity, V

Re_s in fluidized beds, the particle Reynolds number based on the superficial fluid velocity, V_s. Thus $Re_s = \frac{V_s \cdot L}{\nu}$

Sc Schmidt number = $\frac{\nu}{D}$

Sh Sherwood number = $\frac{k_m \cdot L}{D}$ or $\frac{k_d \cdot L}{D}$

Sh' Pseudo-Sherwood number = $\frac{K \cdot L}{D}$

LITERATURE CITED

1. J.W. Mullin
"Crystallization"
Butterworths, London.
(a) First edition, 1961.
(b) Revised second edition, 1972.

2. J. Nyvlt
"Industrial crystallization from solutions"
Butterworths, London, 1971.
(Original Czech edition, 1967)

3. R.F. Strickland-Constable
"Kinetics and mechanism of crystallization"
Academic Press, New York, 1968.

4. H.E. Buckley
"Crystal growth"
Wiley, New York, 1951.

5. A.W. Bamforth
"Industrial crystallization"
Leonard Hill, London, 1965.

6. R.C. Reid et al.
"Crystallization"
Ind. Eng. Chem. 62, 52 and 148 (1970).

7. V.W. Weekman Jr., editor
"Annual reviews of Industrial and Engineering Chemistry"
American Chemical Society, Washington, D.C.

8. A.A. Noyes and W.R. Whitney
"Rate of solution of solid substances in their own solution"
J. Amer. Chem. Soc. 19, 930 (1897).

9. W. Nernst
"Theorie der Reaktiongeschwindigkeit in heterogenen Systemen"
Z. Phys. Chem. 47, 52 (1904).

10. R. Marc
"Über die Kristallisation aus wässerigen Lösungen"
Z. Phys. Chem. 61, 385 (1908); 67, 470 (1909); 68, 104 (1909, 73, 685 (1910); 79, 71 (1912).

11. H.A. Miers
"The concentration of the solution in contact with a growing crystal"
Phil. Trans. A202, 492 (1904).

12. A.Berthoud
"Théorie de la formation des faces d'un cristal"
J. Chim. Phys. 10, 624 (1912).

13. J.W. Mullin and J. Garside
"The crystallization of aluminium potassium sulphate: a study in the assessment of crystallizer design data"
(a) "Single crystal growth rates"
Trans. Inst. Chem. Engrs. (London) 45, T285 (1967).
(b) Growth in a fluidized bed crystallizer"
Ibid. 45, T291 (1967).
(c) "Growth and dissolution rates"
Ibid. 46, T11 (1968).

14. M.M. Osman
"The precipitation and growth of nickel ammonium sulphate crystals in aqueous solution"
Ph.D. thesis, University of London, 1968.

15. J.W. Mullin, M. Chakraborty and K. Mehta
"Nucleation and growth of ammonium sulphate crystals from aqueous solution"
J. Appl. Chem. 20, 367 (1970).

16. J.W. Mullin and C. Gaska
"Potassium sulfate crystal growth rates in aqueous solution"
J. Chem. Eng. Data 18, 217 (1973).

17. J. Garside
"The concept of effectiveness factors in crystal growth"
Chem. Eng. Sci. 26, 1425 (1971).

18. A.A. Chernov
"Laminar-spiral growth of crystals"
Soviet Physics - Usp. 4, 116 (1961).

19. R. Cartier, D. Pindzola and P.F. Bruins
"Particle integration rate in crystal growth"
Ind. Eng. Chem. 51, 1409 (1959).

20. S. Amelinckx
"Sur la vitesse de croissance
des faces d'un cristal et la loi de
Bravais-Donnay-Harker"
J. Chim. Phys. 47, 213 (1950).

21. N.A. Clontz, R.T. Johnson, W.L. McCabe and R.W. Rousseau
"Growth of magnesium sulfate heptahydrate crystals from solution"
Ind. Eng. Chem. Fundam. 11, 368 (1972).

22. F. Rumford and J. Bain
"The controlled crystallisation of sodium chloride"
Trans. Inst. Chem. Engrs. (London) 38, 10 (1960).

23. J.C. Chu, J. Kalil and W.A. Wetteroth
"Mass transfer in a fluidized bed"
Chem. Eng. Progr. 49, 141 (1953).

24. J.C. Brice
"Diffusive and kinetic processes in growth from solution"
J. Cryst. Growth 1, 161 (1967).

25. A.W. Hixson and K.L. Knox
"Effect of agitation on rate of growth of single crystals"
Ind. Eng. Chem. 43, 2144 (1951).

26. G.C. Williams
cited by W.H. McAdams
"Heat transmission," third edition, p. 265.
McGraw-Hill, New York (1954).

27. U. Fasoli and G. Napoli
"Studio della velocita di cristallizzazione"
Chim. Ind. (Milan) 45, 1507 (1963).

28. T. Shirotsuka, K. Toyokura and S. Gotoh
"Rate of crystal growth from aqueous sodium chlorate solution"
Chem. Eng. Japan 3, 179 (1965).

29. P. Watts
"The measurement of crystal growth rates in stirred vessels"
Ph.D. thesis, University of Manchester, 1967.

30. S.H. Bransom, D.E. Brown and P. Watts
"The effect of impeller speed on crystal growth rates in a stirred vessel crystallizer"
Proceedings of the Symposium on Industrial Crystallization presented by the Inst. Chem Engrs. (London), 15-16 April 1969, p. 109.

31. S.H. Bransom, D.E. Brown and G.P. Heeley
"Crystallization studies in continuous flow stirred tank crystallizers: crystal growth rates"
Ibid. p. 24.

32. A. Tanimoto, K. Kobayashi and S. Fujita
"Overall crystallization rate of copper sulfate pentahydrate in an agitated vessel"
Intern. Chem. Eng. 4, 153 (1964).

33. T. Ishii
"Fundamental investigation on crystallization: performance and design of cone-type crystallizer"
Bull. Tokyo Inst. Technol., No. 67, p. 29 (1965).

34. A.D. Randolph and K. Rajagopal
"Direct measurement of crystal nucleation and growth rate kinetics in a backmixed crystal slurry"
Ind. Eng. Chem. Fundam. 9, 165 (1970).

35. J. Nyvlt
"The growth rate of citric acid crystals"
Paper I 3.2 of CHISA 72 Congress, Prague, September 1972.

36. M. Volmer
"Kinetik der Phasenbildung"
Steinkopff, Dresden, 1939.

37. W. Kossel
"Zur Energetik von Oberflächenvorgängen"
Ann. Phys. Lpz. 21, 457 (1934).

38. F.C. Frank
"The influence of dislocations on crystal growth"
Discuss. Faraday Soc. No. 5, p. 48 (1949).

39. W.K. Burton, N. Cabrera and F.C. Frank
"The growth of crystals and the equilibrium structure of their faces"
Phil. Trans. A243 , 299 (1951).

40. J.C. Brice
"The kinetics of growth from solution"
J. Cryst. Growth 1, 218 (1967).

41. P. Bennema
"Interpretation of the relation between the rate of crystal growth from solution and the relative supersaturation at low supersaturation"
J. Cryst. Growth 1, 287 (1967).

42. M. Ohara and R.C. Reid
"Modeling crystal growth rates from solution"
Prentice-Hall, Englewood Cliffs, N.J., 1973.

43. J.A.R. Bennett and J.B. Lewis
"Dissolution of solids in mercury and aqueous liquids: development of a new type of rotating dissolution cell"
AIChE J. 4, 418 (1958).

44. A.G. Mitchell and D.J. Saville
"The dissolution of aspirin and aspirin tablets"
J. Pharm. Pharmac. 19, 729 (1967).

45. C.H. Bovington and A.L. Jones
"Tracer studies of the kinetics of dissolution of lead sulphate"
Trans. Faraday Soc. 66, 2088 (1970).

46. W.L. McCabe and R.P. Stevens
"Rate of growth of crystals in aqueous solutions"
Chem. Eng. Progr. 47, 168 (1951).

47. P.D.B. Bujac
"The growth of ammonium aluminium sulphate crystals from aqueous solution"
Ph.D. thesis, University of London, 1969.

48. J.W. Mullin and J. Garside
"Velocity-voidage relationships in the design of suspended bed crystallizers"
Brit. Chem. Eng. 15, 773 (1970).

49. J.W. Mullin and C. Gaska
"Growth and dissolution of potassium sulfate crystals in a fluidized bed crystallizer"
Can. J. Chem. Eng. 47, 483 (1969).

50. S.H. Bransom
"Factors in the design of continuous crystallizers"
Brit. Chem. Eng. 5, 838 (1960).

51. S.H. Bransom and A.G.C. Palmer
"An experimental 'Oslo' crystallizer"
Brit. Chem. Eng. 9, 673 (1964).

52. W.L. McCabe
"Crystal growth in aqueous solutions"
Ind. Eng. Chem. 21, 30 (1929).

53. H.N. Rosen and H.M. Hulburt
"Growth rate of potassium sulfate in a fluidized-bed crystallizer"
Chem. Eng. Progr. Symp. Ser. 67, No. 110, p. 27 (1971).

54. T.F. Canning and A.D. Randolph
"Some aspects of crystallization theory: systems that violate McCabe's ΔL law"
AIChE J. 13, 5 (1967).

55. C.F. Abegg, J.D. Stevens and M.A. Larson
"Crystal size distributions in continuous crystallizers when growth rate is size dependent"
AIChE J. 14, 118 (1968).

56. M.B. Sherwin, R. Shinnar and S. Katz
"Dynamic behaviour of the well-mixed isothermal crystallizer"
AIChE J. 13, 1141 (1967).

57. S.H. Bransom and G.A.R. Trollope
"Mass transfer in a fluidized bed crystallizer"
AIChE J. 10, 842 (1964).

58. J.W. Mullin, J. Garside and C. Gaska
"A laboratory-scale fluidized bed crystallizer"
Chem. Ind. (London) p. 1704, 1966.

59. C. Gaska
"Nucleation and crystallization of potassium sulphate"
Ph.D. thesis, University of London, 1966.

60. T. Ishii
"Multi-particle crystal growth rates in vertical cones"
Chem. Eng. Sci. 28, 1121 (1973).

61. T. Shirotsuka, K. Toyokura and Y. Sekiya
"Method for calculating the height of the continuous classified bed type crystallizer."
Chem. Eng. Japan 4, 87 (1966).

62. J. Garside, C. Gaska and J.W. Mullin
"Crystal growth rate studies on potassium sulphate in a fluidized bed crystallizer"
J. Cryst. Growth 13/14, 510 (1972).

63. P.D.B. Bujac and J.W. Mullin
"A rapid method for the measurement of crystal growth rates in a fluidized bed crystallizer"
Proceedings of the Symposium on Industrial Crystallization presented by the Inst. Chem. Engrs. (London), 15-16 April 1969, p. 121.

64. J. Glasby and K. Ridgway
"The crystallization of aspirin from ethanol"
J. Pharm. Pharmac. 20, Suppl., 94S (1968).

65. H.J. Graeser III
"Growth of potassium sulfate seed crystals in a fluidized bed crystallizer: temperature and surfactant effects"
Ph.D. thesis, Northwestern University, Evanston, Illinois, 1972.

66. R.G. Paxton
"Crystal growth studies in a fluidized bed crystallizer"
M.Sc. thesis, University of Birmingham, 1968.

67. P.N. Rowe and K.T. Claxton
"Heat and mass transfer from a single sphere to fluid flowing through an array"
Trans. Inst. Chem. Engrs. (London) 43, T321 (1965).

68. M.B. Glaser and G. Thodos
"Heat and momentum transfer in the flow of gases through packed beds"
AIChE J. 4, 63 (1958).

69. G. Wulff
cited by Buckley [4], p. 121.

70. M. Bentivoglio
"An investigation of the rate of growth of crystals in different directions"
Proc. Roy. Soc. A115, 59 (1927).

71. J. Nyvlt, R. Rychly, J. Gottfried and J. Wurzelova
"Metastable zone-width of some aqueous solutions"
J. Cryst. Growth 6, 151 (1970).

72. P. Lumme and J. Peltonen
"Thermogravimetric studies: thermal stability and kinetics of decomposition of hydrated nickel (II) chloride, bromide, iodide, nitrate and sulphate"
Suom. Kemistilehti B37, 162 (1964).

73. J.W. Mullin
"Desupersaturation of seeded solutions in an agitated crystallizer"
Paper I 2.11 of CHISA 72 Congress, Prague, September 1972.

74. J.W. Mullin
"The measurement of supersaturation"
The Chem. Engr., p. 186, 1972.

75. M.A. Larson and S.A. Klekar
"Ammonium sulfate crystallization kinetics from in situ supersaturation measurements"
Paper to be presented at the A.I.Ch.E. 66th Annual Meeting, Philadelphia, November 1973.

76. A.W. Nienow, R. Unahabhokha and J.W. Mullin
"The mass transfer driving force for high mass flux"
Chem. Eng. Sci. 24, 1655 (1969).

77. R. Unahabhokha, A.W. Nienow and J.W. Mullin
"Effect of a receding interface and concentration-dependent physical properties on dissolution mass transfer rates"
Chem. Eng. Sci. 26, 357 (1971).

78. J.M. Coulson and J.F. Richardson
"Chemical Engineering," Revised second edition,
Pergamon, Oxford, 1964.

79. American Society for Testing and Materials
Standard Specification E11-70 for wire-cloth sieves for testing purposes.
"Annual book of A.S.T.M. standards, 1972," part 30, p. 88.

80. American Society for Testing and Materials
"Manual on test sieving methods"
A.S.T.M. Special Technical Publication 447,
Philadelphia, 1969.

81. K. Palmer
"Product size performance from Oslo-Krystal crystallizers"
Proceedings of the Symposium on Industrial Crystallization presented by the Inst. Chem. Engrs. (London), 15-16 April 1969, p. 190.

82. R.H. Hedrick
Struthers Scientific and International Corp., Warren, Pennsylvania, private communication, 1972.

83. J. Garside
"Crystallization and dissolution of aluminium potassium sulphate"
Ph.D. thesis, University of London, 1966.

84. J.F. Richardson and W. N. Zaki
"Sedimentation and fluidization"
Trans. Inst. Chem. Engrs.(London) 32, 35 (1954).

85. R.P. Ayerst
in discussion after the paper by Bujac and Mullin [63].

86. M.A. van Damme-van Weele
Ibid.

87. L.W. Oholm
"Diffusion rates of nickel and cobalt salts in aqueous solution"
(a) Chemical Abstracts 31, 2904 (1937).
(b) Finska Kemistsamfundets Medd. 45, 133 (1936).

88. A.W. Nienow
"Diffusivity in the liquid phase"
Brit. Chem. Eng. 10, 827 (1965).

89. J.H. Masliyah and N. Epstein
"Numerical solution of heat and mass transfer from spheroids in steady axisymmetric flow"
Progress in heat and mass transfer 6, 613 (Pergamon, New York, 1972).

90. E.G. Cooke
in discussion after the paper by Rumford and Bain [22].

91. C.F. Moore and A.G. Fowler
"LQF: Least squares fit routines"
Computer Centre, University of British Columbia, 1970.

92. C.W. Bunn
"Crystal growth from solution: concentration gradients and the rates of growth of crystals"
Discuss. Faraday Soc. No. 5, p. 132 (1949).

93. K. Palmer
Power-Gas Limited, Stockton-on-Tees, England, private communication, 1972.

94. D.A. Busch, J.R. Stone and G. Chiszar
"Production of refined nickel sulfate at ASARCO's Perth Amboy plant," in "Extractive metallurgy of copper, nickel and cobalt" (P. Queneau, ed.)
Interscience, New York, 1961.

95. W.F. Berg
"Crystal growth from solutions"
Proc. Roy. Soc. A164, 79 (1938).

96. S.P.F. Humphreys-Owen
"Crystal growth from solution"
Proc. Roy. Soc. A197, 218 (1949).

97. L. I. Kuznetsova and I.V. Gavrilova
"A laboratory method of growing crystals of pentaerythritol"
"Growth of crystals" (A.V. Shubnikov and N.N. Sheftal, eds.) 3, 203.
(Translated from Russian by Consultants Bureau, New York, 1962).

98. A.G. Mitchell and F. Jamali
Acta Pharmaceutica Suecica
To be published.

99. F. Jamali
"Recrystallization and dissolution of acetylsalicylic acid"
M.Sc. thesis, University of British Columbia, 1973.

100. G. Matz
(a) "Untersuchungsmethoden für die klassifizierende Kristallization" Wärme 70, 99 and 137 (1964)
(b) "Methods for the examination of classifying crystallizers" Technical Translation No. 1411, National Research Council, Ottawa, 1970.

101. J. Garside and J.W. Mullin
"Continuous measurement of solution concentration in a crystallizer" Chem. Ind. (London) p. 2007, 1966.

102. N. Bauer and S.Z. Lewin
"Determination of density"
Chap. 4 in Vol. 1, Pt. 1 of "Technique of organic chemistry" (A. Weissberger, ed.) Third edition, Interscience, New York, 1959.

103. R.C. Weast, editor-in-chief
"Handbook of Chemistry and Physics"
Fifty-third edition
C.R.C. Press, Cleveland, Ohio, 1972

104. E.W. Washburn, editor-in-chief
"International Critical Tables," Vol. 3, p. 69.
McGraw-Hill, New York, 1928.

105. R.W. Gelbach and H.M. Louderback
"Partial molal volumes of nickel sulfate solutions"
J. Amer. Chem. Soc. 64, 2379 (1942).

106. G.N. Dobrokhotov
"Yield of nickel sulfate by crystallization"
J. Appl. Chem. U.S.S.R. 23, 1191 (1950).

107. S. Alamelu and C.V. Suryanarayana
"A study of viscosity of aqueous solutions of nickel sulfate"
Acta Chim. Hung. 20, 339 (1959).

108. C.V. Suryanarayana
Central Electrochemical Research Institute, Karaikudi, India, private communication, 1971.

109. American Society for Testing and Materials
Standard method D445-72 for kinematic viscosity of transparent and opaque liquids.
"Annual book of A.S.T.M. standards," 1972, part 17, p. 181.

110. J. Wagner
"Untersuchungen über die innere Reibung von Flüssingkeiten"
Z. Phys. Chem. 5, 31 (1890).

111. D. Sri Rama Rao
"Viscosity of supersaturated solutions of some ionic crystals"
J. Indian Chem. Soc. 36, 188 (1959).

112. W.F. Linke, editor
"Solubilities of inorganic and metal organic compounds," fourth edition, Vol. 2, p. 1219
Van Nostrand, Princeton, N.J., 1958.

113. J.A. Hesek
J.T. Baker Chemical Co., Phillipsburg, New Jersey, private communication, 1971.

114. L. Borghijs
"Over het tetragonale, enantiomorfe nikkelsulfaat met 6 aq."
Natuurw. Tijdschr. (Ghent) 19, 115 (1937).

115. A.S. Foust et al.
"Principles of unit operations," p. 532.
Wiley, New York, 1960.

116. J. Happel
"Pressure drop due to vapor flow through moving beds"
Ind. Eng. Chem. 41, 1161 (1949).

117. C. Orr Jr. and J.M. Dalla Valle
"Fine particle measurement: size, surface and pore volume"
Macmillan, New York, 1959.

118. P. Groth
"Chemische krystallographie" Vol. 2, p. 423.
Engelmann, Leipzig, 1908.

119. D.A. Busch
American Smelting and Refining Co., South Plainfield, N.J., private communication, 1972.

120. J.A. Rutz
Harshaw Chemical Co., Cleveland,
Ohio, private communication, 1972.

APPENDIX A

SOME COMPOUNDS INITIALLY CONSIDERED FOR USE IN THE INVESTIGATION OF CRYSTAL GROWTH RATES

A.1 Sodium chlorate $NaClO_3$

The growth of this compound in a fluidized bed had already been studied to some extent [61]. It crystallizes in cubes under normal conditions and so gives the advantage of a very simple crystal shape. The shape is in fact geometrically regular and so all faces of the crystals grow at the same rate, another advantage. It is also an anhydrous compound so there is not the confusion over different concentration units which occurs with hydrated compounds. Sodium chlorate has industrial importance as a bleaching agent and as a herbicide.

The maximum metastable supersaturation is not well established, however. Bunn [92] quotes 7 wt% for single crystal growth from stagnant solutions but Shirotsuka et al. [61] used supersaturations of no more than 1 wt% in their continuous classified bed type crystallizer. Sodium chlorate is a somewhat hazardous compound as it is toxic, and it is also a powerful oxidizing agent which can explode when exposed to organic substances. This was a major factor in rejecting its use.

A.2 Ammonium iron alum (or "ferric alum") $(NH_4)_2SO_4 \cdot Fe_2(SO_4)_3 \cdot 24H_2O$

Among other alums, potassium alum and ammonium alum had been studied in detail by previous workers [83, 47].

As an alum, ammonium iron alum offered a simple crystal shape with geometric regularity, in this case an octahedron. The compound is used in volumetric analysis. However there were serious disadvantages. The solubility of the compound was not well-established and when in solution at any temperature significantly above room temperature, the ferric sulfate component of the alum was found to hydrolyse to produce ferric hydroxide.

A.3 Caesium alum $Cs_2SO_4 \cdot Al_2(SO_4)_3 \cdot 24H_2O$

As with other alums, this compound gave the advantage of a geometrically regular crystal shape. However, this particular alum has no industrial significance. Tests in an apparatus as described by Nyvlt [71] indicated that the maximum metastable supersaturation was very low.

A.4 Schönites (or Tutton salts) $M'SO_4 \cdot M_2'' SO_4 \cdot 6H_2O$

These make up a large family of salts. M' is a bivalent metal, for example, zinc, magnesium, copper, nickel. M" is monovalent and is usually potassium or ammonium. The crystal shape is usually relatively simple, being a parallelopiped but with some truncated corners. Test crystals grown in this work indicated that the potassium salts had less truncation of the corners than did the ammonium salts. Some schönites have industrial significance: nickel ammonium sulfate is used in electroplating, while ferrous ammonium sulfate is used in photography and in volumetric analysis.

The growth of nickel ammonium sulfate has been studied by

Osman [14], who reports a maximum metastable supersaturation in the presence of seed crystals of about 0.9 wt% hydrate. The growth rates of single crystals of some of the other salts in the family were studied in some very early work by Wulff [69], and later by Bentivoglio [70].

A.5 Pentaerythritol $C(CH_2OH)_4$

This compound gives a tetragonal bipyramidal crystal shape, which although not geometrically regular, does give the same growth rates on all faces. The compound is used industrially in electronics and in the preparation of resins, paints and explosives. However it is reported [97] that the aqueous solutions have a low maximum metastable supersaturation and that the crystals have low mechanical strength.

A.6 Acetylsalicylic acid ("Aspirin") $HOOC(C_6H_4)OCOCH_3$

In the early part of this study, the fluidized-bed crystallizer was used to prepare aspirin crystals by growth from solution in absolute ethanol under known conditions. These crystals were then used by other workers in a study on the mechanism of aspirin dissolution [98].

The system aspirin/ethanol was not seriously considered for use in quantitative work on growth rates in this study, because of the following disadvantages. The aspirin in solution quite quickly began to decompose to give salicylic acid. In this study, the solubility was found to be greater and the maximum metastable supersaturation much less than literature values [99, 64]. Also it was very inconvenient

to work with a non-aqueous system on a laboratory scale. Despite such problems, two studies of aspirin growth from ethanol in a fluidized-bed crystallizer have been reported [100, 64].

APPENDIX B

SPECIFICATIONS OF THE EQUIPMENT

B.1 Temperature controller

Type TCB 9, Fielden Electronics, Manchester, England. On-off type, switching differential ±0.025°C.

Sensor is a platinum resistance valued at 100 Ω at 0°C.

Canadian supplier: Kent Cambridge Ltd., Willowdale, Ontario.

Recommended replacement in future work: Haake Bros. Type TP41.

B.2 Specific gravity meter

Type SGM 1/1, Sangamo-Weston Controls, North Bersted, Bognor Regis, Sussex, England.

North American supplier: Martin Sweets Co., Louisville, Kentucky.

The principle of operation of the meter has been described by Garside and Mullin [101].

The output of the meter is a d.c. signal which is in the range 0-100 mV and which is almost linear with specific gravity (linearity correction available). For the small specific gravity ranges used in this work (0.02 S.G.) the non-linearity was negligible. The specific gravity range represented by 100 mV is variable from a minimum of 0.015 S.G.to a maximum of 0.4 S.G., when using the optimum plummet density.

Density of plummet used in the present work: 1.517 g/cm^3.

All wetted parts are of stainless steel, gold plate, Teflon or of epoxy resin with the composition given below:

Composition of epoxy resin used in the construction of the specific gravity meter. Supplied by C.I.B.A. (A.R.L.) Ltd., Duxford, Cambridge, England.	
Epoxy resin	MY 740
Hardener	HT 972
Mica flour filler	50 wt%

B.3 Centrifugal pump

Type D-11, Eastern Industries, Hamden, Connecticut.

Generates 20 psi at zero flow and 5 psi at 6.2 U.S. gal/min pumping water. Average N.P.S.H. = 2.5 psi.

All wetted parts are Type 316 stainless steel, graphite, Teflon or ceramic.

Crane "Type 9" rotary mechanical seal.

Totally enclosed explosion-proof motor, split phase induction type. It is difficult to vary the r.p.m. of this type of motor.

B.4 Water baths

Type NB with mercury contact thermo-regulator, Colora GmbH, Lorch, W. Germany.

Under the conditions of use in the present work, the half-wave amplitude of the variations of temperature of the water in the bath was approximately 0.05°C.

B.5 Ultrasonic generator

Series 300, Artek Systems, Farmingdale, N.Y. 19 mm diameter dip-type probe. Generating frequency 20 kHz, maximum output 300 W.

APPENDIX C

SPECIFICATIONS OF THE REAGENTS

C.1 Nickel sulfate α-hexahydrate

"Baker Analyzed" Reagent Grade from J.T. Baker Chemical Co., Phillipsburg, New Jersey. Meets or exceeds A.C.S. specifications.

	A.C.S. specifications (Maximum limits)	Manufacturer's actual lot analyses	
		Lot 36060	Lot 38934
Assay ($NiSO_4 \cdot 6H_2O$)	-	99.3%	99.0%
Insoluble matter	0.005%	0.002%	0.003%
pH of 5% solution at 25°C	-	3.8	4.3
Chloride (Cl)	0.001%	0.0005%	0.0005%
Nitrogen compounds (as N)	0.002%	0.002%	0.0005%
Substances not pptd. by $(NH_4)_2S$	0.10%	0.10%	0.04%
Cobalt and manganese (as Co)	0.003%	0.002%	0.001%
Copper (Cu)	0.005%	0.0005%	0.0003%
Iron (Fe)	0.001%	0.0005%	0.0005%

C.2 Water

Singly distilled in a still in which distillate contacted only borosilicate glass and Teflon. Specific resistance not less than 0.4 MΩ · cm. Stored in all-glass containers until used.

C.3 Methanol

Reagent Grade from various suppliers. All met A.C.S. specifications.

C.4 Benzene

Reagent Grade from various suppliers. All met A.C.S. specifications.

C.5 Carbon tetrachloride

Reagent Grade from various suppliers. All met A.C.S specifications.

APPENDIX D

PHYSICAL PROPERTIES OF NICKEL SULFATE SOLUTIONS

Precise data on saturation concentrations and on the relationship between solution specific gravity and concentration were needed for this work. Existing literature values did not cover the whole range of interest and in any case were not in good agreement, so new measurements were made as part of this work.

Viscosity has been measured too, so that crystal Reynolds numbers could be found. Finally, rough measurements were made on the terminal velocities of single crystals of nickel sulfate α-hexahydrate through a saturated solution at 40°C.

The specific gravity, viscosity and solubility measurements were all made using crystals from J.T. Baker Lot No. 36060 and distilled water. Both reagents are fully specified in Appendix C.

D.1 Specific gravity

The specific gravity bottle method [102] was used. The bottles were approximately 25 cm^3 in volume and had previously been calibrated precisely using distilled water. Solutions were prepared by weighing appropriate amounts of nickel sulfate α-hexahydrate and distilled water to the nearest milligram on an analytical balance and mixing (with heating if necessary) to dissolve. Any evaporation loss during dissolving was made up immediately prior to pouring the solutions into the bottles. All weighings were corrected for air buoyancy. Concen-

trations were expressed as wt% real hexahydrate, despite the fact that the manufacturer's assay for $NiSO_4 \cdot 6H_2O$ on the real hexahydrate was less than 100%. As shown later, the influence of hexahydrate purity variations on the properties studied in this work cannot be large at a purity level of 99% or better. The estimated limits of error on the concentration of solutions prepared by this weighing method were ± 0.01 wt% hexahydrate.

A Haake Bros. (Karlsruhe, W. Germany) Model FT water bath was used and the temperature within it measured by a Hewlett Packard (Palo Alto, Calif.) Model 2801A quartz thermometer. Allowing for bath temperature fluctuations and the calibration error of the thermometer, the limits of error on the temperature of the bottles were ± 0.03°C.

By repeating the bottle temperature equilibration and weighing steps on the bottle and contents but at successively higher temperatures, specific gravities at all temperatures could be obtained from just one filling of the bottle for each concentration.

When working in the supersaturated region, nucleation and crystallization of the solutions were always dangers, but by working reasonably fast, measurements could be made without appreciable nucleation on solutions supercooled by up to 10°C. To estimate repeatability, two runs were made on the same batch of solution for each concentration. To estimate reproducibility, two batches of solution made to the same concentration were run in a few cases. To estimate the effect of reagent purity on specific gravity, a few measurements were made on solutions made with nickel sulfate α-hexahydrate Lot No.

38934 which had a manufacturer's assay for $NiSO_4 \cdot 6H_2O$ of 99.0 wt%, as opposed to 99.3 wt% for Lot No. 36060.

Table D.I presents the original specific gravity results. Each reported value is the mean of the values from two runs on the same batch of solution. These duplicate results never differed by more than 0.0003 and in most cases differed by not more than 0.0002. Their pooled estimated standard error was 0.00006. The mean specific gravities from the runs on duplicate batches of solution never differed by more than 0.0002 so there were no significant between-batch differences.

No significant differences of specific gravity were found between solutions with the same concentration and temperature but prepared from the different lots of nickel sulfate having different purities.

By least squares fitting it was found that the equation

$$\begin{aligned} S.G._4^t = {} & 1.00229 + (0.6236 \times 10^{-2})\, c + (0.2311 \times 10^{-4})\, c^2 \\ & + (0.1608 \times 10^{-6})\, c^3 - (0.0135 \times 10^{-2})\, t - (0.0296 \times 10^{-4})\, t^2 \\ & - (0.0470 \times 10^{-4})\, ct + (0.0493 \times 10^{-8})\, c^2 t^2 \end{aligned} \qquad (D1)$$

in which c is the solution concentration in wt% hexahydrate and t is the temperature in degrees Centigrade, fitted the reported data with no statistically significant lack of fit throughout the ranges of temperature and concentration considered, namely 20 to 60°C and 0 to 60 wt% hexahydrate. The standard error of estimate of $S.G._4^t$ from the equation was 0.00017.

Table D.I Specific gravity of nickel sulfate solution as a function of concentration and temperature

The first column contains standard values of $S.G._4^t$ for pure water [103]. Entries which are underlined are in the supersaturated region.

t°C	c wt% hexahydrate									
	0.00	10.00	20.00	30.00	40.00	50.00	52.50	55.00	57.50	60.00
20.00	0.9982	1.0622	1.1317	1.2080	1.2919	1.3838				
25.00	0.9971	1.0609	1.1299	1.2060	1.2899	1.3815	1.4061			
30.00	0.9957	1.0591	1.1281	1.2039	1.2876	1.3791	1.4037	1.4287		
35.00	0.9941	1.0572	1.1259	1.2016	1.2852	1.3767	1.4012	1.4262		
40.00	0.9922	1.0553	1.1237	1.1994	1.2827	1.3742	1.3988	1.4238	1.4497	
45.00	0.9902	1.0531	1.1214	1.1969	1.2802	1.3716	1.3962	1.4211	1.4471	
50.00	0.9881	1.0509	1.1190	1.1944	1.2775	1.3689	1.3935	1.4184	1.4444	1.4705
55.00	0.9857	1.0485	1.1164	1.1917	1.2748	1.3661	1.3907	1.4157	1.4417	1.4679
60.00	0.9832	1.0460	1.1138	1.1889	1.2721	1.3633	1.3879	1.4128	1.4389	1.4650

Of course in fitting a single equation throughout the whole range of concentration, it is assumed that the curves of specific gravity against concentration have no abrupt changes of slope. An abrupt change might be expected, for instance, at the point of saturation. However there was no evidence in the present work for such a change in slope.

Comparing the results from this work with those from previous work, there is good agreement (present values higher by not more than 0.4%) with the values given in the International Critical Tables [104] for solutions of concentrations 1 to 30 wt% hexahydrate at temperatures near 20°C, and good agreement (present values lower by not more than 0.7%) with the values of Gelbach and Louderback [105] for solutions of concentrations 1 to 48 wt% hexahydrate at 25°C. There is poorer agreement (present values higher by not more than 2.8%) with the values of Dobrokhotov [106] for solutions of concentrations between 28 wt% hexahydrate and saturation at temperatures of 20 to 60°C. (Dobrokhotov also reported specific gravities at temperatures between 60 and 100°C). Dobrokhotov reported preparing his solutions, by weighing, from nickel sulfate containing 60.4 wt% anhydrous $NiSO_4$. Since the expected limits on wt% anhydrous $NiSO_4$ in the solid are 55.1 and 58.9, corresponding to pure heptahydrate and pure hexahydrate, respectively, Dobrokhotov's figure may itself be in error and may have led in turn to errors in his concentration calculations. With the values of Alamelu and Suryanarayana [107, 108] for solutions of concentrations up to 47 wt% hexahydrate between 30 and 60°C, there is good agreement (present values lower by not more than 0.3%) at concentrations up to 36 wt% hexahydrate but then

there is a rapid divergence above 36 wt% hexahydrate, so that at 47 wt% hexahydrate the present values are higher by 4.0%.

D.2 Viscosity

Cannon-Fenske viscometers were used to find the kinematic viscosities [109] and these were multiplied by the appropriate smoothed specific gravity values from Equation (D1), the numerical difference between specific gravity values and absolute density values in g/cm^3 being only 0.003% and therefore quite negligible here, to obtain the absolute viscosities. The viscometers were size 50 and had been calibrated using distilled water. Solutions were prepared in the same way as for specific gravity except that evaporation losses were not made up, so it is estimated that the concentrations may be up to 0.1 wt% hexahydrate in error. A Precision Scientific Company (Chicago, Ill.) "Temp-Trol" viscometer bath was used and the temperature within it again measured by the quartz thermometer, this combination giving limits of error of ± 0.03°C on the temperature of the viscometers.

By repeating the timings on the same viscometer but at successively lower temperatures, viscosities at all temperatures could be obtained from just one filling of the viscometer for each concentration, the variations in sample volume with temperature being negligible. The same duplication procedures were used as for the specific gravity experiments.

Table D.II presents the original kinematic viscosity results and the absolute viscosities derived from them. Each value is calculated from the mean of two timings on the same sample. These

Table D.II Kinematic viscosity and absolute viscosity of nickel sulfate solution as a function of concentration and temperature

For each concentration and temperature, the top figure is the kinematic viscosity in centistokes and the bottom one the absolute viscosity derived from it, in centipoises, except in the case of the first column, which lists standard values for the kinematic and absolute viscosities of pure water [103].

Entries which are underlined are in the supersaturated region.

t°C	c wt% hexahydrate									
	0.00	10.00	20.00	30.00	40.00	50.00	52.50	55.00	57.50	60.00
20.00	1.004 1.002	1.223 1.299	1.562 1.768	2.130 2.573	3.178 4.105	5.290 7.321				
25.00	0.893 0.890	1.084 1.150	1.380 1.560	1.872 2.258	2.756 3.554	4.503 6.221	5.194 7.303			
30.00	0.801 0.798	0.971 1.028	1.234 1.392	1.655 1.993	2.416 3.110	3.898 5.377	4.462 6.264	5.290 7.558		
35.00	0.724 0.719	0.876 0.926	1.109 1.249	1.473 1.770	2.137 2.746	3.398 4.679	3.871 5.424	4.569 6.517		
40.00	0.658 0.653	0.795 0.839	1.000 1.124	1.321 1.584	1.903 2.441	2.963 4.100	3.380 4.728	3.963 5.643	4.600 6.668	
45.00	0.602 0.596	0.726 0.764	0.910 1.021	1.194 1.429	1.709 2.188	2.645 3.628	2.983 4.165	3.481 4.947	4.026 5.825	
50.00	0.553 0.547	0.666 0.700	0.832 0.931	1.085 1.296	1.540 1.967	2.360 3.231	2.648 3.690	3.088 4.381	3.556 5.136	4.121 6.080
55.00	0.511 0.504	0.614 0.644	0.764 0.853	0.990 1.180	1.399 1.783	2.119 2.895	2.367 3.292	2.753 3.898	3.160 4.555	3.639 5.342
60.00	0.475 0.467	0.569 0.595	0.704 0.784	0.906 1.077	1.274 1.620	1.911 2.606	2.121 2.944	2.458 3.473	2.810 4.043	3.215 4.710

timings never differed by more than 0.3%. The mean timings from runs on duplicate batches of solution never differed by more than 0.7%. The contributions from viscometer calibration constants and from solution densities to the imprecision in the absolute viscosities were negligible. Full statistical treatment of the results was difficult because of the non-linear dependence of viscosity on concentration and temperature but since the main difference in duplicates was between batches, the standard error was estimated from the mean range of the means from duplicate batches, giving a value of 0.5% for the standard error and hence 3σ limits on viscosity of $\pm$ 1.5%.

Comparing the results from this work with those from previous work, there is good agreement (present results higher by less than 1%) with the values of Wagner [110] for solutions of concentration up to 12 wt% hexahydrate at 25°C, poorer agreement (present results mostly lower; maximum deviation 20% of present value) with the values of Sri Rama Rao [111] for supersaturated solutions of concentrations 56.55 and 53.72 wt% hexahydrate at temperatures between 30 and 60°C, and very poor agreement (present values higher by not more than 50% of present value) with the values of Alamelu and Suryanarayana [107] for solutions of concentration up to 47 wt% hexahydrate at temperatures between 30 and 60°C. Alamelu and Suryanarayana's absolute viscosity values would be increased by not more than 4% if they were re-calculated using the specific gravity values from the present work but this would do little to reduce the 50% difference between them and the present absolute viscosity values.

D.3 Solubility of the α-hexahydrate

The method was basically as outlined by Mullin [1b]. A suitable weight of solution (250 g) contained in a 250 cm^3 Erlenmeyer flask with a ground glass stopper was immersed in the Haake Bros. Model FT water bath. An excess of α-hexahydrate crystals (size about 800 μm) was added and the mixture stirred for 24 hours at about 100 r.p.m. by a magnetic stirrer. After an hour's settling time, two samples were then taken with a warmed pipette fitted with a stainless steel 38 μm screen, their specific gravities found at the temperature of saturation (the specific gravity bottles being held in the same water bath) and hence their concentrations obtained via Equation (D1). The remaining mixture was then stirred for another 12 hours, after which the sampling procedure was repeated.

As with the specific gravity experiments, the limits of error on the temperature were ± 0.03°C.

At each temperature the saturation point was approached from both supersaturated and undersaturated states. The initial solutions were of such concentrations that they were saturated at about 4°C above or below the test temperature.

To estimate the effect of reagent purity on solubility, one run was also made in which both the seed crystals and the crystals used to prepare the solution were from Lot 38934, which had an assay for $NiSO_4 \cdot 6H_2O$ of 99.0 wt%, as opposed to 99.3 wt% for Lot 36060.

After each run, the seed crystals were filtered off, washed of solution with methanol, rinsed with benzene, dried and examined under a low power microscope. In all cases they had retained

the characteristic green-blue colour and bipyramidal shape of the α-hexahydrate.

The solubility results are given in Table D.III, both as the specific gravity measurements on the saturated solutions and as the saturation concentrations derived from these via Equation (D1). The specific gravities of the two samples taken at the same time never differed by more than 0.0002 and the mean specific gravities of pairs of samples taken during the same run after 24 hours' stirring and after 36 hours' stirring never differed by more than 0.00025. A grand mean of these two was calculated for each run, and for the runs at the same temperature on initially supersaturated and initially undersaturated solutions these grand means never differed by more than 0.0002. The final reported specific gravity at saturation is the simple mean of all eight measurements at each temperature. The simple pooled estimated standard error (standard deviation of the mean) was 0.00004, this estimate then incorporating errors due to the different times of sampling and to different initial concentrations as well as to the specific gravity measurements themselves.

No significant effect was found of reagent purity differences on specific gravity at saturation.

The saturation concentrations derived from the final reported specific gravity values using Equation (D1) have an estimated standard error of 0.006 wt% hexahydrate, giving 3σ limits of $\pm$ 0.02 wt% hexahydrate.

By least squares fitting it was found that the equation

Table D.III Solubility of nickel sulfate α-hexahydrate in water as a function of temperature

Temperature t°C	$S.G._4^t$ of a solution saturated at t°C	saturation concentration c_t^* wt% hexahydrate derived from Equation(D1)
32.00	1.4013	52.35
35.00	1.4093	53.30
40.00	1.4233	54.95
45.00	1.4379	56.63
50.00	1.4534	58.38
53.00	1.4629	59.43

$$c_t^* = 43.1726 + 0.2559\ t + 0.0009611\ t^2 \qquad (D2)$$

in which t is the temperature in degrees Centigrade and c_t^* is the saturation concentration of the solution at t°C in wt% hexahydrate, fitted the data with no statistically significant lack of fit over the range of temperature considered, namely 32 to 53°C. The standard error of estimate of c_t^* from the equation was 0.009 wt% hexahydrate.

The solubility results from this work were compared with those from previous work. Linke [112] reviewed work up to 1958, commenting that there was only fair agreement (differences of 1 to 3%) between the results of several individual workers, but presenting a set of "most probable" values. The present results are in good agreement with these values for the temperature range 32 to 53°C (difference of 0.6% at 53°C but less than 0.4% in the range 32 to 50°C), thereby helping to confirm Linke's estimated values.

Since Linke's review, Alamelu and Suryanarayana [107] have published solubility figures which are higher than those from this work by not more than 1.2% in the range 32 to 53°C. However doubt is cast on their data, at least at the lower end of this temperature range, by their failure to report confirmation of the identity of the solid phase in their solubility tests, particularly as they report that their original reagent solid was the heptahydrate rather than the α-hexahydrate. Linke reports that metastable solubilities in which the solid phase remains as heptahydrate can be achieved at up to 40°C.

D.4 Terminal velocity of single α-hexahydrate crystals at 40°C

The terminal velocity is useful in crystallizer design when estimating the liquor circulation rate necessary to suspend the growing crystals.

Crystals without irregularities were selected from sets of seed crystals which had been closely sized using the full U.S.A. Standard Sieve Series. The crystals were allowed to settle one at a time through the 50 mm I.D. crystallization section of the fluidized-bed crystallizer, which contained an accurately saturated solution at 40°C. Between tests, the solution was circulated to maintain temperature control, but the solution was stationary during the tests. The times required for a crystal to fall through 250 mm and 500 mm below the same starting point were measured to 0.1 s, using stopwatches. The crystals fell through about 500 mm of solution before reaching the starting point. Any test in which the crystal was observed to move to the wall instead of falling centrally down the pipe was discounted.

At least ten tests were made for each crystal size and the average settling time was calculated, together with its standard error. The terminal velocities then calculated from the two different distances were not significantly different, indicating that the terminal velocity V_{t50} had indeed been reached. The wall correction used by Mullin and Garside [48] was applied to calculate in addition the terminal velocity in an infinite medium, $V_{t\infty}$. The reported crystal size was the arithmetic average of the adjacent sieve sizes between which the crystal size fell. The crystals were observed to settle with their long axes oriented horizontally. Figure D.1 shows V_{t50} and $V_{t\infty}$

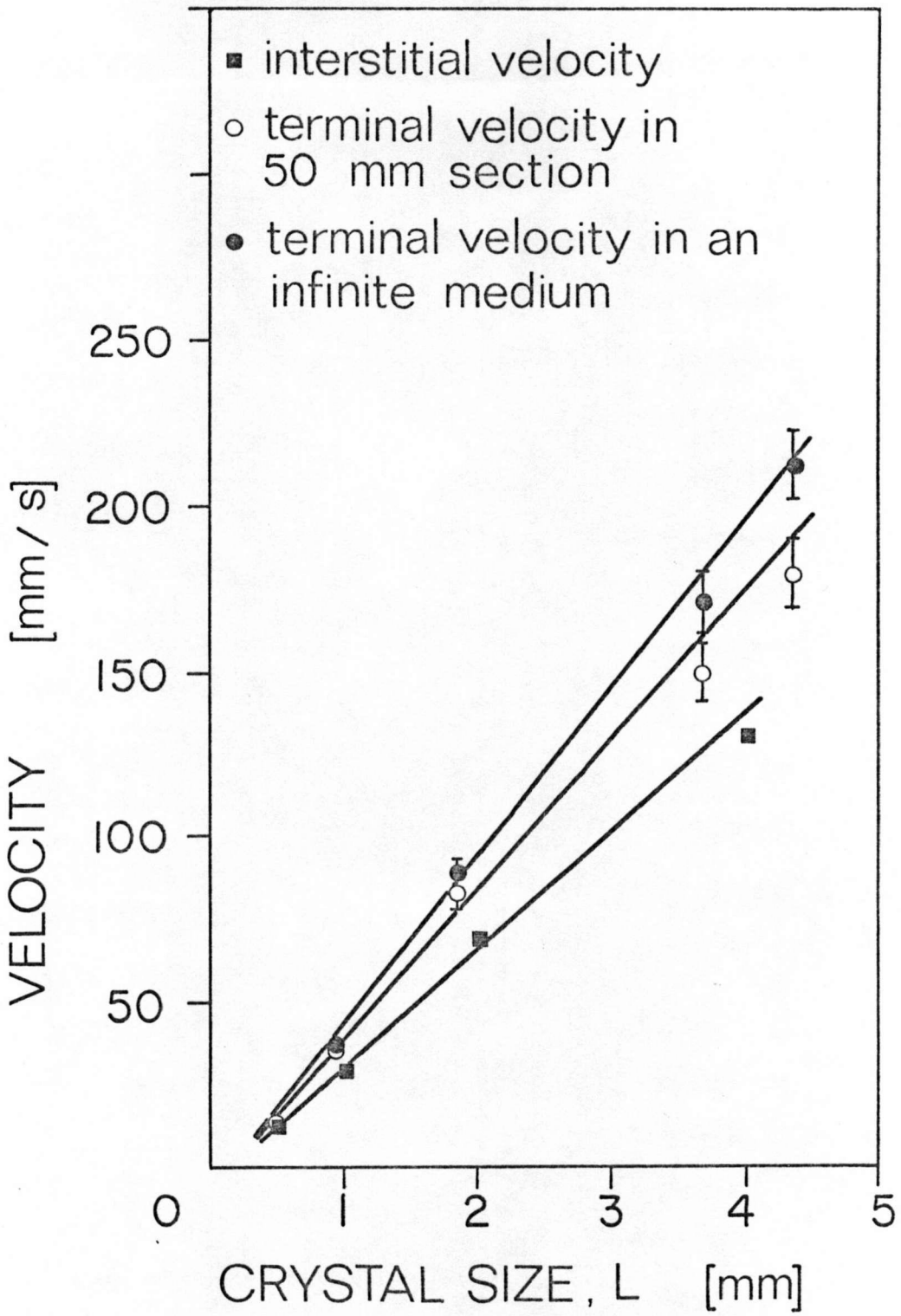

Figure D.1 Interstitial solution velocities during the Batch Method and single crystal terminal velocities, for different crystal sizes at 40°C. Bars show the 95% confidence limits when these extend beyond the point symbols

plotted as functions of crystal size. Also shown, for comparison, are the interstitial solution velocities during the Batch Method, found from the orifice meter measurements (Section 6.3). The lines in Figure D.1 are weighted linear least squares fits.

The terminal velocity measurements made here are not considered highly accurate. The settling times were quite short, in many cases only a few seconds, so systematic errors may have entered at the start and finish of the timings. Also the method of crystal size calculation permits systematic errors of up to 4% [79]. Bamforth [5, Figure 77] presents terminal velocities of single nickel sulfate α-hexahydrate crystals which are roughly half of those reported here. However he does not specify the diameter of the settling chamber nor the temperature used. Temperature differences may account for some of the observed difference in terminal velocity, although the viscosity of saturated nickel sulfate solutions is relatively insensitive to temperature (Appendix D.3). Garside [83] found little effect of temperature on the terminal velocity of single potassium alum crystals, and little effect of temperature on interstitial velocity was found in the present work (Section 6.3).

APPENDIX E

THE DEVELOPMENT OF A QUANTITATIVE PRODUCT CRYSTAL WASHING TECHNIQUE

After the product crystals had been drained from the crystallizer into the 600 cm^3 jacketed Buchner funnel at the end of an experiment and had been filtered of most of the solution which accompanied them, they were still wet with the remaining solution. If left unremoved, this solution would have caused an unwanted increase in the weight of the crystals due to further crystallization and eventually would have caused serious caking together of the crystals. Therefore it was necessary to wash off this remaining solution quantitatively, immediately after filtration.

The ideal washing liquid would have been miscible with the solution but inert to the crystals themselves and also volatile, for quick drying after the washing. However, the best real liquid which could be found was methanol, which was miscible with the solution and was volatile, but in which the crystals had a slight solubility [Reference 103 gives 12.5 g/100 cm^3].

Despite this solubility, it was found that by the following method washing could be effected with negligible weight change to the crystals. Immediately after filtration, while the crystals, damp with solution, were still under suction in the Buchner funnel, a controlled volume of methanol at room temperature was sprayed over them. This was immediately followed by a thorough spray rinse with

benzene, the benzene also being at room temperature. (Benzene is miscible with methanol but fully inert to the crystals.) The rate of suction throughout was such that no volume of methanol or benzene could build up above the sintered glass during spaying. Finally the suction was switched off and the crystals, now damp only with benzene, were given a slow air drying. Rapid drying was avoided because it could cause cooling of the crystals below the moisture dew point of the surrounding air: this led to water vapour condensing on the crystals, causing serious caking.

The time between beginning methanol spraying and beginning benzene spraying was made as short as possible, typically ten seconds. A top-outlet Teflon wash bottle, inverted, was used to give rapid reproducible delivery of the methanol. Two 2000 cm^3 collecting flasks in a T arrangement with a three-way stopcock were used with the Buchner funnel. The first flask collected the nickel sulfate solution from the initial filtration, for re-use. The vacuum was then quickly switched to the other flask, and the Buchner funnel quickly transferred as well, for the washing and rinsing operations. The second flask thus collected a mixture of the small amount of nickel sulfate solution left after filtration, together with the methanol and benzene. This mixture was discarded. The whole procedure, from draining the crystals and solution into the funnel, through filtration, transfer between flasks, washing and rinsing, was completed in forty seconds.

The mechanism by which a controlled volume of methanol washed the crystals without appreciable change in their weight was believed to be as follows. The optimum methanol volume was that volume which

was just sufficient to wash away all the viscous solution left coating the crystals after filtration: if a larger methanol volume had been used, the methanol sprayed on after all the solution was washed away would have started to dissolve the then "unprotected" crystals. A microscopic examination of the crystal surfaces after washing, rinsing and drying, showed none of the etching or rounding of edges which would be expected if partial dissolution had occurred. (When similar washing and rinsing operations were conducted on initially-dry crystals, these did suffer a significant weight loss, and etching and rounding of edges were evident.)

To determine the optimum volume of methanol for washing, pre-heated crystals were put into the Buchner funnel, which was water-jacketed at the appropriate temperature, and with suction already on, 300 cm^3 of saturated solution at that temperature were immediately drained from the crystallizer into the funnel containing the crystals. As soon as this solution had been drawn off (ten seconds) the washing and rinsing operations on the damp crystals were begun. The washing and rinsing operations were repeated with different volumes of methanol. The optimum volume of methanol was then that volume which produced the minimum weight change in the crystals during washing.

In all experiments by the Batch Method, the volume of methanol used for each washing was 40 cm^3. This volume had been found to wash with a weight change not exceeding 15 mg any weight of crystals between five and ten grams, of any crystal size between 0.5 and 4.0 mm at all the temperatures checked (up to 32°C).

During the preparation of seed crystals and during growth

experiments by the Continuous Method, weights of crystals much larger than ten grams had to be washed, and larger volumes of methanol were then used. Although detailed tests for the optimum volume were not made in these cases, where absolutely quantitative washing was not essential, nevertheless a good estimate of the optimum volume could be made by noting the minimum volume necessary to prevent caking (which occurred if residual solution was left on the crystals from incomplete washing) and by microscopic inspection of the crystal surfaces after washing, rinsing and drying for evidence of dissolution. Thus when a batch of newly-grown seed crystals of about 100 g were washed, 60 cm^3 of methanol were used and when about 500 g of product crystals were washed after an experiment by the Continuous Method, 150 cm^3 were used.

The volume of benzene used in rinsing was not critical but in practice not less than 100 cm^3 were used on crystal weights around 10 g and up to 250 cm^3 on crystal weights of 500 g. The benzene was sprayed from a conventional all-glass wash bottle equipped with a polyethylene squeeze bulb.

APPENDIX F

A PROCEDURE FOR REMOVING CRYSTAL DUST FROM THE SURFACES OF THE CRYSTALS

As explained in Section 5.6, the presence of crystal dust (generated mostly by sieving operations) on the surfaces of the seed crystals was believed to lead to increased nucleation. The following method was used to remove this dust when necessary. Seed crystals which had received this treatment then brought about much less nucleation when grown and thus the maximum useable supersaturation could be significantly increased.

The crystals with dusty surfaces, preheated to 40°C, were allowed to settle through an accurately saturated stagnant solution in the crystallizer at 40°C. They were then drained out, washed, rinsed and dried in the normal way (Appendix E). The initial and final weights of the crystals never differed by more than 0.4%. (This is an indication that the solution did not transfer mass to or from the crystals and also that the washing operation caused no great weight change. Hence the crystal dust removal procedure caused no size change either. The weight loss due to the removal of the surface dust itself was certainly negligible.) After drying, the crystals were inspected by microscope. Although most of the surface dust had been removed, no etching of the surfaces or serious rounding of the edges was ever observed.

The removal of the surface dust was believed to occur mainly by a surface tension mechanism as the crystals entered the solution,

because dust could usually be seen on the surface of the solution after the crystals had settled through. It is possible that there was also some mechanical sweeping action of the solution across the crystal surfaces as the crystals settled through the solution.

APPENDIX G

THE PREPARATION OF SEED CRYSTALS

The properties of the seed crystals are important in any experiments on crystal growth and this is particularly true of the present type of experiment, in which the increase of crystal size during a growth experiment was only about 20% of the size of the seed crystals. Thus the average crystal shape and hence the average crystal surface area during an experiment were largely defined by the shape of the seed crystals. Also the surface characteristics of the seed crystals (dislocation density, etc.), which may themselves have been governed by the conditions under which the seed crystals were grown, may influence any growth which is subsequently added to that surface.

It follows then that the seed crystals should be prepared under known, highly controlled conditions and their properties, particularly shape and surface characteristics, should be thoroughly investigated. In line with this reasoning, an initial attempt was made to prepare seed crystals directly from crystals nucleated under controlled conditions in the present fluidized-bed crystallizer. However it was found impossible to control the numbers of nuclei forming after nucleation was initiated. Also microscopic inspection revealed that these nuclei showed many twins, agglomerates and other irregularities of form. Therefore this attempt was abandoned. In

the method which was subsequently adopted, seed crystals were grown in the crystallizer from "sub-seeds," which were smaller crystals selected from among the crystals received from the manufacturer (Appendix C) and prepared, before being grown to seed crystals, as detailed below.

When received, the crystals from the manufacturer were badly caked together (Figure G.1). As an initial stage in the selection of "sub-seeds," the crystals from the manufacturer were quantitatively decaked as follows. It was intended to use as "sub-seeds" only crystals in the size range 600-710 μm from the manufacturer's Lot No. 38934, one of two different lots from which crystals had been received for this work (Appendix C). Therefore all the crystals from this lot were first given a partial decaking by gentle pressure with a pestle (Figure G.2), and were then sieved on a 600 μm sieve (U.S.A. Standard Sieve No. 30). The oversize, a mixture of single crystals and small caked clumps (Figure G.3), were then subjected to ultrasonic action to complete the decaking process. (If the crystals were used as "sub-seeds" without being completely decaked, the resulting seed crystals included many with unacceptably irregular shapes.) Fifty grams at a time were stirred in carbon tetrachloride (a dense and inert suspending medium) by a magnetic stirrer, at the minimum rate necessary for complete suspension, and the suspension was sonated at a rate of 300 W for five minutes with a dip-type ultrasonic generator (Appendix B). The 250 cm^3 stirring vessel was provided with a cold water cooling jacket and there was no appreciable rise in the temperature of the suspension. After sonation, the crystals were filtered of carbon tetrachloride (Appendix C) and allowed to dry

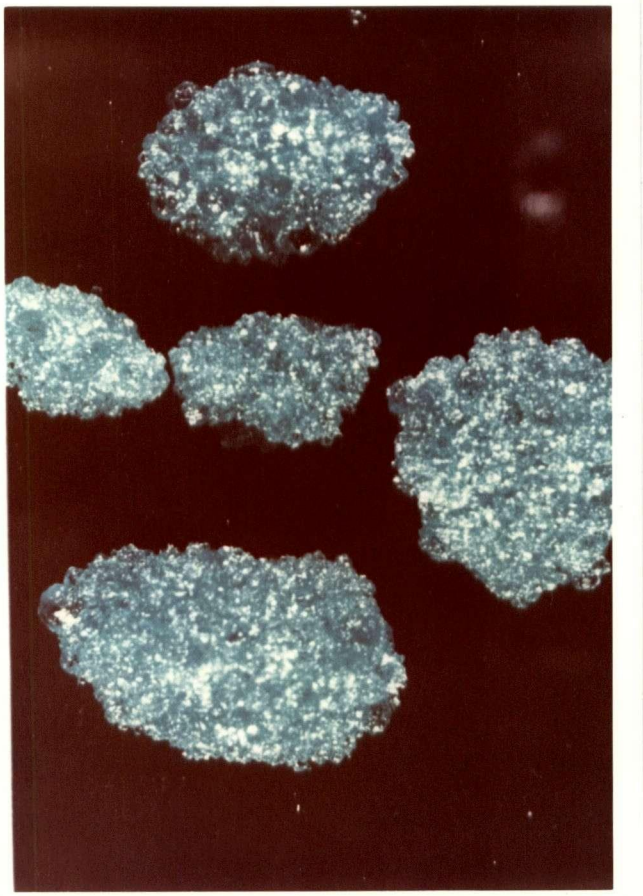

Figure G.1 Caked crystals, as received from the manufacturer

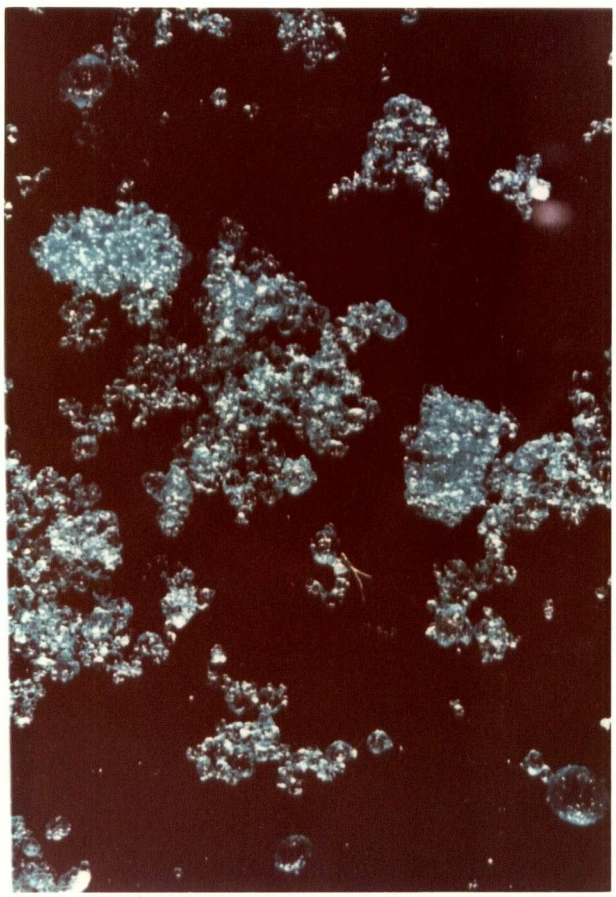

Figure G.2 Crystals from the manufacturer after partial de-caking with a pestle

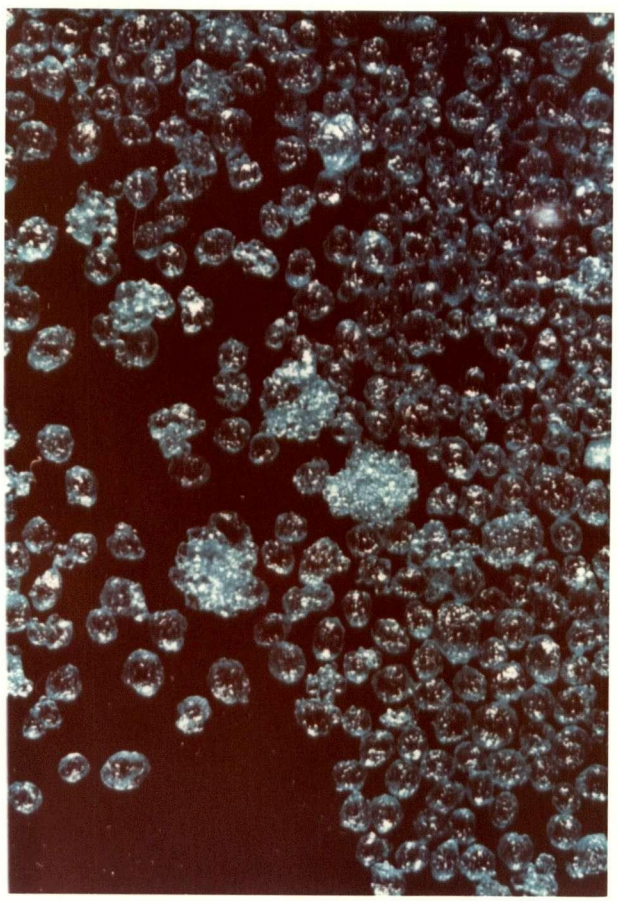

Figure G.3 The size fraction above 600 μm, after partial decaking but before sonation

slowly in the air. They were by then completely decaked (Figure G.4). The ultrasonic treatment caused no observable damage to the crystals. When dry, they were given a thorough sieving according to A.S.T.M. recommendations [80] and the final size fraction 600-710 μm, by then all single crystals (Figure G.5), was used as "sub-seeds" for the growth of seed crystals. Once prepared, the "sub-seeds" never again caked.

The decision to use the size fraction 600-710 μm from Lot No. 38934 as "sub-seeds" was based on several factors. Firstly it was desirable for all "sub-seeds" to be from the same one manufacturer's lot as the average crystal shape differed somewhat between lots: each lot had been crystallized by the manufacturer on separate occasions using a simple batch crystallizer [113]. Secondly it was desirable for the "sub-seeds" to be considerably smaller than the seeds into which they were grown, thus allowing ample opportunity for adjustments of shape (such as growing-out of undesirable secondary faces) to occur during growth, before the final seed crystal size was reached. This was particularly necessary in the present work because the crystals from the manufacturer were highly rounded (probably because of partial dissolution during a purifying wash with undersaturated liquor as a final stage of manufacture) and required considerable growth before they took on a fully smooth-surfaced and sharp-edged shape with only small secondary faces. A third consideration was that of the proportion of "sub-seeds" showing irregularities of shape. Even after complete decaking, some "sub-seeds" showed irregularities, usually twinning.

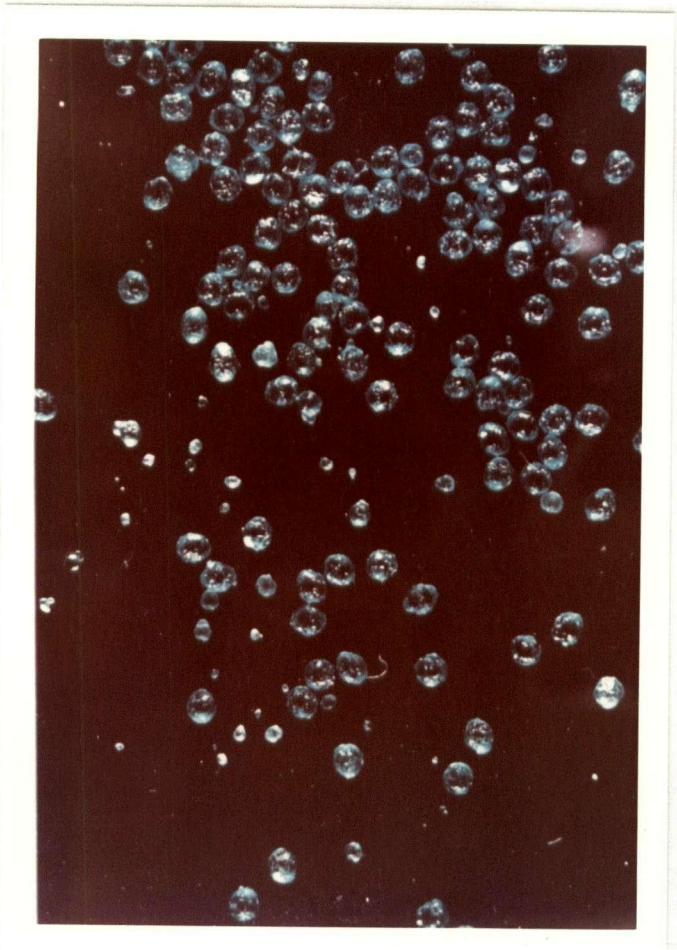

Figure G.4 The size fraction originally above 600 μm, after sonation, but before final sieving

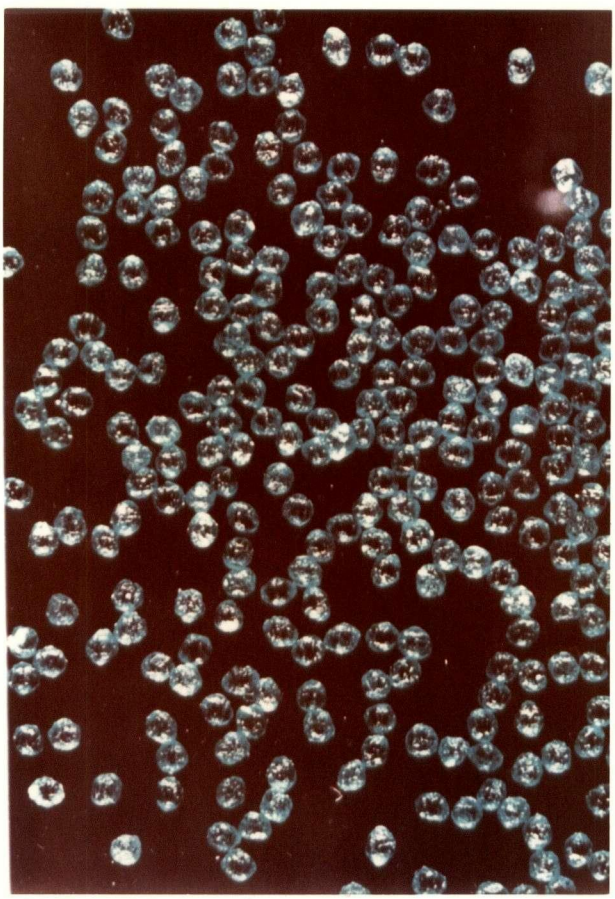

Figure G.5 The finished "sub-seeds": the size fraction 600-710 μm after sonation and final sieving

These could have caused errors in the overall crystal surface area, which was calculated assuming a fully regular crystal shape (Appendix J). The proportion of crystals showing significant irregularities of shape could be reproducibly estimated from ten minutes' hand sorting. The proportion of irregular crystals within a given size range was smaller as crystal size increased. For example, with Lot No. 38934, about 30 wt% showed irregularities at size 600-710 μm and about 45 wt% at size 500-600 μm, while with Lot No. 36060, about 40 wt% showed irregularities at size 600-710 μm and about 50 wt% at size 500-600 μm. Thus from this point of view larger "sub-seeds" were more desirable than smaller "sub-seeds" and "sub-seeds" from Lot No. 38934 were more desirable than "sub-seeds" from Lot No. 36060. A fourth and last consideration was that of availability. "Sub-seeds" in the size range 600-710 μm from Lot No. 38934 were the largest ones which were available in sufficient numbers, as most of the crystals from the manufacturer were much smaller (mode size range 300-355 μm for Lot No. 38934 and 250-300 μm for Lot No. 36060). Thus Lot No. 38934 was used to provide the "sub-seeds" because it offered a lower proportion of irregular crystals at size 600-710 μm and also better availability. Although only crystals from Lot No. 36060 had been used for the main measurements on physical properties, checks had been made (Appendix D) that crystals from Lot No. 38934 gave no significant differences in these measurements.

Standard conditions were used for all the runs in which prepared "sub-seeds" were grown into seed crystals for both crystal

growth and dissolution experiments in the fluidized-bed crystallizer. All runs were made at 40°C with an initial supersaturation of 1.34 wt% hexahydrate (that is, a supercooling of 4°C). A limit of 25% of the initial value was set on the permissible fall-off of supersaturation, so that all the growth would occur not only at the same temperature but also at similar supersaturation levels and hence at similar rates, thus hopefully producing final surfaces having similar microscopic characteristics. The proportion of seed crystals showing irregularities of shape was always observed to be the same as the proportion for the sub-seeds from which they had been grown. Figure G.6 shows some typical finished seed crystals.

Most of the main experiments (Section 5) used seed crystals which were in the size ranges 850 μm - 1.00 mm or 1.00 - 1.18 mm and these could be grown from "sub-seeds" of 600-710 μm in a single stage. (The maximum duration of a stage was determined by the 25% limit on the percent fall-off of supersaturation, the fall-off often being due mainly to nucleation.) To grow the larger seed crystals (up to 4.00 - 4.75 mm) one or more extra growth stages were needed.

In the preparation of seed crystals of sizes 425-500 μm and 500-600 μm only, an additional step was necessary. As with the larger seed crystals, a starting "sub-seed" size of 600-710 μm was desirable, because this size range had a low proportion of irregular crystals. However, because of limited stocks of "sub-seeds" of size 600-710 μm, "sub-seeds" from the same lot (No. 38934) but of size 500-600 μm (with 45 wt% irregular)were substituted in the case of these seeds only. These were partially dissolved down to size 300-

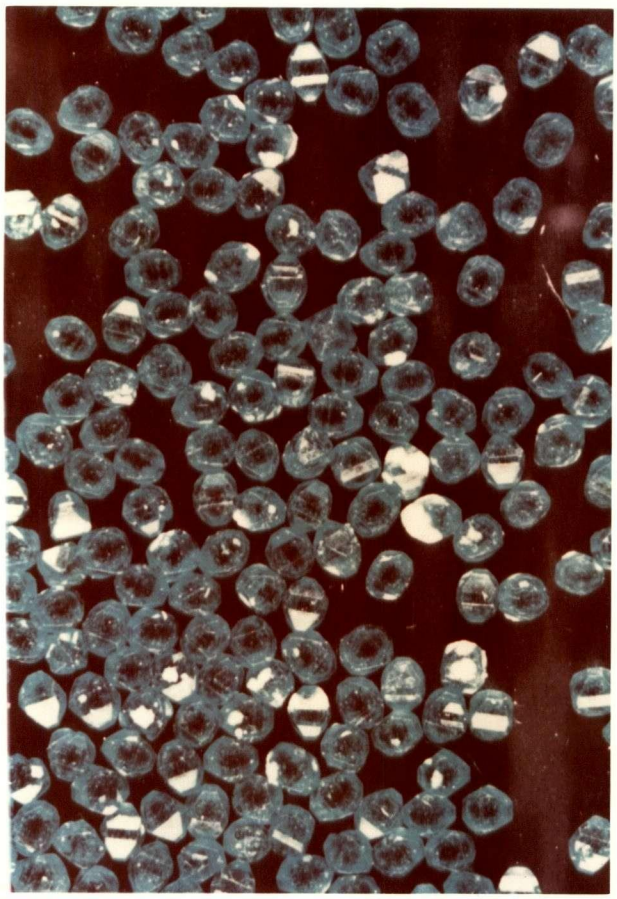

Figure G.6 Typical finished seed crystals

355 μm in the crystallizer at 40°C with a solution of saturation temperature 36°C, and then later regrown under the standard conditions to sizes 425-500 μm and 500-600 μm. The partial dissolution did not affect the proportion of crystals showing irregularities. These seeds could not have been prepared by direct growth from "sub-seeds" of sizes below 425 μm because such "sub-seeds" had a very high proportion of irregular crystals.

Newly-grown seed crystals, after being washed, rinsed and dried by the usual method (Appendix E), were sieved according to A.S.T.M. recommendations [80] to assign them to their final size range. After observing the first few seed growth runs, the growth time could be adjusted to give seed crystals whose sizes were almost all within the desired range. To minimize the amount of surface dust generated during sieving (see Section 5.6), the newly-grown seed crystals were sieved by hand. Nevertheless the A.S.T.M. sieve test end point criterion was satisfied within one or two minutes' sieving, probably because of the thorough sieving on the Ro-tap shaking machine given to the decaked "sub-seeds" before they were grown to seed crystals. (It is remarkable that, in the case of the "sub-seeds" only, even this vigorous machine sieving failed to generate much surface dust, as indicated by both visual observation and by the absence of nucleation when growing the "sub-seeds" afterwards. This was probably due to the "sub-seeds" being very rounded and thus more abrasion-resistant. When attempts were made to sieve sharp-edged crystals by machine, large amounts of surface dust were always generated.)

With each seed crystal size range, quite a few seed growth runs were needed in order to assemble a sufficient number of seed crystals for all the main experiments planned. After sieving, the seed crystals produced in these separate runs were all added together and then thoroughly mixed by several passes through a sample splitter, the two resulting halves of the mixture being added together again after each pass. Thus there should have been no overall differences in the seed crystals of a given size used in any of the main experiments.

As explained above, 30 wt% of the 600-710 μm "sub-seeds" and in turn of the seed crystals 850 μm - 1.00 mm and larger, showed significant irregularities of shape. An attempt was made to reduce this proportion by elutriation in the Stokes flow regime [cf. Rosen and Hulburt, 53] in a separate apparatus, using a viscous oil, but evidently the irregularities of shape were not great enough to permit a significant separation of regular and irregular crystals by this method. To estimate the effect of these irregularities on the crystal surface area and hence on the calculated growth rate, several batch growth experiments were made with 100% regular 850 μm - 1.00 mm seed crystals, which had been separated by hand sorting. Growth rates calculated from these experiments never differed by more than 2% from the corresponding rates calculated when using the normal seeds with 30 wt% irregular.

Nickel sulfate α-hexahydrate crystals are optically active [114]. Nevertheless the laevorotatory and dextrorotatory crystals have identical shapes, as the asymmetry of internal structure which causes the optical activity does not in their case affect the external

shape of the crystals. There is no reason to suppose, nor evidence to indicate, that the laevorotatory and dextrorotatory crystals grow at different rates. Even if they did so, all sets of seed crystals grown under normal circumstances would be expected to be a 50:50 mixture by number of the two forms and thus would give rise to measured growth rates which were reproducible between sets of crystals, even though these measured growth rates were actually the average values of the different true growth rates of the two forms.

APPENDIX H

A REVIEW OF THE GENERAL RELATIONSHIPS BETWEEN PARTICLE SHAPE, VOLUME AND SURFACE AREA

This appendix reviews the background to methods for obtaining the overall surface area of a collection of crystals (or other particles) when starting from a knowledge of the overall weight of the collection.

Consider first a single particle of any shape. The quantities called the "surface area shape factor," f_s, and the "volume shape factor," f_v, are defined by the equations:

$$\text{surface area of particle} = f_s \cdot L^2 \tag{H1}$$

$$\text{volume of particle} = f_v \cdot L^3 \tag{H2}$$

where L is some length parameter of the particle. The choice of a suitable dimension to express L is discussed below. The "overall surface-volume shape factor," F, is then defined by

$$F = f_s/f_v \tag{H3}$$

From Equation (H2) it follows that

$$\text{weight of particle} = \rho_c f_v \cdot L^3 \tag{H4}$$

Hence, on dividing Equation (H1) by Equation (H4),

"specific surface" (=surface area per unit weight)

$$= \frac{f_s}{f_v} \cdot \frac{1}{\rho_c \cdot L} = \frac{F}{\rho_c \cdot L} \qquad \text{(H5)}$$

If we now apply this formula to a collection of particles, whose overall weight is W, the overall surface area of the collection, A, is given by

$$A = W \left(\frac{F}{\rho_c \cdot \bar{L}} \right) \qquad \text{(H6)}$$

where $\bar{L}$ is now the effective average length parameter of the collection. When applying this formula, finding values for W and ρ_c is usually trivial, but finding values for F and $\bar{L}$ is more difficult.

Consider first the problem of finding $\bar{L}$. There are two stages: firstly, the selection of a suitable length parameter L and secondly, the selection of a suitable average $\bar{L}$, in terms of this parameter, to represent all the different sizes L_i present in the collection. The first stage may be examined by considering a collection of particles which is monodisperse as far as the sizing method in question is concerned. The sizing method most commonly used on crystals is sieving. In this case, "monodisperse" means that all the particles have effective sizes between two adjacent sieve sizes and an appropriate value of L is the average (usually the arithmetic average) of these sieve sizes. Other methods of obtaining a measure of the particle size for an effectively monodisperse collection of particles are discussed by

Mullin [1b]. Secondly, consider finding an overall average particle size $\bar{L}$ for a collection of particles which is polydisperse. Although there are several methods of averaging size for a polydisperse collection [1b, 115], the most appropriate average size in the present case, as in all problems of interphase mass transfer, is the "specific surface" average size, also known as the "volume-surface" average size [13b], "Sauter" average size [115] and "reciprocal" average size [116]. From Equation (H5), we can write as a definition of the specific surface average size, $\bar{L}_s$,

$$\text{specific surface of whole collection} = \frac{\bar{F}}{\rho_c \cdot \bar{L}_s} \tag{H7}$$

where $\bar{F}$ is the overall shape factor averaged over the whole collection. But also,

$$\text{specific surface of whole collection} = \frac{\text{surface area of whole collection}}{\text{weight of whole collection}}$$

$$= \frac{\sum_i n_i f_{si} L_i^2}{\rho_c \sum_i n_i f_{vi} L_i^3} \tag{H8}$$

where n_i is the number of particles of effective size L_i.

Hence

$$\frac{\bar{F}}{\bar{L}_s} = \frac{\sum_i n_i f_{si} L_i^2}{\sum_i n_i f_{vi} L_i^3} \tag{H9}$$

Assuming all f_{si} are the same and all f_{vi} are the same, which is a good assumption in the present case (Table J.I), and recalling Equation (H3),

$$\bar{L}_s = \frac{\sum_i n_i L_i^3}{\sum_i n_i L_i^2}$$

$$= \frac{\sum_i w_i}{\sum_i (w_i/L_i)} = \frac{W}{\sum_i (w_i/L_i)} \qquad \text{(H10)}$$

where w_i is the weight of particles of effective size L_i. It is this specific surface average size $\bar{L}_s$ which is then finally substituted in the formula

$$A = \frac{F \cdot W}{\rho_c \cdot \bar{L}} \qquad \text{(H6)}$$

Now we turn to the problem of finding F, that is, of finding f_s and f_v. Strictly, for a polydisperse collection, F should be averaged as was L, but often F can be assumed independent of size. This is a good assumption in the present case (Table J.I). The quantities f_s and f_v can only be found without large errors when the particles considered have a well-defined shape. Values of f_s and f_v can then be found by calculation, using solid geometry. This method has been used in the present work (Appendix J).

When the particle shape is not well-defined, f_s and f_v can only be found by experiment, and the values obtained can be subject

to large errors. The term f_v for each size range can be determined by counting and weighing to find the average volume of a single particle in that size range. This average volume is then divided by the cube of a suitable length dimension to obtain f_v. Since the values of the length dimension are usually subject to large systematic errors, so also are the experimental values of f_v (see Appendix J). No knowledge of particle shape is necessary when finding f_v experimentally. The term f_s is more difficult to determine. An initial estimate can be made by assuming the particles to be spherical. Once the average volume of a single particle in a given size range is known, the diameter of the volume-equivalent sphere can be found, and hence the surface area of the volume-equivalent sphere and finally f_s, again for the volume-equivalent sphere. This value is obviously subject to large errors. To find somewhat better values for f_s, direct experimental measurements must be made of the surface area, for example, by controlled adsorption [117].

APPENDIX J

THE SHAPE OF NICKEL SULFATE α-HEXAHYDRATE CRYSTALS

In calculating crystal growth rates from the results of any experiment measuring an overall weight increase of a crystal or crystals, the most difficult quantity to find with any accuracy is the overall crystal surface area across which the measured overall weight increase is spread. The overall surface area of the crystals, or in general of any collection of particles, can only be found accurately if the particles have a well defined shape, so that their surface area per unit weight (or "specific surface") can be found with some confidence by calculation, using solid geometry. Since the crystals used in the present work were mostly without irregularities (Appendix G) and had a well-defined shape, this method was used here.

The shape of nickel sulfate α-hexahydrate crystals is basically a combination of two tetragonal bipyramids. An idealized shape, showing all the crystallographic types of face which have been observed on crystals of nickel sulfate α-hexahydrate, together with their Miller indices, is shown in Figure J.1, from Groth [118]. The ideal shape shows a perfectly square cross-section, discounting corners, in any (001) plane and identical halves on each side of the (001) plane through the centre.

Faces of different types always incline to one another at constant angles (Haüy's Law) but the "habit" or the relative amount of each type of face occurring on a crystal cannot easily be predicted.

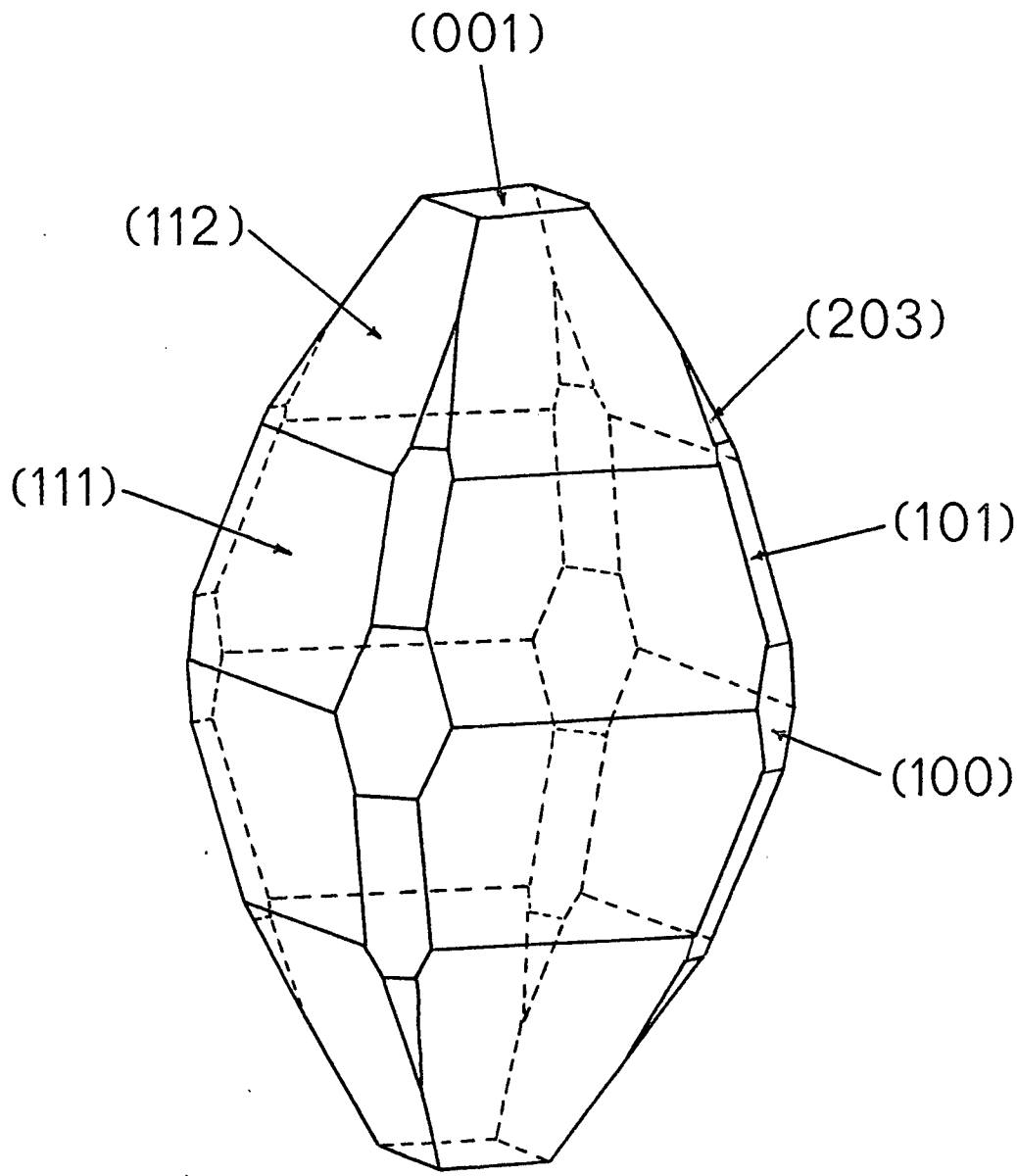

Figure J.1 Idealized shape of nickel sulfate α-hexahydrate crystals

Rather, it depends on the conditions under which that particular crystal was grown. With the seed crystals used in the present work, (100) faces were only present to a small extent, such that ignoring them caused an estimated error of not more than 2% in the surface area, while (101) and (203) faces were even less in evidence. Therefore for this work the general shape was approximated by the simplified form shown in Figure J.2.

In order to complete characterization of the average crystal shape for each of the four seed crystal size ranges used (425-500 μm, 850 μm - 1.00 mm, 1.70-2.00 mm and 3.35-400 mm), the three lengths L, L_1 and L_2 (Figure J.2) were measured for each of one hundred crystals showing no irregularities from each size range. L of course is the effective crystal size for sieving purposes. With each size range, L_1/L and L_2/L were calculated for each of the one hundred crystals and then the average L_1/L and the average L_2/L were found. The measurements were made with a reticle having divisions of 0.1 mm. The crystals and the reticle were observed through a 40-power binocular microscope so L, L_1 and L_2 could be measured to the nearest 0.01 mm. It was found that the variation in the values of L from different sides of the same crystal was much less than the variation of L between different crystals. In other words, although the crystal size L varied within the seed size range, the cross-section in the (001) plane through the centre of any given crystal was close to a perfect square. Therefore all three lengths L, L_1 and L_2 were always measured on one and only one side of each of the one hundred crystals.

Once the average values of L_1/L and L_2/L had been obtained,

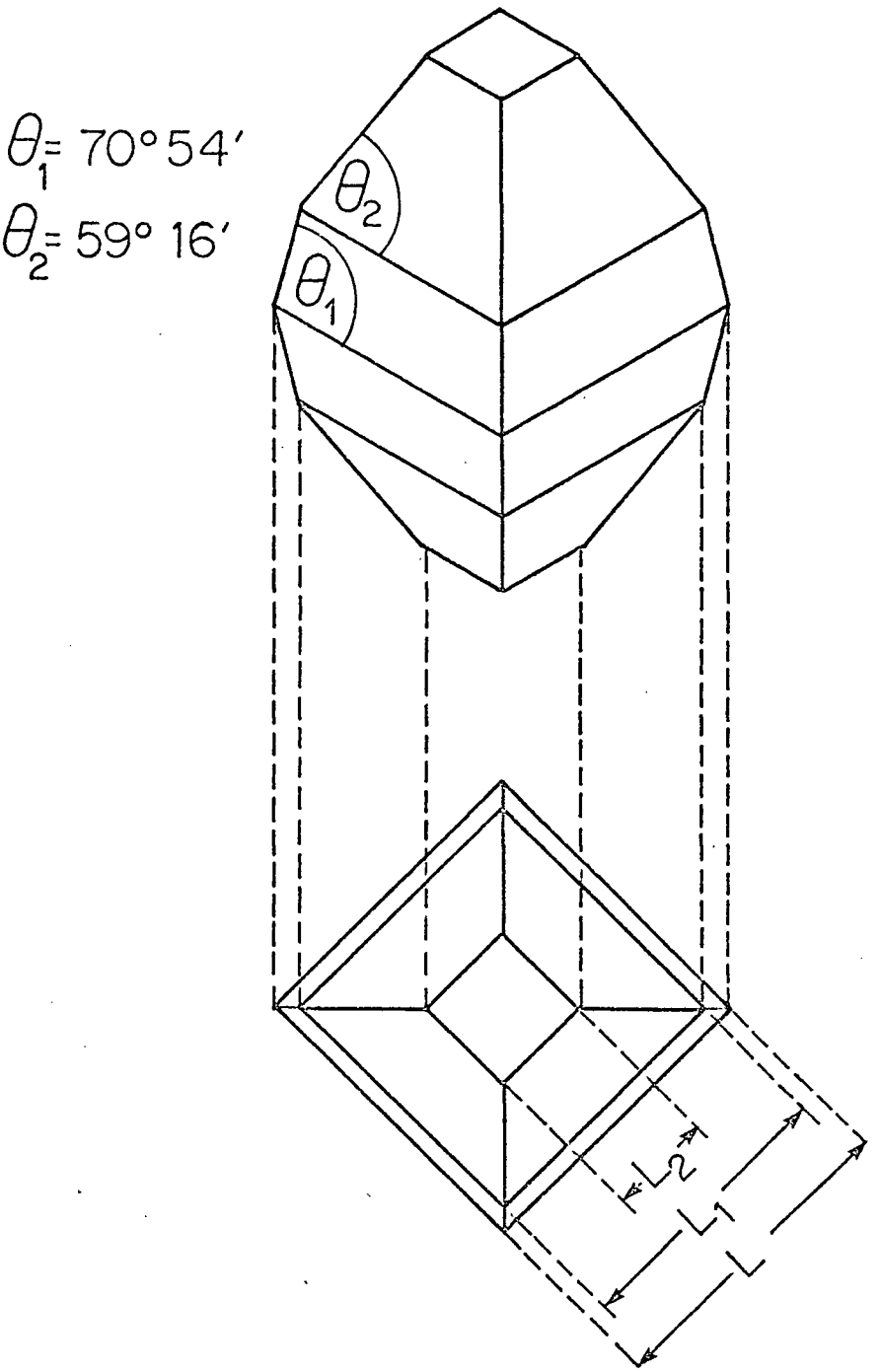

Figure J.2 Simplified shape of nickel sulfate α-hexahydrate crystals

the surface area shape factor f_s and the volume shape factor f_v (Appendix H) were calculated by solid geometry. The overall shape factor F is then given by f_s/f_v, and it is via F that the overall surface area of the crystals can be found, given the weight of crystals, as detailed in Appendix H. Values of f_s, f_v and F for each of the four seed crystal size ranges used are given in Table J.I. It will be seen that the crystal shape, as expressed by f_s and f_v, is quite similar for all four size ranges. This is good evidence that the crystal shape observed during this work was close to the steady state shape, or "Endkörper" [4] for nickel sulfate α-hexahydrate under the present conditions of growth: a crystal shape independent of crystal size (or "invariant") is a sufficient but not necessary condition that the Endkörper has been attained.

It should be noted however that having a crystal shape independent of crystal size does not necessarily imply that equal rates of growth occur on all faces of the crystal. Figure J.3 shows a hypothetical crystal whose faces must grow at different rates for the crystal to hold the same shape. In fact the necessary and sufficient condition on crystal shape for growth rates to be the same on all faces is that all faces of the crystal have the same Miller index, that is, have the same lattice density. (This usually, but not always, implies that the crystal shape is geometrically regular.) This condition is not met by nickel sulfate α-hexahydrate crystals so the overall growth rates found in the present experiments are strictly rates averaged over the different rates on the different faces. Never-

Table J.I Parameters of the crystal shape for different crystal sizes

crystal size range	425-500 μm	850 μm-1.00 mm	1.70-2.00 mm	3.35-4.00 mm
average (L_1/L)	0.787 (s.e. 0.6%)	0.787 (s.e. 0.9%)	0.839 (s.e. 0.7%)	0.820 (s.e. 1.2%)
average (L_2/L)	0.368 (s.e. 1.1%)	0.320 (s.e. 1.3%)	0.335 (s.e. 1.2%)	0.366 (s.e. 1.6%
f_s	4.093 (s.e. 0.5%)	4.138 (s.e. 0.6%)	3.922 (s.e. 0.6%)	3.968 (s.e. 1.0%)
f_v	0.659 (s.e. 0.6%)	0.667 (s.e. 0.9%)	0.618 (s.e. 0.9%)	0.631 (s.e. 1.4%)
F	6.211 (s.e. 0.8%)	6.204 (s.e. 1.1%)	6.346 (s.e. 1.1%)	6.288 (s.e. 1.6%)

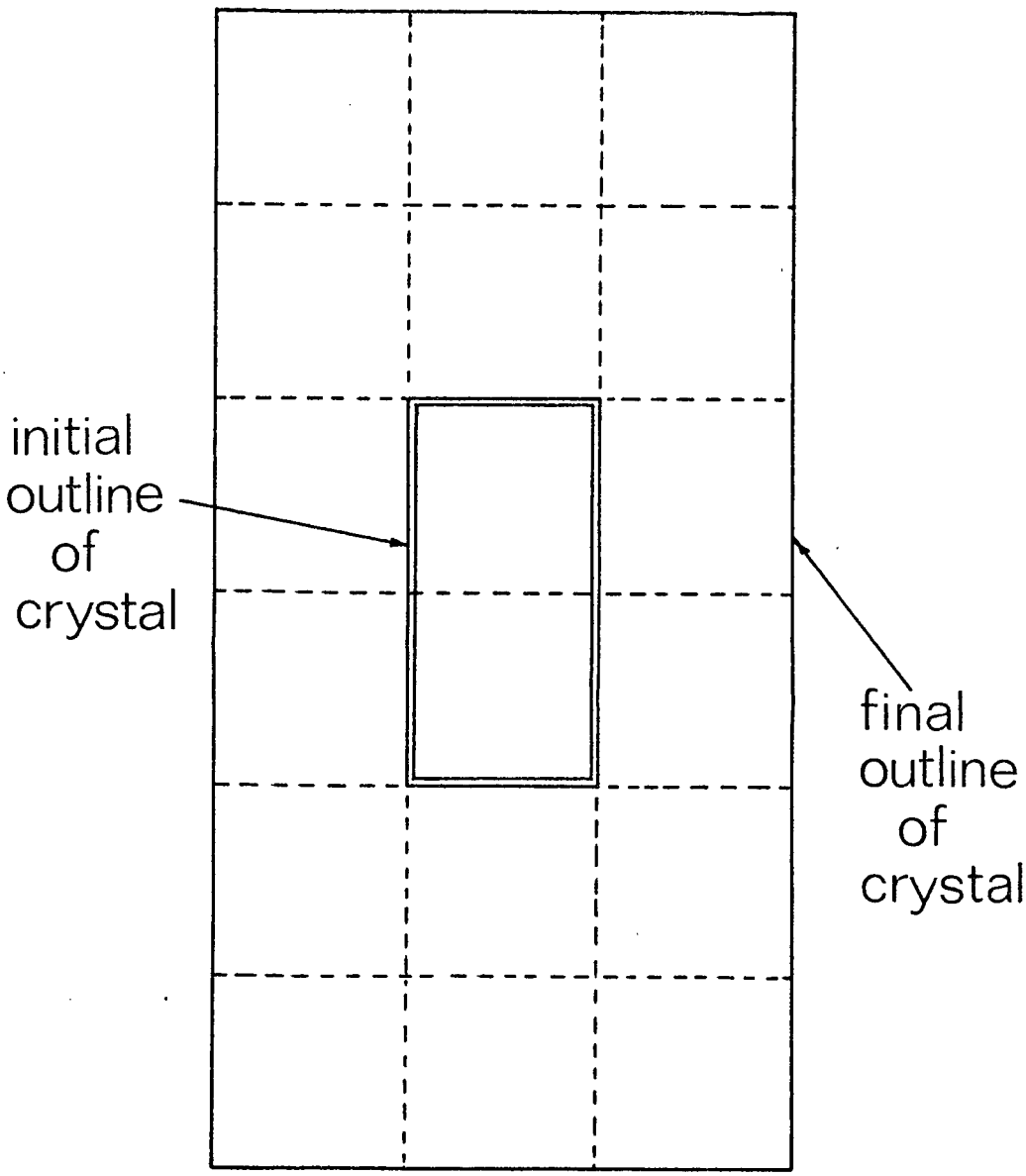

Figure J.3 A hypothetical crystal whose faces must grow at different rates for it to hold the same shape

theless, in the case of nickel sulfate α-hexahydrate crystals, the different faces have lattice densities which are not too different, so the rates on the different faces are expected to be not too different. This prediction was borne out by rough observations on crystals which had been grown in stages and had veils which showed previous positions of their surfaces, and also by scale drawings of the crystal shape, assuming this to be truly independent of crystal size: experimentally the shape is almost independent of size (Table J.I). The drawings indicated relative rates of growth of about 1:1.1:1.4 on the (111), (112) and (001) faces respectively. Using these ratios the separate absolute growth rates on each type of face could have been estimated. The relationship between growth rates on different types of face and overall growth rates is considered in more detail by Mullin and Gaska [16] and by Clontz et al. [21].

Because of the use of a sample size of 100 for the measurements of L, L_1 and L_2, the final values of F had relatively small standard errors (Table J.I). However, in obtaining the specific surface, F is divided by $\bar{L}$, the mean crystal size. As is common for small ranges of size, the arithmetic average sieve size was used for the mean crystal size, but the arithmetic average sieve size may have a systematic error of up to 4% due to tolerances in the manufacture of the sieves [79]. It was not necessary to consider this error when analysing growth rates at any given crystal size (unless it was necessary to state absolutely that crystal size), but a systematic error of up to 4% did enter when growth rates at different crystal sizes were compared.

As detailed above, f_s and f_v have been found by calculation, based on an average shape. While a value of f_s is very difficult to find by experiment, a value of f_v can be found very easily by experiment, even without investigating the crystal shape. Although this experimental value of f_v is by no means accurate, it does afford some degree of check on the calculated value of f_v. To find f_v by experiment, a sufficiently large known number of crystals from the size range in question are weighed together. The average weight and thus the average volume of one crystal can then be found. This average volume must be divided by the cube of some average crystal size to give f_v, and it is here that large errors may enter. One could use the arithmetic mean size of the appropriate sieve size range, but the absolute sieve sizes and hence also the mean size may have systematic errors of up to 4% [79]. The systematic error in f_v could therefore be up to 12% from this source alone, and other systematic errors may enter if the distribution of true sizes within the range is such that the true average size is far from the arithmetic mean size. Alternatively one could find the average crystal size directly by microscopic measurement. This should be more accurate although questions of sampling efficiency arise. It is difficult to be sure that the crystals used in the microscopic size measurements are an unbiased sample of those which were weighed, or, even if all those weighed are measured for size, whether these were an unbiased sample of all the crystals in the size range. (It should be noted that while unbiased sampling is very important when measuring microscopically for the average size, it is not as important when measuring microscopically for the average shape, as in

this case the size L is required only as a step in finding L_1/L and L_2/L.)

For the present crystals, the results of this rough check on f_v were as follows. A calculated value for f_v of 0.66 was obtained, from values of L_1/L and L_2/L found by measurements on ten crystals showing no irregularities, for a batch of seed crystals in the sieve size range 1.00-1.18 mm. Although the sample size of ten was small, this calculated value of f_v was close to the calculated value of 0.67 found with a sample size of one hundred for crystals 850 μm - 1.00 mm. The average volume of one crystal was found from weighing one hundred crystals. When the average sieve size (1.09 mm) was used for the real average crystal size, f_v found by experiment took the value 0.83. When the average microscopic size from the sample of ten crystals (1.20 mm) was used, f_v found by experiment took the value 0.63. There is a large difference between the sieve and microscopic average sizes, which in turn causes the large difference between the two experimental values of f_v. This is a common occurrence with many types of particles but in the present instance it may have been at least partly due to lack of precautions to ensure random sampling from the batch of the ten crystals investigated.

In this particular case, use of the microscopic average size led to much better agreement with the calculated value of f_v than did use of the arithmetic average sieve size. Nevertheless, as is common, use of the arithmetic average sieve size as a measure of the true average crystal size was retained because it was much more convenient than was the microscopic average size.

As mentioned in Appendix G, nickel sulfate α-hexahydrate

crystals are optically active [114], but in their case the asymmetry of the arrangement of ions in the crystal lattice which generates the optical activity does not influence the external shape: the laevorotatory and dextrorotatory crystals are visually indistinguishable.

Although the angles between the faces on any crystals of the same compound crystallized in the same form are constant, the "habit" or the linear proportions of the crystal, as expressed in this work by the average values of L_1/L and L_2/L, may vary, depending on the conditions of growth of the set of crystals considered. Thus even between the two manufacturer's lots, with very similar chemical specifications (Appendix C), which were used in this work, there were small but significant differences in the average values of L_1/L and L_2/L at comparable sizes, while the average shapes from samples of the nickel sulfate α-hexahydrate crystals grown in two different industrial "Krystal" crystallizers [93, 119] and an industrial stirred tank crystallizer [120] were each a little different again. In principle, the methods used in this work for finding crystal growth rates can be used on crystals of any shape, provided only that the different shapes occurring in each case are taken into account when finding the average overall crystal surface area.

APPENDIX K

SAMPLE CALCULATIONS OF GROWTH RATE

K.1 Batch Method

We shall use Experiment BG10.

K.1.1 Calculation of corrected weight increase

Weight of seed crystals = 5.030 g

Weight of product crystals, excluding nuclei = 8.471 g

Hence, uncorrected average weight = 6.751 g

Supersaturation, $(c - c^*)$ = 0.54 wt% hexa.

Therefore, from Figure L.1, end correction per gram of average weight = 0.0221 g

Therefore, total end correction (to be subtracted), = 0.149 g

Hence corrected weight increase = 8.471 - 5.030 - 0.149 = 3.292 g

Duration of steady growth period = 46.00 mins

K.1.2 Calculation of specific surface average crystal sizes

Seed crystals are all 0.85 - 1.00 mm (between U.S.A. Standard Sieve Nos. 20 and 18).

Therefore initial specific surface average crystal size = 0.925 mm

Product crystals have the size distribution shown below

Size range [mm] (U.S.A. Standard Sieve Nos.)	L_i [mm]	w_i [g]	w_i/L_i [g/mm]
0.85 - 1.00 (No. 20 - No. 18)	0.925	0.112	0.121
1.00 - 1.18 (No. 18 - No. 16)	1.09	8.359	7.669
Total		8.471	7.790

Using Equation (H10):

Final $\bar{L}_s$

$$= \frac{\Sigma w_i}{\Sigma(w_i/L_i)} = \frac{8.471}{7.790}$$

$$= 1.087 \text{ mm}$$

K.1.3 Calculation of average overall crystal surface area

We use Equation (H6):

$$A = W \left(\frac{F}{\rho_c \cdot \bar{L}_s} \right) \qquad \text{(H6)}$$

From Table J.I, for 1 mm crystals, F = 6.204. Density of crystals $\rho_c = 2.07$ g/cm^3. (Literature values of ρ_c [118, 114] and experimental values found in this work by the bottle method, using benzene as the auxiliary liquid, were all in good agreement.) We apply Equation (H6) to both seed and product crystals.

Hence overall surface area of seed crystals $= 5.030 \left(\frac{6.204}{2.07 \times 0.0925}\right)$ cm^2

$= 163.0$ cm^2

and overall surface area of product crystals = $8.471\ (\frac{6.204}{2.07 \times 0.1087})\ cm^2$

$= 233.6\ cm^2$

So average overall surface area of crystals = $198.3\ cm^2$

K.1.4 Calculation of growth rate

$$\text{Growth rate}\quad r = \frac{1}{A} \cdot \frac{\Delta W}{\Delta t} \tag{K1}$$

$$= \frac{1}{198.3} \times \frac{3.292}{46} \times \frac{10^4}{10^3} \times \frac{1}{60}\ kg/m^2 \cdot s$$

$$= 6.02 \times 10^{-5}\ kg/m^2 \cdot s$$

K.2 Continuous Method

We shall use the experiments over the supersaturation range 0.00 - 0.67 wt% hexa.

Twenty-two points were picked from the recorder trace. The least squares fit equation for these points was

$$\bar{c} = 55.614 - (1.4233 \times 10^{-2})\ t + (1.3668 \times 10^{-4})\ t^2$$

$$- (6.5677 \times 10^{-7})\ t^3 + (1.2065 \times 10^{-9})\ t^4 \tag{K2}$$

where $\bar{c}$ is the solution concentration in the sampling chamber, in wt% hexa., and t is the time after starting, in minutes.

We convert $\bar{c}(t)$ to $c(t)$ via Equation (44) (Section 6.2)

$$c = \bar{c} + \tau \frac{d\bar{c}}{dt} \qquad (44)$$

Here, residence time τ = 35 s = 0.583 mins

Hence

$$c = 55.606 - (1.4074 \times 10^{-2})t + (1.3553 \times 10^{-4})t^2 - (6.5396 \times 10^{-7})t^3 + (1.2065 \times 10^{-9})t^4 \qquad (K3)$$

and $$\frac{dc}{dt} = -1.4074 \times 10^{-2} + (2.7106 \times 10^{-4})t - (1.96188 \times 10^{-6})t^2 + (4.8260 \times 10^{-9})t^3 \qquad (K4)$$

As in the Batch Method calculation above, $\frac{F}{\rho_c \cdot L_{init}} = 32.401\ cm^2/g$

Weight of seed crystals = 320.0 g

Initial volume of solution at 40°C = 11200 cm^3

Initial s.g. of solution at 40°C = 1.4301

Therefore absolute density of solution at 40°C

= 1.4301 x 0.99997 g/cm^3

= 1.4301 g/cm^3

Therefore initial weight of solution = 11200 x 1.4301 g

Initial concentration of solution = 55.62 wt% hexa.

Therefore weight of water = 11200 x 1.4301 (1 - 0.5562) g

= 7108 g

For the mass balance, we must temporarily convert the concentration c(t), in wt% hexa., into $\hat{c}(t)$, in kg hexa/kg water. This is done via

$$\hat{c} = \frac{c}{100 - c} \tag{K5}$$

$$\text{and } \frac{d\hat{c}}{dt} = \frac{d\hat{c}}{dc} \cdot \frac{dc}{dt} = \frac{100}{(100 - c)^2} \cdot \frac{dc}{dt} \tag{K6}$$

The above values are substituted in the relationships given in Section 6.2. These relationships are then solved together on a computer, using t as a dummy variable, to produce values of r for corresponding values of (c - c*).

APPENDIX L

SUMMARY OF DATA

L.1 Growth end corrections for the Batch Method

The growth end corrections for the Batch Method are given in graphical form in Figures L.1 and L.2 on the two following pages.

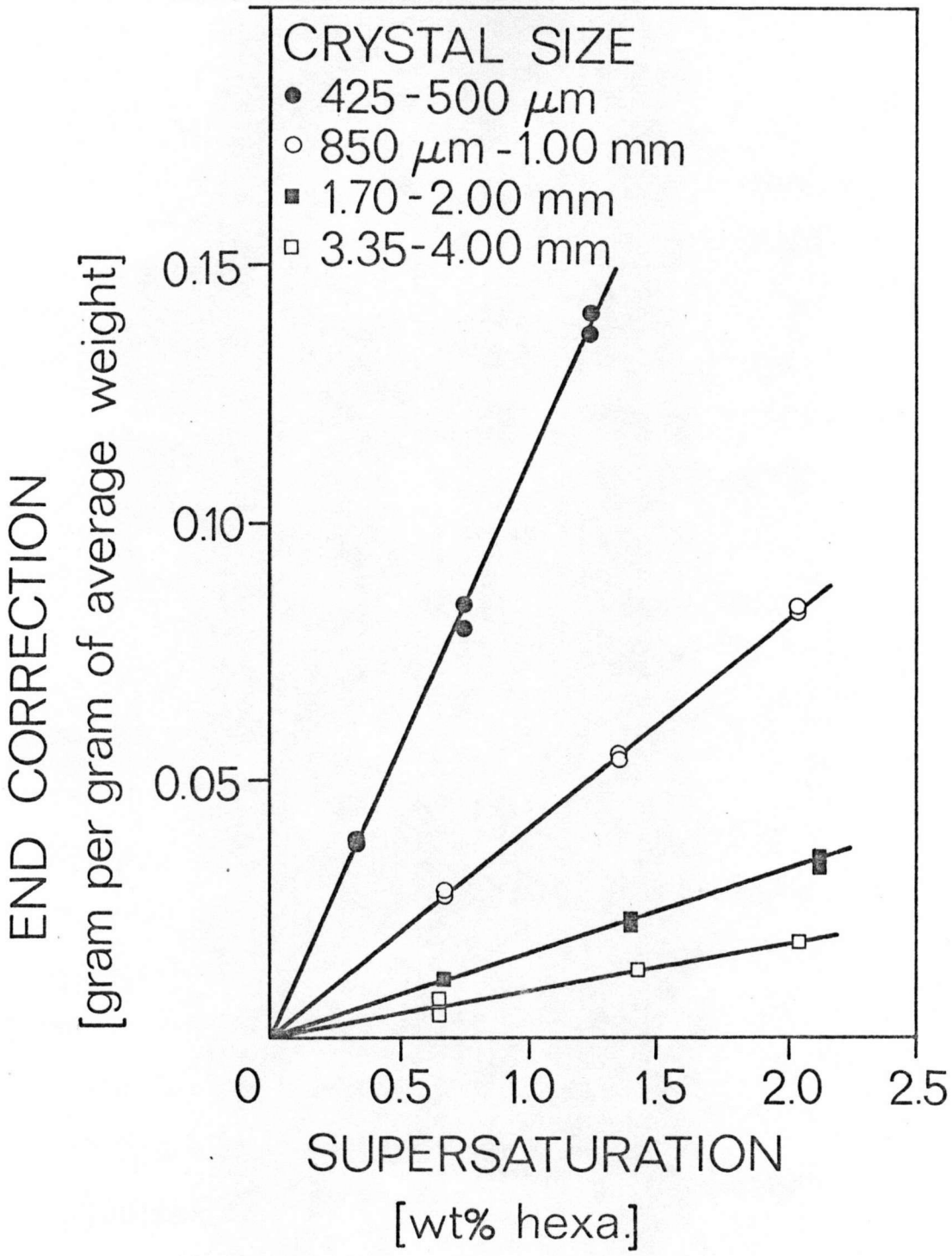

Figure L.1 Growth end corrections in the Batch Method for different sized crystals at 40°C

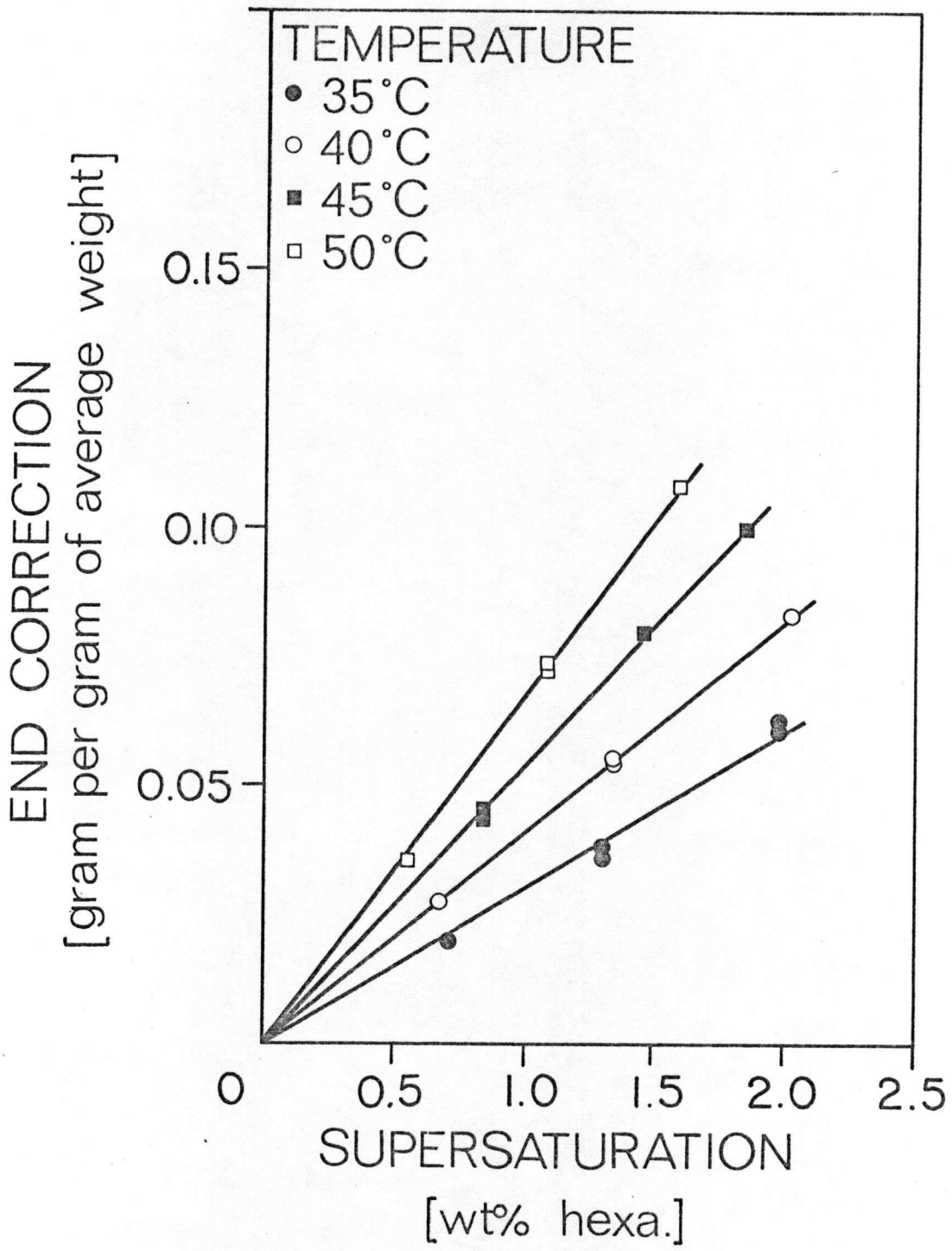

Figure L.2 Growth end corrections in the Batch Method for 1 mm crystals at different temperatures

L.2 Growth rates by the Batch Method

Temperature = 40.00°C c* = 54.95 wt% hexa.

Average crystal size for the series = 0.51 mm
Average interstitial solution velocity for this crystal size = 12.1 mm/s

Experiment No.	Crystal size L [mm]	Supersaturation c - c* [wt% hexa]	Growth rate [$kg/m^2 \cdot s$]
425G8	0.51	0.19	1.24×10^{-5}
425G7	0.51	0.36	2.71×10^{-5}
425G6	0.51	0.51	4.24×10^{-5}
425G5	0.51	0.67	6.08×10^{-5}
425G4	0.51	0.67	6.18×10^{-5}
425G3	0.51	0.82	7.99×10^{-5}
425G2	0.51	0.98	9.63×10^{-5}

Temperature = 40.00°C c* = 54.95 wt% hexa.

Average crystal size for the series = 1.01 mm

Average interstitial solution velocity for this crystal size = 29.5 mm/s

Experiment No.	Crystal size L[mm]	Supersaturation c - c* [wt% hexa.]	Growth rate [kg/m^2·s]
BG 14	1.01	0.13	1.15×10^{-5}
BG 13	1.01	0.23	2.02×10^{-5}
BG 12	1.01	0.32	3.09×10^{-5}
BG 11	1.01	0.44	4.50×10^{-5}
BG 10	1.01	0.54	6.02×10^{-5}
BG 9	1.01	0.64	7.59×10^{-5}
BG 8	1.01	0.64	7.54×10^{-5}
BG 7	1.01	0.74	9.23×10^{-5}
BG 6	1.00	0.85	10.98×10^{-5}
BG 5	1.01	1.00	13.17×10^{-5}
BG 4	1.01	1.09	15.06×10^{-5}
BG 3	1.01	1.16	16.49×10^{-5}
BG 2	1.01	1.25	18.26×10^{-5}
BG 1	1.01	1.34	19.15×10^{-5}
BG 15	1.01	1.34	19.22×10^{-5}
BG 16	1.01	1.44	21.22×10^{-5}
BG 17	1.01	1.53	23.50×10^{-5}
BG 18	1.01	1.66	26.10×10^{-5}
BG 19	1.01	1.78	28.76×10^{-5}
BG 20	1.01	1.89	31.19×10^{-5}
BG 21	1.01	2.00	34.19×10^{-5}
BG 22	1.01	2.00	34.02×10^{-5}
BG 23	1.01	2.13	37.25×10^{-5}
BG 24	1.01	2.26	40.87×10^{-5}
BG 25	1.01	2.39	44.51×10^{-5}

Temperature = 40.00°C c* = 54.95 wt% hexa.

Average crystal size for the series = 2.03 mm

Average interstitial solution velocity for this crystal size = 69.0 mm/s

Experiment No.	Crystal size L [mm]	Supersaturation c - c* [wt% hexa.]	Growth rate [$kg/m^2 \cdot s$]
1.70G5	2.02	0.34	4.13×10^{-5}
1.70G4	2.04	0.69	8.92×10^{-5}
1.70G3	2.06	1.02	14.72×10^{-5}
1.70G2	2.02	1.40	22.33×10^{-5}
1.70G1	2.02	1.40	22.30×10^{-5}
1.70G6	2.02	1.64	27.36×10^{-5}
1.70G7	2.02	1.97	34.85×10^{-5}
1.70G8	2.02	2.20	42.92×10^{-5}

Temperature = 40.00°C c* = 54.95 wt% hexa.

Average crystal size for the series = 4.03 mm

Average interstitial solution velocity for this crystal size = 130 mm/s

Experiment No.	Crystal size L [mm]	Supersaturation c - c* [wt% hexa.]	Growth rate [kg/m^2·s]
4.00G7	4.03	0.21	3.25×10^{-5}
4.00G6	4.03	0.44	6.55×10^{-5}
4.00G5	4.03	0.70	11.51×10^{-5}
4.00G4	4.03	0.93	17.07×10^{-5}
4.00G3	4.03	0.93	16.84×10^{-5}
4.00G2	4.03	1.16	22.57×10^{-5}
4.00G1	4.03	1.32	27.32×10^{-5}
4.00G8	4.03	1.57	37.43×10^{-5}
4.00G9	4.03	1.80	44.59×10^{-5}

Temperature = 35.00°C c* = 53.30 wt% hexa.

Average crystal size for the series = 1.01 mm

Average interstitial solution velocity for this crystal size = 29.5 mm/s

Experiment No.	Crystal size L [mm]	Supersaturation c - c* [wt% hexa]	Growth rate [kg/m^2·s]
35G5	1.01	0.31	1.80×10^{-5}
35G4	1.01	0.66	5.02×10^{-5}
35G3	1.01	0.99	8.72×10^{-5}
35G2	1.01	1.33	13.37×10^{-5}
35G1	1.01	1.33	13.30×10^{-5}
35G6	1.01	1.64	17.78×10^{-5}
35G7	1.01	1.98	23.40×10^{-5}
35G8	1.01	2.35	30.29×10^{-5}

Temperature = 45.00°C c* = 56.63 wt% hexa.

Average crystal size for the series = 1.01 mm

Average interstitial solution velocity for this crystal size = 29.5 mm/s

Experiment No.	Crystal size L [mm]	Supersaturation c - c* [wt% hexa.]	Growth rate [$kg/m^2 \cdot s$]
45G7	1.01	0.33	4.98×10^{-5}
45G6	1.01	0.63	10.90×10^{-5}
45G5	1.01	0.98	18.36×10^{-5}
45G4	1.01	1.24	24.95×10^{-5}
45G3	1.01	1.24	24.89×10^{-5}
45G2	1.01	1.51	31.94×10^{-5}
45G1	1.01	1.84	39.92×10^{-5}

Temperature = 50.00°C c* = 58.38 wt% hexa.

Average crystal size for the series = 1.01 mm

Average interstitial solution velocity for this crystal size = 29.5 mm/s

Experiment No.	Crystal size L [mm]	Supersaturation c - c* [wt% hexa.]	Growth rate [$kg/m^2 \cdot s$]
50G8	1.01	0.24	4.94×10^{-5}
50G7	1.01	0.44	9.75×10^{-5}
50G6	1.01	0.65	15.22×10^{-5}
50G5	1.01	0.89	22.31×10^{-5}
50G4	1.01	0.89	22.00×10^{-5}
50G3	1.01	0.89	22.36×10^{-5}
50G2	1.01	1.10	29.18×10^{-5}
50G1	1.01	1.34	35.26×10^{-5}

L.3 Growth rates by the Continuous Method

Supersaturation range 0.00 - 0.67 wt% hexa.	
Temperature = 40.00°C c* = 54.95 wt% hexa. Average crystal size = 1.01 mm Average interstitial solution velocity = 33.1 mm/s	
Supersaturation $c - c^*$ [wt% hexa.]	Growth rate [$kg/m^2 \cdot s$]
0.66	8.07×10^{-5}
0.63	7.60×10^{-5}
0.60	7.16×10^{-5}
0.55	6.38×10^{-5}
0.51	5.70×10^{-5}
0.46	5.11×10^{-5}
0.42	4.58×10^{-5}
0.39	4.11×10^{-5}
0.36	3.70×10^{-5}
0.32	3.33×10^{-5}
0.28	2.84×10^{-5}
0.25	2.43×10^{-5}
0.22	2.09×10^{-5}
0.19	1.79×10^{-5}
0.16	1.47×10^{-5}
0.13	1.16×10^{-5}
0.10	0.90×10^{-5}
0.07	0.71×10^{-5}
0.04	0.58×10^{-5}
0.00	0.50×10^{-5}

Supersaturation range 0.67 - 1.30 wt% hexa.	
Temperature = 40.00°C c* = 54.95 wt% hexa. Average crystal size = 1.01 mm Average interstitial solution velocity = 33.1 mm/s	
Supersaturation c - c* [wt% hexa.]	Growth rate [kg/m^2•s]
1.29	16.66×10^{-5}
1.26	16.06×10^{-5}
1.23	15.49×10^{-5}
1.20	14.95×10^{-5}
1.15	13.94×10^{-5}
1.10	13.03×10^{-5}
1.07	12.61×10^{-5}
1.02	11.81×10^{-5}
0.97	11.08×10^{-5}
0.92	10.40×10^{-5}
0.88	9.76×10^{-5}
0.83	9.17×10^{-5}
0.79	8.61×10^{-5}
0.75	8.08×10^{-5}
0.69	7.34×10^{-5}

L.4 Dissolution end corrections for the Batch Method

The dissolution end corrections for the Batch Method are given in graphical form in Figures L.3 and L.4 on the two following pages.

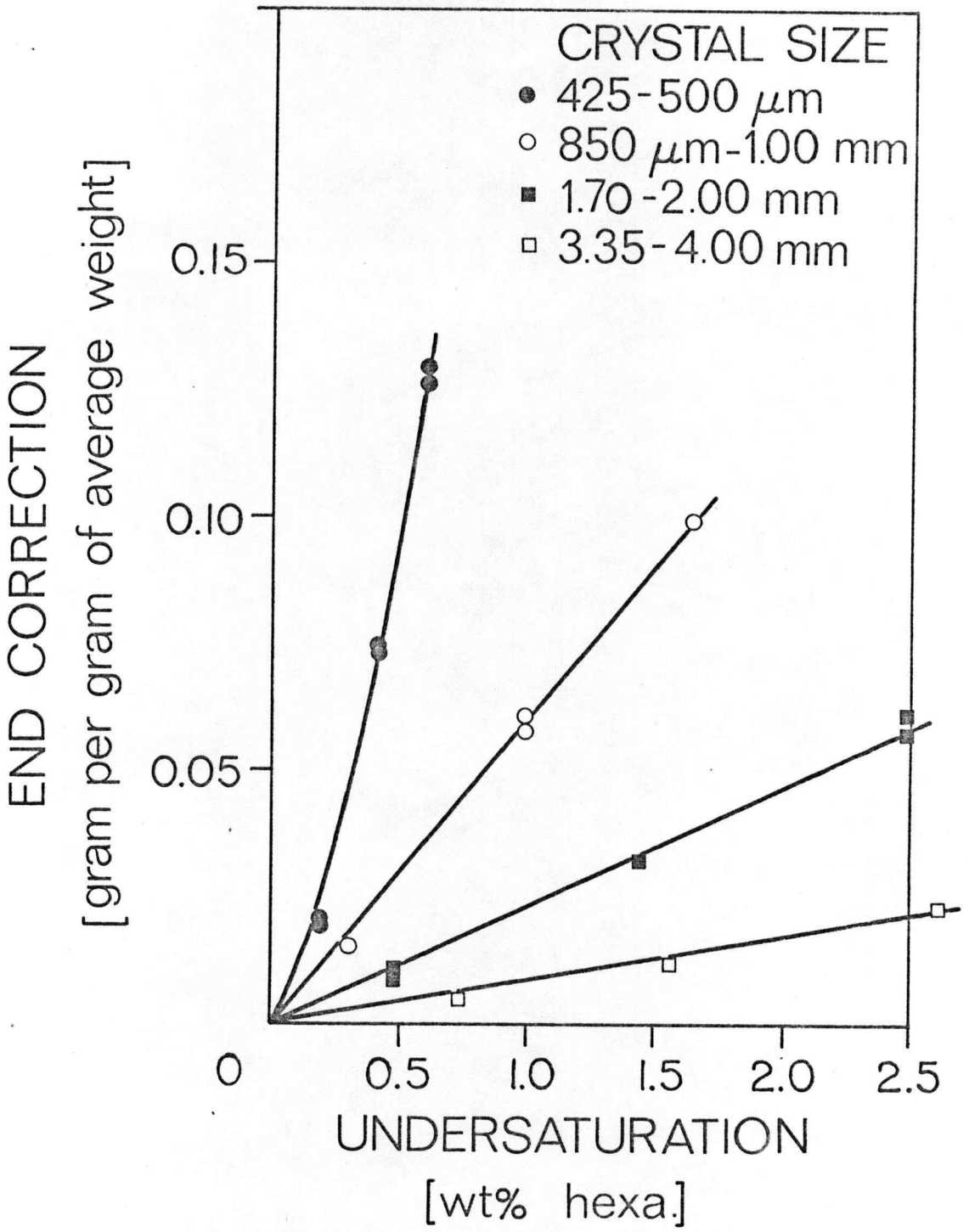

Figure L.3 Dissolution end corrections in the Batch Method for different sized crystals at 40°C

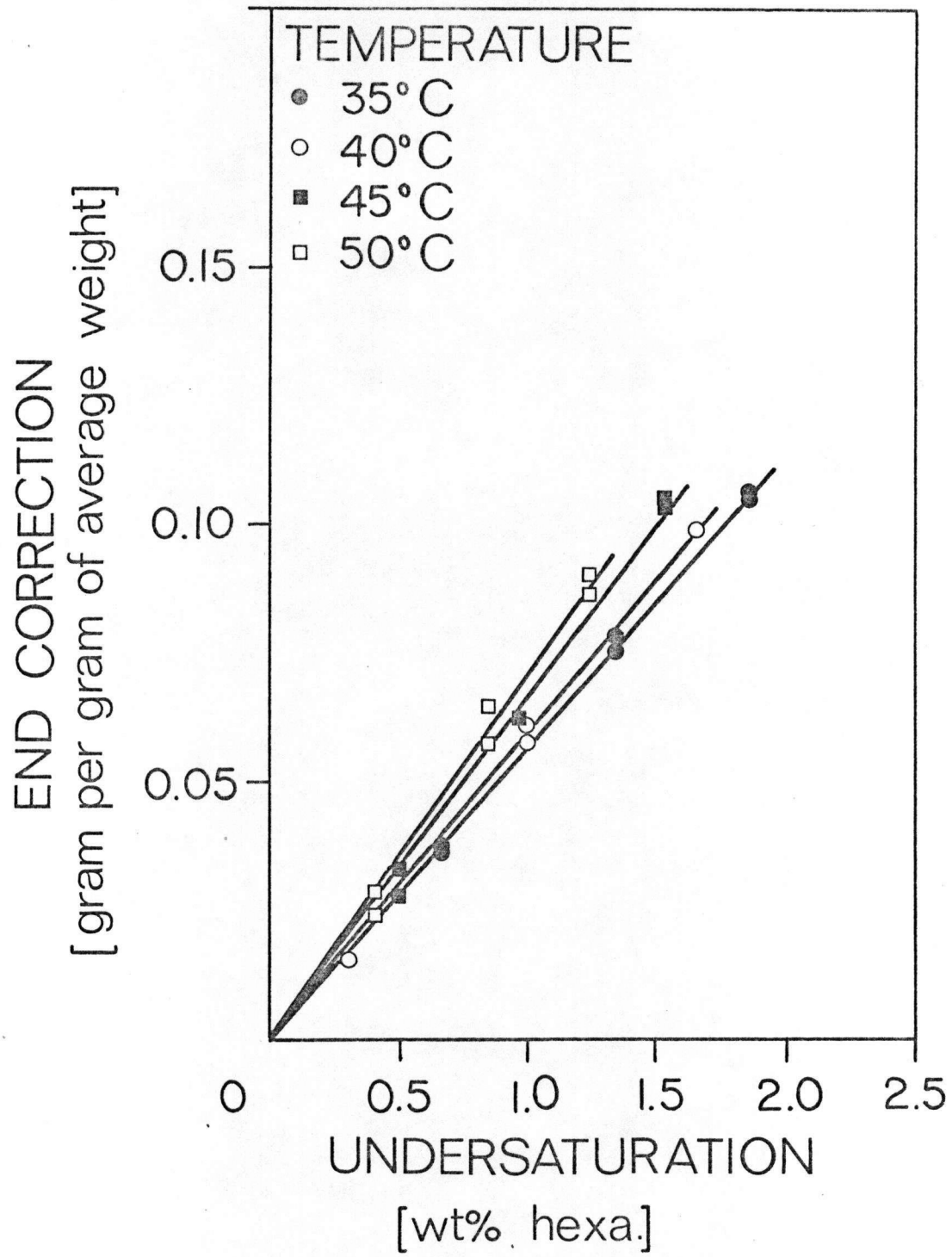

Figure L.4 Dissolution end corrections in the Batch Method for 1 mm crystals at different temperatures

L.5 Dissolution rates by the Batch Method

Temperature = 40.00°C c* = 54.95 wt% hexa.

Average crystal size for the series = 0.50 mm

Average interstitial solution velocity for this crystal size = 12.1 mm/s

Experiment No.	Crystal size L [mm]	Undersaturation c* - c [wt% hexa.]	Dissolution rate [$kg/m^2 \cdot s$]
425D6	0.50	0.13	3.31×10^{-5}
425D5	0.51	0.20	7.39×10^{-5}
425D4	0.51	0.29	11.11×10^{-5}
425D3	0.51	0.29	11.51×10^{-5}
425D2	0.51	0.37	15.42×10^{-5}
425D1	0.50	0.49	22.43×10^{-5}

Temperature = 40.00°C c* = 54.95 wt% hexa.

Average crystal size for the series = 1.00 mm

Average interstitial solution velocity for this crystal size = 29.5 mm/s

Experiment No.	Crystal size L [mm]	Undersaturation c* - c [wt% hexa.]	Dissolution rate [$kg/m^2 \cdot s$]
40D3	1.01	0.32	13.47×10^{-5}
40D4	1.01	0.64	29.52×10^{-5}
40D5	1.01	0.97	46.92×10^{-5}
40D6	1.01	0.97	45.99×10^{-5}
40D2	1.01	1.25	61.00×10^{-5}
40D1	0.99	1.63	79.11×10^{-5}

Temperature = 40.00°C c* = 54.95 wt% hexa.

Average crystal size for the series = 2.00 mm

Average interstitial solution velocity for this crystal size = 69.0 mm/s

Experiment No.	Crystal size L [mm]	Undersaturation c* - c [wt% hexa.]	Dissolution rate [$kg/m^2 \cdot s$]
1.70D3	2.02	0.46	21.38×10^{-5}
1.70D4	2.02	0.91	44.66×10^{-5}
1.70D5	2.02	1.35	69.03×10^{-5}
1.70D6	2.02	1.35	67.56×10^{-5}
1.70D2	1.96	1.91	97.62×10^{-5}
1.70D1½	1.94	2.42	124.13×10^{-5}

Temperature = 40.00°C c* = 54.95 wt% hexa.

Average crystal size for the series = 4.03 mm

Average interstitial solution velocity for this crystal size = 130 mm/s

Experiment No.	Crystal size L [mm]	Undersaturation c* - c [wt% hexa.]	Dissolution rate [$kg/m^2 \cdot s$]
4.00D3	4.03	0.48	21.24×10^{-5}
4.00D4	4.03	0.93	47.97×10^{-5}
4.00D5	4.03	1.42	77.69×10^{-5}
4.00D6	4.03	1.42	78.39×10^{-5}
4.00D2	4.03	1.86	101.09×10^{-5}
4.00D1	4.03	2.40	130.75×10^{-5}

Temperature = 35.00°C c* = 53.30 wt% hexa.

Average crystal size for the series = 1.01 mm

Average interstitial solution velocity for this crystal size = 29.5 mm/s

Experiment No.	Crystal size L [mm]	Undersaturation c* - c [wt% hexa]	Dissolution rate [$kg/m^2 \cdot s$]
35D1	1.01	0.31	12.23×10^{-5}
35D2	1.01	0.58	24.21×10^{-5}
35D3	1.01	0.86	36.25×10^{-5}
35D4	1.01	0.86	36.32×10^{-5}
35D5	1.01	1.16	49.91×10^{-5}
35D6	1.01	1.37	58.66×10^{-5}

Temperature = 45.00°C c* = 56.63 wt% hexa.

Average crystal size for the series = 1.00 mm

Average interstitial solution velocity for this crystal size = 29.5 mm/s

Experiment No.	Crystal size L [mm]	Undersaturation c* - c [wt% hexa.]	Dissolution rate [$kg/m^2 \cdot s$]
45D1	1.01	0.26	11.70×10^{-5}
45D2	1.01	0.49	23.43×10^{-5}
45D3	1.00	0.72	38.94×10^{-5}
45D4	1.00	0.72	37.73×10^{-5}
45D5	1.00	0.97	52.16×10^{-5}
45D6	1.00	1.20	66.27×10^{-5}

Temperature = 50.00°C c* = 58.38 wt% hexa.

Average crystal size for the series = 1.00 mm

Average interstitial solution velocity for this crystal size = 29.5 mm/s

Experiment No.	Crystal size L [mm]	Undersaturation c* - c [wt% hexa.]	Dissolution rate [$kg/m^2 \cdot s$]
50D1	1.01	0.21	9.98×10^{-5}
50D2	1.00	0.40	23.24×10^{-5}
50D3	1.00	0.59	35.28×10^{-5}
50D4	1.00	0.59	34.82×10^{-5}
50D5	1.01	0.80	49.73×10^{-5}
50D6	1.00	0.98	61.75×10^{-5}